Synthesis of nanocapsules for emerging contaminants detection

Javier Pérez Piñeiro

TESE DE DOUTORAMENTO
2017 Mención internacional

Universidade Vigo

EIDO
Escola Internacional
de Doutoramento

Universidade Vigo
Escola Internacional de Doutoramento

Javier Pérez Piñeiro

TESE DE DOUTORAMENTO

Synthesis of nanocapsules for emerging contaminants detection

Dirixido polos doutores:

Miguel Ángel Correa Duarte y

Moisés Pérez Lorenzo

ANO 2017

"Mención internacional"

Contents

THESIS SCOPE

The main goal of the present manuscript consists in the design, synthesis and application of engineered plasmonic nanocapsules as multifunctional platforms. Along these lines, we pay special attention to their use as sensing devices for the detection of relevant contaminants such as pharmaceuticals and drugs, species that have recently acquired great relevance, becoming an environmental problem worldwide. In this manner, the presence of these contaminants in aquatic ecosystems imply a great risk for human health given the development of antimicrobial resistance among aquatic microorganisms. We herein introduce in detail the use of these plasmonic nanocapsules as sensing nanoplatforms for the detection of trace amounts of such chemicals by means of surface enhanced Raman spectroscopy (SERS). In another order of things, the same plasmonic capsules have been used as molecular probes within Raman tweezers, leading to the development of local SERS platforms that may pave the way towards the design of

novel tools which may allow the dragging and location of cargo in a locally-controlled fashion.

The results obtained in the course of this Thesis have been developed at the Department of Physical Chemistry of Universidade de Vigo. Moreover, a scientific stay at Adolphe Merkle Institute in Switzerland and an important collaboration with Case Western University (USA) and CNR-IPCF (Italy) have had a positive impact in the final output of this work. The manuscript herein presented has been divided in four chapters. Chapter 1 corresponds to a General Introduction section in which special attention is given to the fundamentals of SERS spectroscopy and the synthetic protocols used for the formation of the hybrid nanocapsules used. The subsequent chapters correspond to the main results obtained and are classified as follows:

Chapter 2 is focused in the use of plasmonic nanocapsules for the detection of trimethoprim (TMP), a pharmaceutical compound with antibacterial activity that is currently prescribed for the treatment of chest and urine infections. In this particular case, a direct detection approach is performed due to the affinity between TMP and the metallic component of the capsules, given the presence of amine groups in the molecule. TMP diffuses through the mesoporous silica shell and is anchored to the gold nanoparticles located at the inner wall of the inorganic capsule. In this manner, the use of hollow nanostructures provides a protected environment where the detection can be performed even in harsh environments. This characteristic is particularly valuable, given that the detection of such molecules will be performed in wastewaters, where high ionic strength and the presence of other contaminants or macromolecules could jeopardize the correct operation of the nanosensor. Moreover, in our work the detection has been also performed in the presence

of other contaminants such as ibuprofen or diclofenac. Even in this scenario the same sensitivity can be attained, showcasing the high specificity of this approach under more realistic conditions.

In Chapter 3, an indirect detection methodology is reported. Emerging contaminants such as diclofenac, carbamezapine and ethinylestradiol can be detected in this fashion. In this case, the contaminants do not have a strong chemical affinity for the metallic surface, thereby highlighting the need to introduce a linker that may provide the necessary interaction between both species and lead therefore to the desired SERS fingerprint of each contaminant. In this case, the linker used has been modified in order to obtain a functional group that may present higher reactivity towards the aromatic component of the analytes (all the emerging contaminants studied are aromatic compounds). In this way, the modified linker can react with different emerging contaminants allowing the multiplex detection even at low concentrations.

In Chapter 4, plasmonic nanocapsules have been applied as platforms in optical trapping. This work has been developed as a proof of concept idea, aiming at performing the optical trapping of the plasmonic capsules, thus using them as local SERS probes in Raman tweezers. Along these lines, we hereby demonstrate a high trapping efficiency due to plasmon-enhanced optical trapping of the gold component present in the inner walls of the sub-micrometric capsules. The relevance of effective optical trapping in hollow plasmonic mesocapsules is twofold for detection and delivery technologies: positioning and activation processes. In fact, the presented system allows for the opportunity to drag and locate cargo mesocapsules embedded with specific molecules that can be activated and released in situ when a precise localization is required.

Chapter 1

General Introduction

1.1 Nanoparticles

In the last years, Nanotechnology have acquired great importance and the publications in this field have increased exponentially. Nanotechnology focuses on the preparation, characterization and manipulation of materials and structures at the nanometer scale.

In general, it is widely accepted that Nanotechnology deals with structures with sizes ranging from 1 to 100 nanometers (nanoparticles). Along these lines, while bulk materials have constant physical and chemical properties regardless their size and shape, the morphological aspects of nanoparticles often define the physical and chemical properties of the substance.

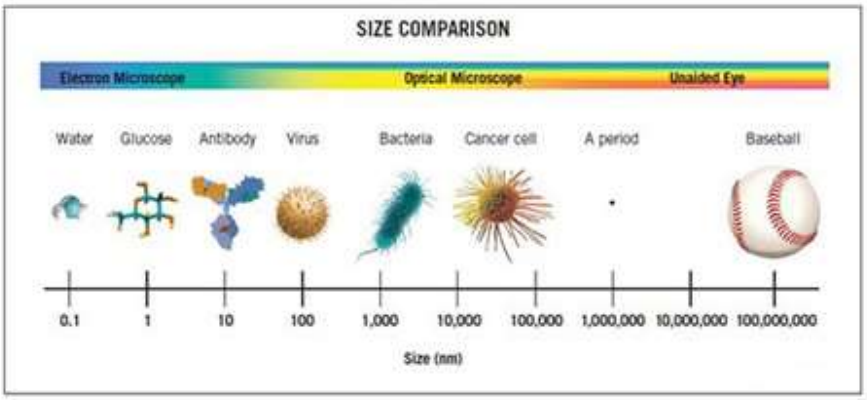

Figure 1. Comparison of sizes is shown

Thus, the properties of materials may be altered as their size approaches the nanoscale and thus, as the percentage of atoms at the surface of the material becomes significant. Other properties likely to undergo changes are those related with the electromagnetic, thermodynamic and spectroscopic factors.

The novel properties arising from the fabrication of nanomaterials have attracted great attention from the scientific community due to the possibility to create a wealth of new materials and manufacturing possibilities, which will deeeply impact the economy, the environment, and society.[1] In this regard, one of the most notable aspects of this field is their potential in many areas of science. In the figure 2 are shown some examples, among others.

Nanoparticles are characterized for a high surface/volume ratio but the particles tend to aggregate to reduce their surface area. For this reason, nanoparticles are thermodynamic unstable being necessary repulsion methods to avoid the aggregation and acquire kinetic stability, allowing colloids to be dispersed for long

[1] X. W. Lou; L. A. Archer; Z. Yang, *Adv. Mater.* **2008**, 20, 3987–4019.

periods of time. Indeed, some of gold colloids synthesized by Faraday more than a hundred years ago are stable nowadays.

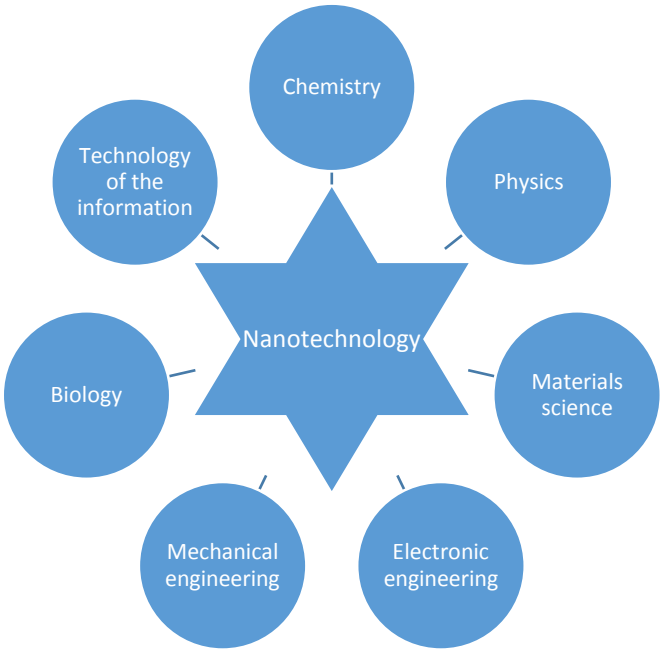

Figure 2. Some fields where nanotechnology is applied

DLVO theory[2,3] explain perfectly the stability of colloids due to the equilibrium between the repulsive and attractive forces. Therefore, DLVO theory is an equilibrium between Van der Waals forces and the repulsive intermolecular forces.

The factor that avoid the aggregation of the particles is the electric double layer that provide the necessary kinetic stability. There are several models to explain the electric double layer. For that, it is considered a charged surface (an electrode) introduced in a solution where this charge performs an attraction in the ions of the solution with different charge.

---

[2] B. Derjaguin; L. Landau, *Acta Physicochim. URSS* **1941**, 14, 633-662.
[3] E. J. W. Verwey; J. T. Overbeek; K. Nes, Theory of the stability of lyophibic colloids: the interaction of sol particles having an electric doublé layer, *Elsevier* **1948**.

In 1879, Helmholtz proposed a compact layer of ions in contact with the charged surface metal. At the beginning of the 20th century, Gouy and Chapman proposed a double diffuse layer in which consider the thermal motion of ions near a charged surface.[4,5] Stern, in 1924 improved the model combining the two previous models and he proposed that the counterions have a finite size and the charge can approach a minimum distance equal to the radius of the counterion.[6]

In the colloid surface is not possible measure the potential, so it is necessary measure the zeta potential that is the potential in the point where the diffuse layer and the Stern layer are joined. This zeta potential value indicates the charge accumulation on the colloid surface and therefore if repulsion between the colloids exceeds the tendency to the aggregation. For this reason, zeta potential is used to know the colloidal stability of the nanoparticles.

Colloids can be stabilized by two different strategies:

- Stabilization by coating: it consists in creating a polymer layer or a surfactant layer that avoids the aggregation of colloids.
- Stabilization by electric charge: controlling the charge surface.

[4] G. Gouy, *Compt. Rend.* **1910**, 149, 654.
[5] D. L. Chapman, *Philos. Mag.* **1913**, 25, 475.
[6] O. Stern, *Z. Elektrochem.* **1924**, 30, 508.

1.1.2 Metallic nanoparticles

Among metallic nanoparticles, gold, silver and copper have great importance due to their characteristic optical properties. For example the gold has experienced an unprecedented growth in publications in the fields of Nanoscience and Nanotechnology over the past two decades, despite it has been a very common topic of investigation for many years.

Gold changes the color depending on the size. Its colorful features have allowed the use of gold nanoparticles in decorative elements, for example, the stained glass windows in Notre-Dame de Paris. However, one the main examples is sited in the British Museum where the Lycurgus cup is located. This cup made in Roma and dating from the 4th century, changes its color depending on where the light comes from. Being green if the light comes from the outside and red when the cup is illuminated from the inside. This is due to the presence of gold and silver nanoparticles that provide it with characteristically optical properties.[7]

Figure 3. Left: picture of the Rose Window in Notre Dame Cathedral. Right: picture of Lycurgus cup.

[7] I. Freestone; N. Meeks; M. Sax; C. Higgitt, *Gold Bull.* **2007**, 40, 4, 270-277.

Science about metallic nanoparticles starts in 1857 with Michael Faraday's experiments.[8] Faraday demonstrated the formation of gold colloids with a red color reducing tetrachloroauric acid with phosphorous acid as a reducing agent. Faraday could not determine the size of the nanoparticles but afterwards J. M. Thomas reproduced the experiments estimating that gold nanoparticles had a size between 3–30 nm.[9]

In the 20th century, gold nanoparticles were synthesized with several sizes and several shapes by different ways producing a very important increase in applications. Nowadays, among those applications stands out the use of nanoparticles in the treatment of diseases.[10]

Choosing the synthesis method, it is possible to control the size, the shape and the dispersion. Modifying these factors, the optical, catalytic and electrical properties can be changed.

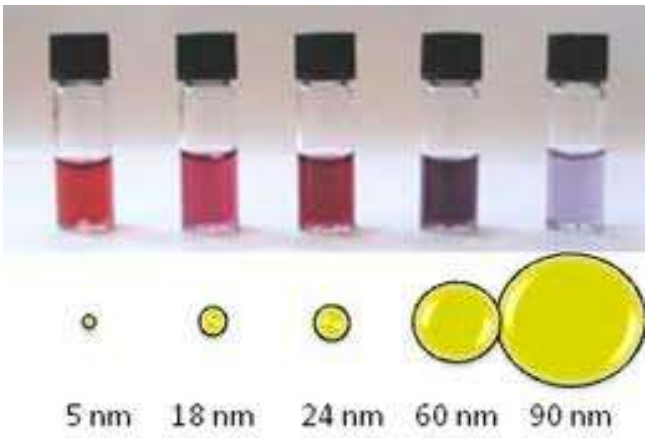

Figure 4. Color of gold nanoparticles change depending on the size nanoparticles.

[8] M. Faraday, *Phil. Trans. Roy. Soc.* **1857**, 147, 145-153.
[9] J. M. Thomas, *Pure and Appl. Chem.* **1988**, 60, 1517-1528.
[10] E. C. Dreaden; A. M. Alkilany; X. Huang; C. J. Murphy; M. A. El-Sayed, *Chem. Soc. Rev.,* **2012**, 41, 2740–2779.

There are several factors that affect the morphology of the nanoparticles: the reducing agent, the ratio between the amounts and concentrations of the reactants, the temperature and the reaction time.

The typical synthesis to obtain gold nanoparticles is the Turkevich method[11] that use citrate to reduce tetrachloroauric acid in water. This method is very common because is simple and reproducible obtaining a size of 20 nm. In 1973, this method was improved by Frens[12] obtaining a size between 16 and 150 nm changing the ratio between the reducing agents and the stabilizers.

Other common synthesis of gold nanoparticles is the Brust method[13] where gold nanoparticles of 1–3 nanometers are obtained using borohydride as a reducing agent and an alcanothiol as a stabilizer agent.

Recently, other method is used to obtain gold nanoparticles between 5 and 110 nm.[14] Such a method consist in two steps. In the first, the spherical gold seeds (5–20 nm, depending on the reducing agent/stabilizer agent ratio) are prepared and in the second, the growth of the seeds is performed (20–110 nm) reducing Au(III) with ascorbic acid on the surface of the seeds.

The syntheses of gold nanoparticles with a growth step are controlled by LaMer method[15]. This model explains that it is necessary a supersaturated solution of reagent to create the nucleus. The formation of these nucleus consumes reagent so the solution is no longer supersaturated and the formation of nucleus is not favored giving rise to the growth of the nucleus. Ostwald

[11] J. Turkevich; P. C. Stevenson; J. Hillier, *Discuss.Faraday Soc.* **1951**, 11, 55-75.
[12] G. Frens, *Nature* 1973, 241, 20-22.
[13] M. Brust; M. Walker; D. Bethell; D. J. Schiffrin; R. Whyman, *Chem. Commun.* **1994**, 801-802.
[14] T. K. Sau; A. Pal; N. R. Jana; Z. L. Wang; T. Pal, *J. Nanopart. Res.* **2001**, 3, 257-261.
[15] V. K. LaMer; R. H. Dinegar *J. Am. Chem. Soc.* **1950**, 72, 4847-4854.

ripening process explains that bigger particles grow at the expense of the small ones.

Besides the importance of gold nanoparticles, silver nanoparticles have a great interest and are very common in nanoscience and in nanotechnology. There are several ways to synthesize silver nanoparticles, the main one consist in the reduction of silver nitrate using borohydride as a reducing agent. Through this method it is possible to obtain silver nanoparticles with a size of 12 nm. These nanoparticles are yellow, transparent and dispersed.

Silver nanoparticles have unique optical and catalytic features. Besides, sometime they are used because of their antibacterial properties. However, the main disadvantage of the silver nanoparticles is that can be oxidized very easily.

Generally, silver nitrate is the reagent chosen to synthesize silver nanoparticles. In the several methods avaliable, the reducing agent, the ratio between amount and concentration of the reagents, the reaction time and the temperature obtaining different sizes of silver nanoparticles can be changed.[16]

1.2 Hollow nanostructures

Synthesis of nanocapsules has a great interest because of their many application in several fields. For example, catalysis[17],

[16] S. D. Solomon; M. Bahadory; A. V. Jeyarajasingam; S. A. Rutkowsky; C. Boritz, *J. Chem. Educ.* **2007**, 84, 322-325.
[17] X. Huang; C. Guo; J. Zuo; N. Zheng; G. D. Stucky, *Small* **2009**, 5, 361-365.

chromatography, nanomedicine[18], rechargeable batteries,[19] sensors[20] or antibacterial materials,[21] among others.

Modifying the chemical composition of this kind of structures (hollow nanostructures), it is possible to change its properties and its applications. This versatility allow the synthesis of capsules that respond to specific stimuli (pH, electromagnetic field, heat, etc.). In this way, it would be possible to achieve a high degree of spatiotemporal control over the release of their contents.

For this reason, one of the most interest applications in the field of the nanomedicine is drug delivery.[22]

There are a lot of ways to synthesize hollow nanostructures: spry-drying method[23], auto-assembly technique[24], polymerization with a sol-gel process[25], among others. Although the more common technique is the template method because allows synthesizing nanocapsules with homogenous layers. This method is based in four steps: 1) Template preparation. 2) Surface functionalization on the template to acquire the desired surface properties. 3) Template coating to protect and stabilize the structure. 4) Removal of the template obtaining a hollow structure.

---

[18] J.-F. Chen; H.-M. Ding; J.-X. Wang; L. Shao, *Biomaterials* **2004**, 25, 723-727.
[19] X. W. Lou; Y. Wang; C. Yuan; J. Y. Lee; L. A. Archer, *Adv. Mater.* **2006**, 18,2325-2329.
[20] M. Sanlés-Sobrido; W. Exner; L. Rodríguez-Lorenzo; B. Rodríguez-González; M. A. Correa-Duarte; R. A. Álvarez-Puebla; L. M. Liz-Marzán, *J. Am. Chem. Soc.* **2009**, *131*, 2699–2705.
[21] J.-X. Wang; L.-X. Wen; Z.-H. Wang; J.-F. Chen, *Mater. Chem. Phys*. **2006**, 96, 90-97.
[22] J. Kim; J. E. Lee; J. Lee; J. H. Yu; B. C. Kim; K. An; Y. Hwang; C.-H. Shin; J.-G. Park; J. Kim; T. Hyeon, *J. Am. Chem. Soc.* **2006**, 128, 688-689.
[23] Y. Lu; H. Fan; A. Stump; T. L. Ward; T. Rieker; C. J. Brinker, *Nature* **1999**, 398, 223–226.
[24] B. M. Discher; Y. Y. Won; D. S. Ege; J. C. M. Lee; F. S. Battes; D. E. Discher; D. A. Hammer, *Science* **1999**, 284, 1143–1146.
[25] I. Tissot; J. P. Reymond; F. Lefebvre; E. Bourgeat-lami, *Chem. Mater.* **2002**, 14, 1325–1331.

In this method there are two kind of templates[26]. The soft templates that are formed by organic materials such as liposomes[27], ionic liquids[28], monomers or solvents[29]. With these templates, it is not possible obtain a homogenous size and shape, being an important disadvantage.

The other kind of templates are the hard templates (as copper oxide[30], silica[31], carbon[32] or organic polymers). With these templates it is possible to obtain monodisperse nanocapsules, with the desired size and thickness.

In the final step, the template is removed to obtain a hollow structure by etching using a specific solvent or calcination at high temperatures.

1.3 Surface modification

Nanoparticles have a high surface/volume ratio. For this reason, surface modification is very important because allows to tune the properties of the nanoparticles since the surface properties determine the system properties.

Changing the properties, it is possible to provide new characteristics to the nanoparticles depending on their application.[33] To obtain this, Layer-by-layer (LbL) assembly

[26] W. Leng; M. Chen; S. Zhou; L. Wu, *Langmuir* **2010**, 26, 14271–14275.
[27] H. T. Schmidt; A. E. Ostafin, *Adv. Mater.* **2002**, 14, 532–535.
[28] T. Nakashima; N. Kimizuka, *J. Am. Chem. Soc.* **2003**, 125, 6386–6387.
[29] H. Wang; Y. Song; C. J. Medforth; J. A. Shelnutt, *J. Am. Chem. Soc.* **2006**, 128, 9284-9285.
[30] Z. Zhang; J. Sui; L. Zhang; M. Wan; Y. Wei; L. Yu, *Adv. Mater.* **2005**, 17, 2854–2857.
[31] P. M. Arnal; C. Weidenthaler; F. Scheuth, *Chem. Mater.* **2006**, 18, 2733–2739.
[32] M. Titirici; M. Antonietti; A. Thomas, *Chem. Mater.* **2006**, 18, 3808–3812.
[33] F. Caruso, *Chem. Soc. Rev.* **2007**, 36, 707-718.

technique is a simple method to modify the surface. Being possible to form several layers around the particle and even introduce new materials.

The first scientific who described an assembly by layers was Iler in 1966 publishing the formation of multilayer by adsorption of colloidal particles with positive and negative charge.[34] Although, it was Decher, in the 90s, who described the LBL technique[35].

Decher reported a substrate with a positive surface charge is immersed in a solution of a negatively charged polyelectrolyte. Then, a monolayer of this negative polyelectrolyte is adsorbed onto the substrate changing the surface charge. After that, the substrate is immersed in a solution of a positively polyelectrolyte obtaining a monolayer with a positive charge. In this way, it is possible to add several layers to acquire the surface charge desired.

The formation of these multilayers by LbL method does not depend on the shape of substrate. In 1998, Caruso et al. demonstrated that LBL method can be used in different shapes and sizes.[36,37]

Other advantage of this technique is that allows controling the thickness of the particles (with high precision, nanometric resolution) varying the material, the number of layers and the conditions used in the adsorption (temperature, ionic strength and solvent polarity).

The most common interaction between layers is that of electrostatic nature. Other kinds of interactions are hydrogen

[34] R. K. Iler, *J.Colloid Interface Sci.* **1966**, 21, 569-594.
[35] G. Decher, *Science* **1997**, 277, 1232-1237.
[36] F. Caruso, *Angew. Chem. Int. Ed.* **1998**, 37, 2201-2205.
[37] F. Caruso; R. A. Caruso; H. Möhwald, *Science* **1998**, 282, 1111-1114.

bond,[38] covalent bond,[39] DNA hybridization[40] and charge transfer.[41] In addition, it can be used specific kinds of reaction as click chemistry,[42] step-by-step reactions,[43] or electrochemical deposition[44] to acquire an interaction between layers.

1.3.1 Silica coating

As aforementioned, surface modification changes the nanoparticles properties. It is very common in the synthesis of nanoparticles modifying the properties with a silica coating. This coating can be prepared by the Stöber method[45] that consist in the hydrolysis and condensation of tetraethyl orthosilicate (TEOS) in a mixture of water, alcohol and ammonia. Reactions are shown in the figure 5.[46]

[38] W. B. Stockton; M. F. Rubner, *Macromolecules* **1997**, 30, 2717-2725.
[39] P. Kohli; G. J. Blanchard *Langmuir* **2000**, 16, 4655-4661.
[40] A. P. R. Johnston; H. Mitomo; E. S. Read; F. Caruso, *Langmuir* **2006**, 22, 3251-3258.
[41] Y. Shimazaki; M. Mitsuishi; S. Ito; M. Yamamoto, *Langmuir* **1997**,13, 1385-1387.
[42] G. K. Such; J. F. Quinn; A. Quinn; E. Tjipto; F. Caruso, *J .Am. Chem. Soc.* **2006**, 128, 9318-9319.
[43] H. Lee; L. J. Kepley; H. G. Hong; T. E. Mallouk, *J. Am. Chem. Soc.* **1988**, 110, 618-620.
[44] H. Wang; S. Ishihara; K. Ariga; Y. Yamauchi, *J. Am. Chem. Soc.* **2012**, 134, 10819-10821.
[45] W. Stöber; A. Fink; E. Bohn, *J. Colloid Interface Sci.* 1968, 26, 62-69.
[46] C. J. Wrinker, *J. Non-Cryst. Solids* **1988**, 100, 31-50.

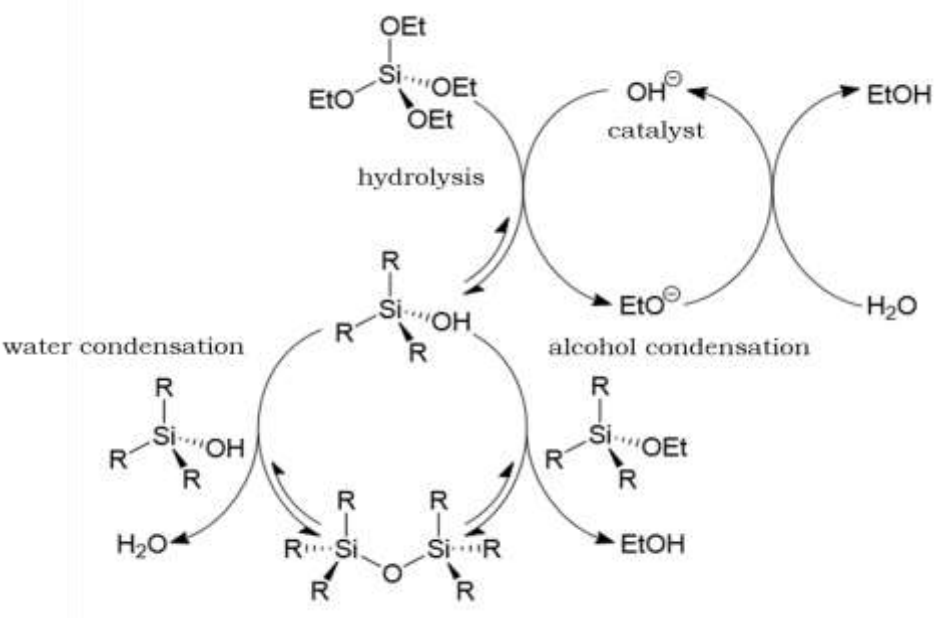

Figure 5. Chemical reactions that happen in the silica coating process.

From this method, several modifications have been performed. For example, adsorbing some polymers to the colloidal surface before the silica coating to facilitate the coupling of the silica.[47]

In the hydrolysis step, the alcoxysilane is replaced by a molecule of water that act as a nucleophile. Then, a condensation reaction occurs that consist in the union between two molecules of TEOS eliminating a molecule of water in the process.

Silica coating is a very common method due to their stability. But silica has more properties that make silica an ideal material. It is chemically inert, it is possible to control its porosity and it has optical transparency. Therefore, silica layers provide steric and electrostatic protection, and also act as dispersant agents providing a high stability. Also, silica coatings give the possibility to continue with the surface modification (it is easy functionalize

[47] C. Graf; D. L. J. Vossen; A. Imhof; A. van Blaaderen, *Langmuir* **2003**, 19, 6693-6700.

the silica surface) and provide biocompatibility allowing the use of these nanomaterials in bio-applications.

1.4 Optical properties

The optical properties of some materials are dominated by a phenomenon called Surface Plasmon Resonance. This phenomenon has more importance in metals as gold, silver and copper since the resonance frequency is in the visible region of the electromagnetic spectrum.

A plasmon is a collective oscillation of the conduction electrons in the metal surface. When an electromagnetic wave interacts with a metallic surface, the wave excites localize surface plasmon resonance (LSPR) on the surface, resulting in amplification of the nearby electromagnetic fields.

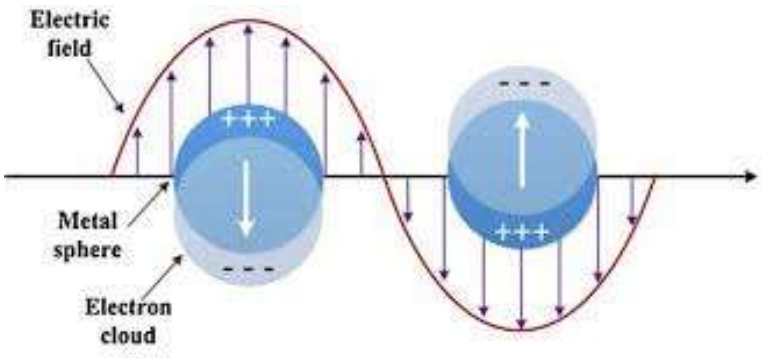

Figure 6. Scheme of the interaction between an electromagnetic radiation with a metal sphere.

The resonance frequency has a close relation with the size and shape of the nanoparticles. For this reason, it is very important to

predict theoretically the plasmonic resonance frequency in order to know the relation between the optical properties and the nanoparticles structure.

The simplest theory that can explain this relation is the Mie theory[48] that solves the Maxwell equations for the light interaction with spherical particles of small size. The problem of this theory is that only works for spherical particles, although some modification was performed in the Gans-Mie theory[49] to apply it in ellipsoidal particles.

Applying the Mie theory several simulations were performed to obtain the UV-visible spectra of different metallic spherical colloids, verifying that few metals have the plasmonic resonance in the visible range.[50]

1.5 Raman spectroscopy

A technique that is based on the optical properties is Raman spectroscopy. This was experimentally discovered by C. V. Raman[51] and K. S. Krishnan in India in 1928 and, at the same time and independently, in the Soviet Union by Leonid Mandelstam and Grigory Landsberg.[52]

When a beam of monochromatic light interacts with the matter, it can be refracted, reflected, absorbed or scattered. When the light is scattered, the phenomenon is known as scattering.

---

[48] G. Mie, *Ann. Phys.* **1908**, 25, 377-445.
[49] R. Gans, *Ann. Phys.* **1912**, 37, 881-900.
[50] J. A. Creighton; D. G. Eadon, *J. Chem. Soc.; Faraday Trans.* **1991**, 87, 3881-3992.
[51] C. V. Raman; K. S. Krishnan, *Nature* **1928**, 121, 501-502.
[52] G. Landsberg; L. Mandelstam, *Naturwissenschaften* **1928**, 16, 557.

When a collision is produced between a photon and a molecule, two effects can occur. If the collision is elastic, that is, the photon and the molecule maintain the same energy, the incident radiation has the same frequency that the dispersed radiation. This effect is called Rayleigh scattering.

However, the collision could be inelastic. In this case, the molecule gains or loses energy (rotational or vibrational) emitting a photon with more or less energy than the incident radiation. This effect is known as Raman Scattering.

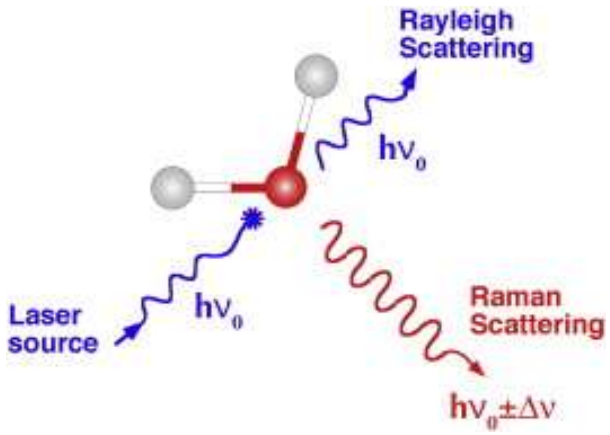

Figure 7. Scheme of the difference between Raman and Rayleigh Scattering.

The energy difference between the incident radiation frequency and the dispersed radiation frequency is called Raman shift. This difference in energy must correspond to the necessary energy to produce a transit between two energy levels of the molecule according to the principle of energy conservation.

If the energy of the molecule increases with the incident radiation, that is, the incident light gives part of his energy to the molecule, this implies that the dispersed radiation has less energy than the incident radiation. In this case, it is named Stokes Raman. In the opposite way, the effect is called Anti-Stokes Raman and consists in the energy decrease of the molecule due to the interaction with

the incident radiation, decreasing the energy of molecule to a lower energy level and giving energy to the photon. In this case, the dispersed radiation has more energy than the incident radiation.

If the transit is produced between rotation levels, Stokes and Anti-Stokes bands have a similar energy. However, if the transit is produced between vibrational levels, Anti-Stokes bands have a low intensity because few molecules can decrease their energy since most of them (at room temperature) are in the lower vibrational level.

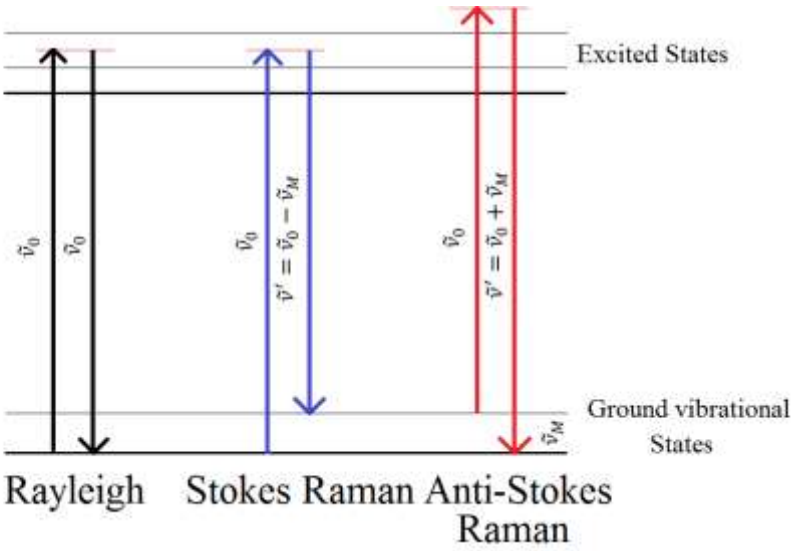

Figure 8. Diagram of the Rayleigh and Raman Scattering process.

The property responsible of the interaction mechanism between radiation and matter that provokes the Raman effect is the polarizability. If the polarizability changes during the rotation or vibration there will be Raman scattering.

Polarizability can be explained as the tendency of a molecule to displace the electrons cloud with respect to the nuclei creating a dipole.

When an incident electromagnetic field interacts with a molecule, an electric dipole is induced in the molecule, being the electric dipole equal to the electromagnetic field.

The Raman spectroscopy provides a lot of information about the chemical structure and composition of matter. For this reason, this technique is used in several fields such as food industry, petrochemical industry, biomedicine and environmental sciences.

1.6 Surface Enhanced Raman Spectroscopy (SERS)

However, the Raman effect is very weak. SERS is a technique to study the surfaces and consist in increasing the Raman dispersion in molecules adsorbed onto rough metal surfaces.

Spectroscopic effects are higher if they happen close enough to the surface and metallic nanostructures due to the coupling with the metallic surfaces.

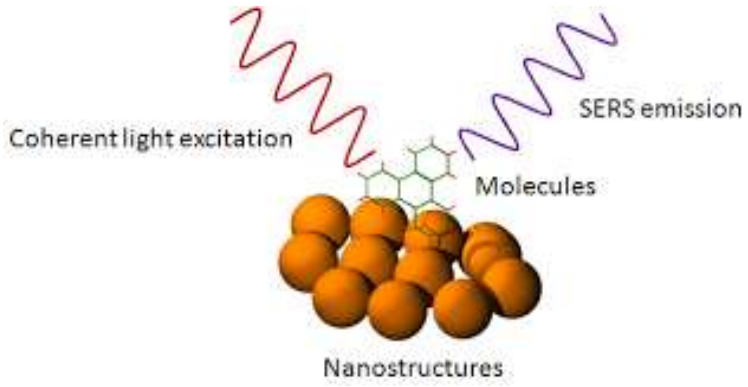

Figure 9. Scheme of SERS effect in molecule that is attached on a metallic surface.

Due to resonances between the optical field and the plasmon surfaces, the electromagnetic fieds are stronger. This allows a redistribution of the field intensities near the nanoparticles obtaining some areas where the Raman scattering is higher.

To obtain this enhancement in the Raman signal the best metallic nanoparticles are gold, silver and copper due to their surface plasmon resonance in the visible and infrared range.

Therefore, the surface plasmons of these metals are excited by laser light giving rise to an increase in the electromagnetic fields around the metal. Since the Raman intensities are proportional to the electromagnetic fields there is a very important increase in the Raman signal.

This signal is, basically, a vibrational spectrum that provides a lot of information about the chemical structure of the molecules adsorbed on the metallic surfaces. For this reason, Raman spectroscopy is considered an analytical technique with a good sensibility. Intensifying Raman signal can be until 10^{14}.[53]

This technique was discovered in 1974 by Fleischmann, Hendra and McQuillan.[54] They observed this phenomenon for first time in a pyridine electrochemical adsorbed to a rough silver electrode. But the great advance happened in 1977 when Jeanmaire and Van Duyne, and independently Albrecht and Creighton, analyzed that the silver electrode produced a Raman spectrum one million times more intense than the expected spectrum.[55][56]

This technique has a limitation due to it is restricted to noble metal substrates. For this reason, SERS is not more common in surface

[53] J. Kneipp; H. Kneipp; K. Kneipp, *Chem. Soc. Rev.* **2008**, 37, 1052–1060.
[54] M. Fleischman; P. J. Hendra; A. McQuillan, *J. Chem. Phys. Lett.* **1974**, *26*, 163-166.
[55] D. L. Jeanmair; R. P. Van Duyne, *J. Electroanal. Chem.* **1977**, *84*, 1.
[56] M. G. Albrecht; J. A. Creighton, *J. Am. Chem. Soc.* **1977**, *99*, 5215-5217.

science because SERS activity depends strongly on the metal nature and the rough of the surface.

The smoothness of the surface is not active for SERS. So, only the metals with rough surfaces at the nanoscale can improve the Raman signal.

Composition, shape, size and interstitial distance between particles of the metallic nanostructures are critical factors that affect the surface plasmon resonance.[57] Also, a condition to obtain the SERS enhancement is that the molecule is very close to the metallic surface. The molecule can be adsorbed spontaneously on the metallic surface by physisorption or chemisorption. In the case that the molecule and the metallic surface have not affinity, a surface modification to improve this affinity can be performed.

The molecules adsorbed on the first layer have the best improvement but the enhancement also happens to tens nanometers from the metallic surface.

So, the enhancement factor of the Raman signal in SERS depends on the:

- Laser wavelength
- Substrate nature
- Surface morphology, the nanometric roughness
- Distance and orientation of the molecule respect to the surface

This technique is very sensible and allows the detection of molecules. Also, it exists an improvement in the selectivity due to vibrational spectrum act as a fingerprints. For this reason, this method is very useful in bioanalytical areas because provides a

[57] S. L. Kleinman; R. R. Frontiera; A.-I. Henry; J. A. Dieringer; R. P. Van Duyne, *Phys. Chem. Chem. Phys.* **2013**, 15, 21-36.

high level of structural information and ultrasensible limits of detection.

Nowadays, it is well known that the enhancement of the Raman signal is due to two mechanisms:

- Electromagnetic mechanism (EM): radiation is extremely higher near the rough metallic surface.
- Chemical mechanism or transfer charge (TC): the cross-section of a molecule is intensified by the formation of a molecule-metal complex and the transfer charge between them.

Both mechanisms affect to the Raman improvement but the most important is the Electromagnetic mechanism based on the efficient coupling between the incident radiation and the surface plasmon resonance of the nanostructure. In this regard, it is considered that the SERS effect does not occur in the absence of the EM.

1.6.1 Electromagnetic mechanism (EM)

This enhancement depends on the nature of the metal and the morphology of the nanoparticle.

In the nature of the metal its dielectric constant has a great importance due to real part of this constant is associated with the scattering (the imaginary part is associated with absorption). For this reason, metals with a preferably large and negative real part (Au, Ag or Cu) are appropriate for SERS applications, being the real part larger in silver, thus providing a higher SERS signal.

According to EM, other factors influence in the SERS enhancement. Size and shape of nanoparticles, and distance and orientation of the molecule to the metal surface. Also, the interstitial space between nanoparticles where the so-called hot-

spots are located. In these hot-spots the electromagnetic field is higher due to the coupling between two or more nanoparticles with closely spaced features. This distance between nanoparticles is a few nanometers.

1.6.2 Transfer charge (TC)

As aforementioned, EM is the main responsible of the Raman enhancement and the SERS effect does not occur without this mechanism but also, there are other mechanisms that can explain why all the molecules do not show the same SERS effect.

This mechanism is called chemical mechanism or transfer charge and consists in the formation of a bond between the molecule and the metal surface. This makes possible the transfer charge (electrons or holes) from the metal surface to the molecule. This considerably increases the molecular polarizability of the molecule due to the interaction with the metal electrons.

The CT mechanism can occur from the HOMO orbital of the adsorbed molecule to the Fermi level of the metal or from the Fermi level of the metal to the LUMO orbital of the adsorbed molecule.

This mechanism is directly connected to the nature of the molecule and the metal. For example, molecules with pi electrons (such as molecules with a high aromatic character) in their structure transfer the charge to the metal more easily. Related to the metal, the nanoroughness is considered responsible in the process of charge transfer between the metal and the adsorbate.

1.7 SERS substrates

There are several ways to classify the materials used as SERS substrates. Following the classification performed by Wang, X. A. et al.[58], the SERS substrates will be separated in plasmonic nano-structures, design materials and hybrid materials.

1.7.1 Plasmonic nanostructures

The SERS enhancement obtained is highly dependent on the interaction between the adsorbed molecules and the plasmonic surface. Classic SERS substrates are gold, silver and copper because of their optical properties. These three metals have the Localized Surface Plasmon Resonance (LSPR) that cover most of the visible and near-infrared range where the Raman measurements are collected.

It was discovered that size and shape have a great influence in the electromagnetic field around the molecule and therefore a great influence in the SERS enhancement. For this reason, controlling the size and the shape of the metallic nanoparticles in the synthetic process has acquired a great importance.

Plasmonic nanoparticles

The process to obtain Au NPs and Ag NPs with spherical shape is simple, rapid and cost-effective. It was demonstrated that the diameter of these spherical nanoparticles have a great influence in the electromagnetic field.[59] Using the Natan's and Frens's methods the diameter of the Au NPs can be modified by changing

[58] X. A. Wang; X. Kong, *Materials* **2015**, 8, 3024-3052.
[59] A. C. Sant'Ana; T. C. R. Rocha; P. S. Santos; D. Zanchet; M. L. A. Temperini, *J. Raman Spectros*. **2009**, 40, 183-190.

the amount of added sodium citrate.[60,61] Ag NPs produce a higher enhancement factor than using similar AuNPs. Kneipp's group have obtained a great enhancement factor of 10^{14} measuring the Raman spectroscopy of a single molecule on the surface of Ag nanostructures.

Core-shell

The main problem of Au and Ag nanoparticles is their stability under ambient conditions. For example, oxidation in air or aggregation in saline solutions or in presence of high amount of salts. To avoid these problems Au and Ag nanoparticles can be coated with a shell forming a core-shell structure.[62,63,64] These structures are more stable and also allow incorporating new functionalities to the SERS substrate. For example, Nie's and Natan's group performing a silica coating in a core embedded with a molecule (with a good Raman signal) called as a SERS tag.[65,66] The core-shell structure Raman tags were successfully applied in biomolecule detection.

Plasmonic nanoparticle with different shapes

As previously mentioned, LSPs of metal materials are highly dependent on the morphology of the nanomaterials. There are many syntheses to obtain nanoparticles with different shape.[67]

---

[60] G. Frens, Controlled Nucleation for the Regulation of the Particle Size in Monodisperse Gold
Suspensions. *Nature* **1972**, 20–22.
[61] K. C. Grabar; R. G. Freeman; M. B. Hommer; M. J. Natan, *Anal. Chem.* **1995**, *67*, 735–743.
[62] L. M. Liz-Marzán; M. Giersing; P. Mulvaney, *Langmuir* **1996**, 12, 4329-4335.
[63] W. Wang; Z. Meng; Q. Zhang; X. Jia; K. Xi, *J. Colloid Interface Sci* **2014**, 418, 1-7.
[64] X. Kong; Q. Yu; X. Zhang; X. Du; H. Gong; H. Jiangb, *J. Mater. Chem.* **2012**, 22, 7767-7774.
[65] W. E. Doering; S. Ni, *Anal. Chem.* **2003**, *75*, 6171–6176.
[66] S. P. Mulvaney; M. D. Musick; C. D. Keating; M. J. Natan, *Langmuir* **2003**, *19*, 4784–4790.
[67] M. Shah; V. Badwaik; Y. Kherde; H. K. Waghwani; T. Modi; Z. P. Aguilar; H. Rodgers; W. Hamilton; T. Marutharaj; C. Webb; M. B. Lawrenz; R. Dakshinamurthy, *Front. Biosci.* **2014**, 19, 1320-1344.

Nanowires

The monolayers of nanowires exhibit a high performance for SERS due to the plasmon coupling between individual plasmonic nanowires that provide a good enhancement factor.[68,69]

Nanorods

This kind of structure has two plasmonic bands, the transverse band at lower wavelengths that corresponds to electron oscillations perpendicular to the long axis, and the longitudinal band in the longer wavelength position that corresponds to the electron oscillations along the long axis.[70]

Nanoprisms

Sharp edges or branches of metallic nanoparticles can concentrate the charge and cause greater electric fields than in spherical nanoparticles.[71]

The sharp features on nanoprisms with wavy edges are very active for SERS.

Nanocubes

The intensity of SERS signals on nanocubes with sharp edges were dependent on the polarization of the excitation laser.[72]

Nanostars

It is a very common substrate to obtain a very good enhancement factor due to the sharp tips where the electric field is so high. Also, the plasmon hybridization between tips and core provide an increase in the local electric field.[73]

---

[68] L. Vigderman; E. R. Zubarev, *Langmuir* **2012**, 28, 9034-9040.
[69] J. Song; Y. Huang; Y. Fan; Z. Zhao; W. Yu; B. A. Rasco; K. Lai, *Nanomaterials* **2016**, 6, 175/1-10.
[70] Y. Huang; S. Liao; M. Xiong; Y. Ma; J. Zhao; S. Zhaoa, *Analytical Methods* **2017**, 9, 786-791.
[71] S:-H. Ciou; Y.-W. Cao; H.-C. Huang; D.-Y. Su; C.-L. Huang, *J. Phys. Chem.* **2009**, 113, 9520-9525.
[72] J. M. McLellan; A. Siekkinen; J. Chen; Y. Xia, *Chem. Phys. Lett.* **2006**, 427, 122-126.
[73] L. Rodríguez-Lorenzo; R. A. Álvarez-Puebla; F. J. García-de-Abajo; L. M. Liz-Marzán, *J. Phys. Chem. C* **2010**, 114, 7336–7340

Nanosheets

Nanosheets assemblies are reproducible, highly sensitive and easily synthesized. The size and the density of these nanostructures can be easily modified in the synthesis process.

Plasmonic nanoparticles made of alloy metals

Also, can be combined with some metal forming bimetallic alloy nanoparticles to improve the SERS signal.[74]

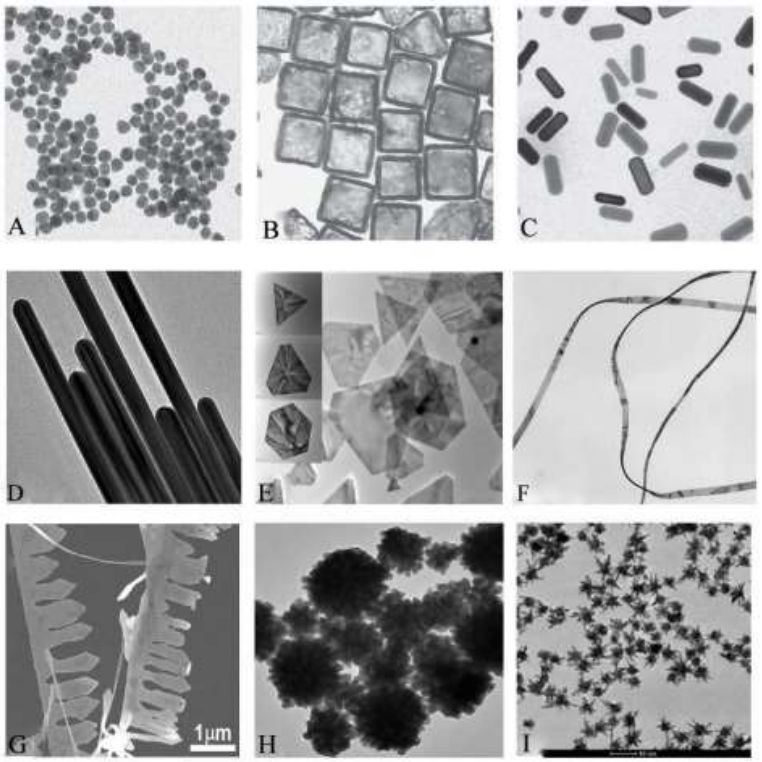

Figure 10. Gold Nanoparticles with different shapes. TEM images of: A) Nanospheres; B) Nanocages; C) Nanorods; D) Nanowires; E) Nanoplates; F) Nanobelts; G) Nanocombs; H) Nanoflowers; I) Nanostars. Image reproduced from reference 67.

[74] X. Dong; J. Zhou; X. Liu; D. Linb; L. Zha, *J. Raman Spectrosc.* **2014**, 45, 431-437.

1.7.2 Designed SERS substrates

In this section designed SERS substrates using bottom up and top down fabrication techniques will be shown. This kind of substrates try to obtain a higher sensitivity, tunability, robustness and reproducibility. To fabricate them, it has a great importance the advances in nanotechnology.

Nanosphere lithography[75] is an example where nano-triangles with sharp edges in their vertex can be synthesized. This technique is inexpensive and versatile. Nanosphere lithography can control the inter-spatial distance between nanoparticles that is a very important parameter in the electromagnetic enhancement mechanism.

On-wire lithography consists in introducing some unusual architectural changes to simple building blocks.[76] For nanowires, it is a powerful way of synthesize a segmented structure and then introduce architectural changes through the post-chemical treatment. Nanostructures with gaps as small as 2 nm and disks as about 20 nm can be created. This technique also allows to control the gap size between metal nanoparticles.

Other examples of designed SERS substrate are:

-Nanocapsules[77]

Plasmonic nanocapsules due to the confinement of metallic nanoparticles provide a large number of hot-spots.

---

[75] X. Zhao; J. Wen; M. Zhang; D. Wang; Y. Wang; L. Chen; Y. Zhang; J. Yang; Y. Du, *ACS Appl. Mater. Interfaces* **2017**, 9, 7710-7716.

[76] K. D. Osberg; M. Rycenga; N. Harris; A. L. Schmucker; M. R. Langille; G. C. Schatz; C. A. Mirkin, *Nanoletters* **2012**, 12, 3828-3832.

[77] M. Sanles-Sobrido, W. Exner, L. Rodríguez-Lorenzo, B. Rodríguez-Gonzalez, M. A. Correa-Duarte, R. A. Álvarez-Puebla, L. M. Liz-Marzán, *J. Am. Chem. Soc.* **2009**, 131, 2699 –2705.

-Electrical tweezers[78,79]

It is a nanomanipulation technique. Combined DC and AC electric fields can be controlled the transport and the alignment of the nanoparticles.

-Plasmonic nanoantennas by e-beam lithography[80]

Optical nanoantennas are devices that convert freely-propagating optical radiation into localized energy at nanometer scale.

-Nanogaps created by non-conventional methods[81]

To acquire smaller metallic nanogaps E-Beam Lithography was combined with electrochemical methods for the fine-tuning of gap dimensions.

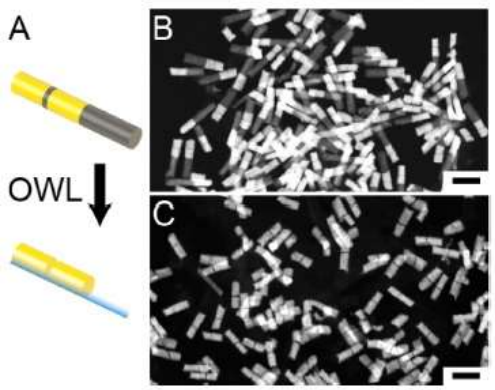

Figure 11. Example of designed SERS substrate. Preparation of gold nanorods dimers using the technique on-wire lithography (OWL). A) Scheme; B) STEM image of precursor Au-Ni nanorods; C) STEM image of resulting Au nanorod dimers. Image reproduced from reference 75.

[78] L. Lin; X. Peng; M. Wang; L. Scarabelli; Z. Mao; L. M. Liz-Marzán; M. F. Becker; Y. Zheng, *ACS Nano* **2016**, 10, 9659-9668.
[79] X. Xu; K. Kim; C. Liu; D. Fan, *Sensors* **2015**, 15, 10422-10451.
[80] C. David; N. Guillot; H. Shen; T. Toury; M. L. de la Chapelle, *Nanotechnology* **2010**, 21, 475501/1-6.
[81] T. Ding; L. O. Herrmann; B. de Nijs; F. Benz; J. J. Baumberg, *Small* **2015**, 11, 2139-2143.

1.7.3 Hybrid materials

The integration of nanoparticles into advanced materials to generate novel hybrid materials which may offer flexibility and functionality is a key in sensor engineering. Some examples are plasmonic NPs with photonic crystals[82] or dielectric gratings[83]; SERS substrates using bio-enabled materials; SERS sensing using optical fibers[84]; SERS sensing in micro-fluidics[85]; SERS substrates on graphene[86].

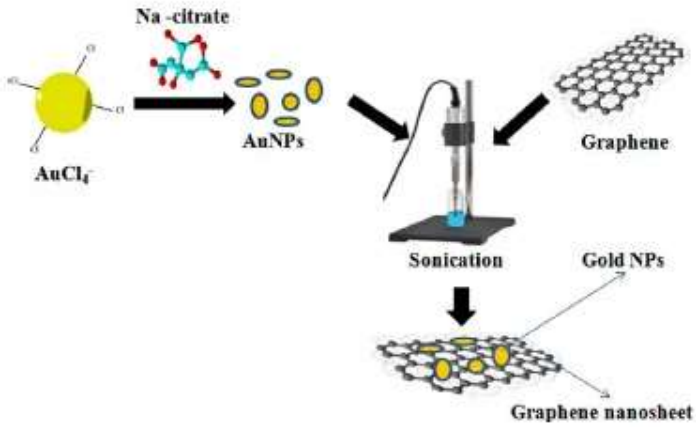

Figure 12. Example of hybrid materials as SERS substrate. In this case, gold nanoparticles on graphene. Image reproduced from reference 86.

[82] S. Lin; W. Zhu; Y. Jin; K. B. Crozier, *Nanoletters* **2013**, 13, 559-563.
[83] J. Li; D. Fattal; Z. Li, *Appl. Phys. Lett.* **2009**, 94, 263114.
[84] A. Foti; C. D'Andrea; F. Bonaccorso; M. Lanza; G. Calogero; E. Messina; O. Maria-Maragò; B. Fazio; P. G. Gucciardi, *Plasmonics* **2013**, 8, 13-23.
[85] O. Péron; E. Rinnert; F. Colas; M. Lehaitre; C. Compère, *Appl. Spectrosc.* **2010**, 64, 1086-1093.
[86] M. Manikandan; H. N. Abdelhamid; A. Talib; H. F. Wu, *Biosens. Bioelectron.* **2014**, 55, 180-186.

1.8 Emerging contaminants

In the last years, emerging contaminants,[87] have acquired great importance due to their bioaccumulation in environmental media because in very small concentrations are not so dangerous but in prolonged exposure can cause damages in the organisms.[88,89] This kind of pollutants are mainly pharmaceutical compounds that are consumed in high quantities worldwide, in the range of tons per year per pharmaceutical compound.[90]

Wastewater plants are not ready to remove completely this kind of compounds.[91,92,93] Only about half of the prescription drugs and other newly emerging contaminants are removed. For this reason, emerging contaminants can get into the aquatic environment where they are of particular concern given their global distribution, environmental persistency, bioaccumulation and potential harm that can cause adverse effects in human and aquatic species.

Some of the more common pharmaceutical drugs are:

Trimethoprim

Trimethoprim is an antibacterial medicine prescribed for treating infections, mainly chest or urine infections. Also, it is commonly

[87] S. Sauvé and M. Desrosiers, *Chemistry Central Journal* **2014**, 8, 15.
[88] M. F. Rahman, E. K. Yanful and S. Y. Jasim, *J. Water Health* **2009**, 7, 224.
[89] K. Kümmerer, *Chemosphere* **2009**, 75, 417.
[90] A. C. Johnson, V. Keller, E. Dumont and J. P. Sumpter, *Science of the Total Environment* **2015**, 511, 747.
[91] J. Margot, C. Kienle, A. Magnet, M. Weil, L. Rossi, L. F. de Alencastro, C. Abegglen, D. Thonney, N. Chèvre, M. Schärer and D.A. Barry, *Science of the Total Environment* **2013**, 461-462, 302.

[92] J. M. Choubert; S. M. Ruel; M. Esperanza; H. Budzinski; C. Miège; C. Lagarrigue; M. Coquery, *Water Sci. Technol.* **2011**, 63, 57-65.
[93] K. E. Murray, S. M. Thomas and A. A. Bodour, *Environmental pollution* **2010**, 158, 3462.

used in the veterinarian medicine in combination with the sulfonamides for prevention and treatment of respiratory or gastro-intestinal tract infections in cattle, swine and poultry.[94,95]

Trimethoprim is rapidly absorbed following oral administration. It exists in the blood as unbound, protein-bound and metabolized forms. Ten to twenty percent of trimethoprim is metabolized, primarily in the liver; the remaining is excreted unchanged in the urine.[96]

Diclofenac

Diclofenac is an anti-inflammatory agent to relieve pain. This medicine works by reducing the substances in the body that cause pain or inflammation and it is mainly used to treat pain or inflammation caused by arthritis or ankylosing spondylitis. Taking into account that 65% of the drug consumed is excreted in the urine without modification[97], it is one of the drugs most commonly detected in wastewater treatment plants.

Ethinylestradiol

Ethinylestradiol is an oral contraceptive.[98] It inhibits ovulation and changes in the endometrium. It is used to control the symptoms of menopause and in cases of female hypogonadism. It can also be used in treatment of inoperable prostate cancer and in the treatment of breast cancer in some cases of postmenopausal women.

---

[94] A. Iglesias, C. Nebot, J. M. Miranda, B. I. Vázquez and A. Cepeda, *Environ. Sci. Pollut. Res.* **2012**, 19, 3235.
[95] B. Kolar, L. Arnuš, B. Jeretin, A. Gutmaher, D. Drobne and M. K. Durjava, *Chemosphere* **2014**, 115, 75.
[96] J. O. Straub, *Antibiotics* **2013**, 2, 115.
[97] I. Forrez; M. Caballa; K. Verbeken; L. Vanhaecke; M. Schlüsener; T. Ternes; N. Boon and W. Verstraete, *Environ. Sci. Technol.* **2010,** 44, 3449–3454.
[98] R. Vallejo-Rodríguez; M. Murillo-Tovar; J. Navarro-Laboulais; E.León-Becerril; A. López-López, *J. Environ. Chem. Eng.* **2014**, 2, 316-322.

Ibuprofen

Ibuprofen is an anti-inflammatory and analgesic medicine One of the most widely used drugs for muscle pain and inflammatory disorders.[99]

Carbamezapine

Carbamezapine is an important antiepileptic and analgesic agent specific for trigeminal neuralgia. And it is widely used worldwide with a consumption of more than one thousand tons per year.[100]

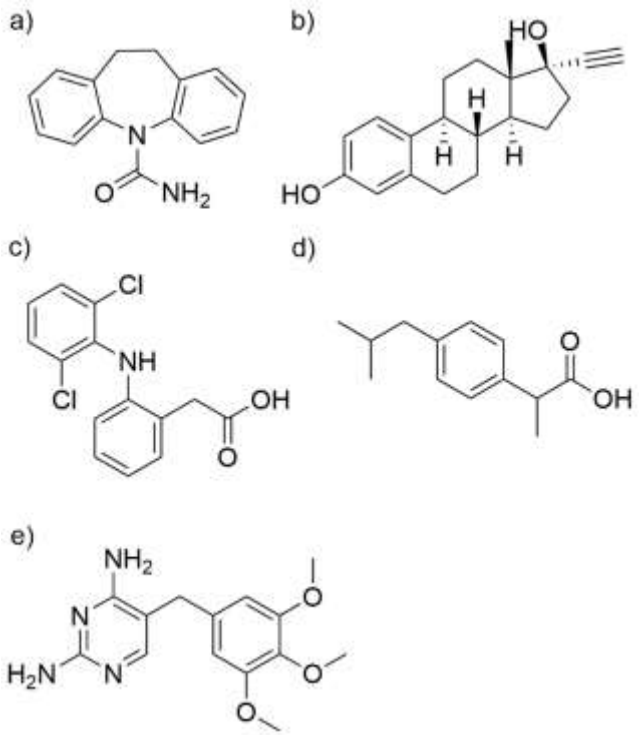

Figure 13. Emerging contaminants used in this work: a) Carbamacepine. b) Ethinylestradiol. c) Diclofenac. d) Ibuprofen. e) Trimethoprim.

[99] J. Siemens; G. Huschek; C. Siebe; M. Kaupenjohann, *Water Res.* **2008**, 42, 2124-2134.
[100] V. Calisto; M. R. M. Domingues; G. L. Erny; V. I. Esteves, *Water Res.* **2011**, 45, 1095-1114.

1.8.1 Effect of emerging contaminants

Many tons of drugs are produced per year and applied in human and veterinarian medicine. Due to this high application level, detectable concentrations of drugs may be expected in sewage. This has lead to an increasing concern about environmental risks than can be produced for this kind of compounds because although the concentration levels detected after the wastewater treatment process seem not toxic on human health the concern comes from the long exposition of aquatic organisms to this pharmaceuticals.

The emergence of resistance is a highly complex process that is not yet fully understood with respect to the interaction between bacteria populations and antibiotics. It is known that antibiotic at sub-inhibitory concentrations can have an impact on cell functions and change the genetic expression of virulence factors or the transfer of antibiotic resistance.

Approx. 70% of the consumed amount of antibiotics is excreted unchanged. Antibiotics are only partially removed in wastewater treatment plants, if they are not removed they reach the aquatic environment with potential adverse effects.[101]

Bacteria, fungi and microalgae are the organisms primarily affected by antibiotics. Fishes are also affected[102], changing the hormonal processes and affecting to their reproductive behavior.[103,104]

---

[101] K. Kümmerer; A. Henninger, *Clin. Microbiol. Infec.* **2003**, 9, 1203-1214.
[102] T. Vieira-Madureira; C. Cruzeiro; M. J. Rocha; E. Rocha, *Environ. Toxicol. Phar.* **2011**, 32, 212-217.
[103]K. Kümmerer, *Chemosphere* **2009**, 75, 417-434.
[104] N. Bolong; A. F. Ismail; M. R. Salim; T. Matsuura, *Desalination* **2009**, 239, 229-246.

Chapter 2

Plasmonic capsules for label-free detection of trimethoprim in wastewater

Emerging contaminants are an important concern in the environmental media, in particular, pharmaceutical compounds that are used worldwide. In this chapter, trimethoprim, a common antibacterial drug, was detected by SERS using plasmonic nanocapsules as a sensing platform. The identification of trimethoprim can potentially allow the in situ monitoring of the performance of water treatment plants.

2.1 Introduction

The occurrence of contaminants of emerging concern (CECs) - pharmaceuticals, illicit drugs and personal care products- in the environment has received considerable attention.[1] These CECs are ubiquitous in the aquatic environments, mainly derived from the discharge of municipal wastewater effluents. CECs are important because the risk they pose to human health and the environment is not yet fully understood.[2,3]

Pharmaceuticals represent an important group of CECs concern widely used in human and veterinary medicine.[4] They can enter the environment either as parent compounds or metabolites, conjugates or both. Pharmaceuticals have been found in wastewaters at levels of up to a few $\mu g \cdot L^{-1}$. Antibiotics, followed by steroid compounds, analgesics/nonsteroidal and anti-inflammatory drugs, are the most widely studied classes of pharmaceuticals.[5] There is a growing interest about their presence, persistence and fate in the environment because low levels of antibiotics can favor the proliferation of antibiotic resistant bacteria. The use of antibiotics in animal agriculture has been linked to the increased emergence of resistant strains of pathogenic bacteria that have potential to impact human health.[6] Therefore, pharmaceuticals have to be removed to protect water resources. However, the available water treatment technologies are time-consuming, expensive and ineffective to eliminate these CECs.[7,8,9] For instance, trimethoprim (TMP), an antibacterial

[1] S. Sauvé; M. Desrosiers, *Chem. Cent. J.* **2014**, 8, 15, 1-7.
[2] M. F. Rahman; E. K. Yanful; S. Y. Jasim, *J. Water Health* **2009**, 7, 224-243.
[3] K. Kümmerer, *Chemosphere* **2009**, 75, 417-434.
[4] A. C. Johnson; V. Keller; E. Dumont; J. P. Sumpter, *Sci. Total Environ.* **2015**, 511, 747-755.
[5] G. Yilmaz; Y. Kaya; I. Vergili; Z. B. Gönder; G. Özhan; B. Ozbek Celik; S. M. Altinkum; Y. Bagdatli; A. Boergers; J.Tuerk, *Environ. Monit. Asses.* **2017**, 189:55, 1-19.
[6] A. Van Epps; L. Blaney, *Curr. Pollution Rep.* **2016**, 2, 135-155.
[7] J. Margot; C. Kienle; A. Magnet; M. Weil; L. Rossi; L. F. de Alencastro; C. Abegglen; D. Thonney; N. Chèvre; M. Schärer; D.A. Barry, *Sci. Total Environ.* **2013**, 461-462, 302-316.
[8] J. M. Choubert; S. Martin-Ruel; M. Esperanza; H. Budzinki; C. Miège; C. Lagarrigue; M. Coquery, Water Sci. Technol. **2011**, 63, 57-65.
[9] K. E. Murray; S. M. Thomas; A. A. Bodour, *Environ. Pollut.* **2010**, 158, 3462-3471.

medicine prescribed for urine infections, presents high stability that difficults its removal from wastewater.[10,11,12] Thus, the development and implementation of novel water treatment technologies are mostly driven by three primary factors: the discovery and detection of CECs, the promulgation of new water quality standards (WQS), and cost.

The current methods -total organic carbon and chromatographic techniques associated to mass spectroscopy- for detection of antibiotic have limitations with respect to selectivity, speed, and technological restrictions. Nowadays, there is a growing interest about the potential use of surface-enhanced Raman scattering (SERS) for single and multiplex detection of organic contaminants in a range of environmental milieu.[13,14] SERS offers unique advantages as an analytical tool with a high selectivity and sensitivity without matrix interference. It can provide high throughput chemical information on particles with sizes down to the nanometric scale.[15,16] SERS is based on the enhancement of the Raman signal by several order of magnitude for molecules adsorbed on a plasmonic surface.[17] This enhancement is principally caused by the excitation of the collective oscillations of the conduction electrons in a metal nanostructure, the so-called localized surface plasmon resonance (LSPR).[18] Together with the recent outstanding advances in nanofabrication

[10] A. Jelic; M. Gros; A. Ginebreda; R. Céspedes-Sánchez; F. Ventura; M. Petrovic; D. Barceló, *Water Res.* **2011**, 45, 1165-1176.
[11] M. Gros; M. Petrović; A. Ginebreda; D. Barceló, *Environ. Int.* **2010**, 36, 15-26.
[12] E. Gracia-Lor; J. V. Sancho; R. Serrano; F. Hernández, *Chemosphere* **2012**, 87, 453-462.

[13] L. Rodríguez-Lorenzo; R. Álvarez-Puebla; I. Pastoriza-Santos; S. Mazzucco; O. Stéphan; M. Kociak; L. M. Liz-Marzán; F. J. García de Abajo, *J.Am. Chem. Soc.* **2009**, 131, 4616-4618.
[14] X. Ding; L. Kong; J. Wang; F. Fang; D. Li; J. Liu, *ACS Appl. Mater. Interfaces* **2013**, 5, 7072-7078.
[15] J. Kneipp; H. Kneipp; K. Kneipp, *Chem. Soc. Rev.* **2008**, 37, 1052-1060.
[16] P. L. Stiles; J. A. Dieringer; N. C. Shah; R. P. Van Duyne, *Annu. Rev. Anal. Chem.* **2008**, 1, 601-626.
[17] L. Gutierrez-Rivera; R. F. Peters; S. K. Dew; M. Stepanova, *J. Vac. Sci. Technol. B* **2013**, 31, 06F901.
[18] K. Kneipp, *Physics Today* **2007**, 60, 40-46.

techniques,[19,20,21,22] SERS substrates with optimized, uniform and reproducible response can be designed, which allows the successful translation of the great analytical potential of SERS to reliable, widely accepted and commercially viable sensing applications, addressing several limitations posed by conventional analytical techniques.

Therefore, the advancement of SERS as well in nanofabrication has remarkably improved the detection and quantification of organic pollutants in aquatic environmental samples.

In line with this, we show here the design and fabrication of a SERS-based sensing platform based on silica capsules containing gold nanoparticles. This platform offers not only reproducible SERS signal and ultradetection of TMP, but also a very high specificity avoiding any interference from the aquatic matrix.

This SERS-based sensing platform is expected to allow the detection and monitoring the presence of CECs in urban wastewater using TMP as WQS, which may help to optimize water treatment plants. TMP was selected as excellent candidate to be used as WQS because is one of the most relevant antibiotic since it is commonly used in human and veterinarian medicine worldwide.[23,24] In this regard, ninety per cent is excreted unchanged to wastewaters.[25]

---

[19] X. Zhao; J. Wen; M. Zhang; D. Wang; Y. Wang; L. Chen; Y. Zhang; J. Yang; Y. Du, *ACS Appl. Mater. Interfaces* **2017**, 9, 7710-7716.

[20] K. D. Osberg; M. Rycenga; N. Harris; A. L. Schmucker; M. R. Langille; G. C. Schatz; C. A. Mirkin, *Nanoletters* **2013**, 13, 559-563.

[21] L. Lin; X. Peng; M. Wang; L. Scarabelli; Z. Mao; L. M. Liz-Marzán; M. F. Becker; Y. Zheng, *ACS Nano* **2016**, 10, 9659-9668.

[22] C. David; N. Guillot; H. Shen; T. Toury; M. L. de la Chapelle, *Nanotechnology* **2010**, 21, 475501/1.

[23] A. Iglesias; C. Nebot; B. I. Vázquez; J. M. Miranda; C. M. Franco-Abuín; A. Cepeda, *Environ. Sci. Pollut. Res.* **2014**, 21, 2367-2377.

[24] B. Halling-Sørensen; H. C. Holten-Lützhøft; H. R. Andersen; F. Ingerslev, *J. Antimicrob. Chemother.* **2000**, 46, 53-58.

[25] J. O. Straub, *Antibiotics* **2013**, 2, 115-162.

2.2 Experimental section

2.2.1 Sample collection

Pharmaceuticals selected here were Trimethoprim (TMP) as WQS and two non-steroidal anti-inflammatory drugs, ibuprofen (Ibu) and diclofenac (DCF), one steroid hormone, ethinylestradiol (EE2), and one anticonvulsive drug, carbamazepine (CBZ), as possible interferences in wastewater. All these pharmaceuticals were supplied by Sigma-Aldrich.

Ultrapure water was provided by a Milli-Q system (18.2 mΩ·cm, resistivity) and the wastewater samples (1000 mL) were collected 3 times per season from return sludge containers. The samples were stored in plastic bottles at room temperature until analysis. The compounds were previously dissolved in ethanol (1.0×10^{-2} M) with subsequent dissolutions in ultrapure water or wastewater in a desired concentrations.

2.2.2 Fabrication of plasmonic silica capsules

Polystyrene beads functionalization

Plasmonic hollow mesocapsules were synthesized by a templating procedure described previously in our group with slight modifications.[26] Briefly, surface functionalization of polystyrene (PS, 530 nm; Ikerlat Polymers) beads was carried out by a layer-by-layer assembly method[27,28] using positively charge poly(allylamine hydrochloride) (PAH Mw=17500; Sigma-Aldrich) and negatively

[26] C. Vázquez-Vázquez; B. Vaz; V. Giannini; M. Pérez-Lorenzo; R. A. Álvarez-Puebla; M. A. Correa-Duarte, *J. Am. Chem. Soc.* **2013**, 135, 13616-13619.
[27] E. Donath; G. B. Sukhorukov; F. Caruso; S. A. Davis; H. Möhwald, *Angew. Chem. Int. Ed.* **1998**, 37, 2201-2205.
[28] H. Ejima; J. J. Richardson; K. Liang; J. P. Best; M. P. van Koeverden; G. K. Such; J. Cui; F. Caruso, *Science* **1998**, 282, 1111-1114.

charged poly(sodium styrene sulfonate) (PSS Mw= 70000; Sigma-Aldrich), until an external and uniform positive surface is obtained.

Synthesis and adsorption of the gold seeds

AuNPs (3 nm [Au]= 10^{-4}M) were produced as described Duff et al.[29] and subsequently adsorbed on functionalized PS beads. In this case, 6 mL of 3 nm AuNPs were added to 50 mL positively charged PS beads (0.25 mg/mL) under sonication. The suspension was then centrifuged to remove the excess of 3 nm AuNPs (3500 rpm, 20 min) and redispersed in ultrapure water (18.2 MΩ cm). The final concentration was 1.25 mg/mL.

Mesoporous silica coating and capsule preparation

Mesoporous silica coating was carried out following the method described by Yonghui Deng et al.[30] Briefly, 3nm AuNPs-coated PS particles (PS@Au seed) were added dropwise and under sonication to a solution containing 312.5 mg of cetyl trimethylammonium bromide (CTAB; Sigma-Aldrich), 100 mL of ultrapure water, 50 mL of ethanol (Sigma-Aldrich) and 1.5 mL of an ammonia aqueous solution (28 wt %, Sigma-Aldrich). After 20 min, 1.88 mL of a 5% (v/v) tetraethoxysilane (TEOS; Sigma-Aldrich) ethanolic solution was added dropwise under sonication for 5 min. Then, the mixture was stirred for 18 h to obtain a homogenous silica growth. The silica-coated PS@Au particles were washed by three centrifugation (3500 rpm, 20 min)-redispersion (ethanol) cycles. The organic templates, PS and CTAB, were removed by calcination at 550 °C for 6 h, obtaining the Au-containing silica capsule (Au@SiO_2).

[29] D.G.Duff; A. Baiker, *Langmuir* **1993**, 9, 2301-2309.
[30] Y. Deng; D. Qi; C. Deng; X. Zhang; D. Zhao, *J. Am. Chem. Soc.* **2008**, 130, 28-29.

Confined growth of gold nanoparticles

AuNPs in the inner of the capsule were grown *via* Au^+ reduction with formaldehyde.[31] Briefly, the Au^+ solution was obtained mixing 474.4 µL of 0.11 M $HAuCl_4 \cdot 3H_2O$ (Sigma-Aldrich) and 120 mL of 1.80 mM K_2CO_3 (Sigma-Aldrich) for 1 h. Then, 5 mL of this Au^+ solution and 30 µL of formaldehyde solution (37 wt%; Sigma-Aldrich) were added to 2 mL of a $Au@SiO_2$ suspension (1.25 mg/mL) under vigorous stirring. After 10 min, the color changed from pink to purple-blue (Au(Growth 1)@SiO_2). The sample was centrifuged and washed with ethanol (4500 rpm, 15 min). All these steps were repeated to obtain a second growth (Au(Growth 2)@SiO_2).

2.2.3 SERS Measurements

Enhanced optical properties in average SERS were collected with a Renishaw InVia Raman system equipped with high resolution grating (visible: 1800 or NIR: 1200 g mm^{-1}) with additional band-pass filter optics, a confocal microscope and a 2D-CCD detector. Samples were excited with two different laser lines at 633 (He-Ne) and 785 nm (diode). The power at the sample was set at 65 mW, with accumulation time of 10 s. The laser beam was focused inside of cuvette with 1 mm optical path length, which contains the capsules in suspension. The latter ensure the reproducibility by recording the average SERS signal coming from the capsules that cross the laser beam during the measurement.

The SERS optical activity of the prepared plasmonic capsules was tested with 4-aminothiophenol (4-ATP; Sigma-Aldrich), a well-known SERS probe. Samples were prepared by mixing 200 µL of a 4-ATP solution (10 µM) with 200 µL of capsules (1 mg/mL). After

[31] M. Sanles-Sobrido; W. Exner; L. Rodríguez-Lorenzo; B. Rodríguez-González; M. A. Correa-Duarte; R. A. Álvarez-Puebla; L. M. Liz-Marzán, *J. Am. Chem. Soc.* **2009**, 131, 2699-2705.

24 h in a rotary shaker, samples were centrifugated and redispersed in 200 µL of ultrapure water.

For TMP detection, samples were prepared by mixing 200 µL of plasmonic nanocapsules (1 mg/mL) with 200 µL of TMP at different concentrations (either in ultrapure water or wastewater) for 24h in a rotary shaker. The samples were then centrifuged at 4500 rpm for 15 min and redispersed in ultrapure water or wastewater. SERS spectra were collected in liquid with a NIR (785 nm) laser line.

2.2.4 Statistical analysis

The linearity of the SERS method was assessed by analyzing the calibration standards in three replicates. Average integral of 1652 cm^{-1} band area was plotted against respective concentration level and subjected to least square linear regression. The sensitivity of the method was given by the slope of the linear regression. The limit of detection (LOD) and limit of quantification (LOQ) were calculated as following: LOD = $3\sigma \cdot a^{-1}$ and LOQ = $10\sigma \cdot a^{-1}$, where σ is the noise of SERS measurements and 'a' is the slope of the fitted curve.[32] Precision of the method was estimated *via* three replicates of TMP samples prepared at different concentration in wastewater. The results of precision were expressed as coefficients of variation (% CVs = (SD/mean)·100). The matrix effect (loss or gain of SERS signal) was expressed as matrix factor (%ME = $((TMP_{signal\ in\ the\ presence}/TMP_{signal\ in\ the\ absence})-1)\cdot 100$). SERS signal of TMP at three different concentrations was acquired in the presence and absence of other pharmaceuticals. % ME < ±15 % are acceptable.

[32] Analytical Methods Committee, *Analyst* **1987**, 112, 199-204.

2.3 Results and discussion

We selected gold nanoparticles (AuNPs) confined inside silica nanocapsules as SERS active substrates to detect TMP, which have already shown a wide applicability as nanoreactors,[26] catalysts,[33] drug carriers,[34] and sensors.[35] A sketch representing the fabrication of a plasmonic capsule is shown in Figure 1a. First, the PS bead is coated with 3 nm AuNPs and subsequently coated with silica, generating a structure with a size of 530 nm in diameter. Then, the PS is removed by calcination. In this step, AuNPs grow due to the high temperatures. Finally, we carried out the Au growth (Figure 1b): from 12 (Au@SiO_2) to 19 (Au (Growth 1)@SiO_2) and 25 nm (Au (Growth 2)@SiO_2) (size histograms are shown in Figure 2). We also prepared Au Grown assemblies-coated PS beads (PS@Au-Grown) to compare the sensing capabilities of these nanostructures with those of their hollow counterparts (the plasmonic capsules) (Figure 1b).

[33] A. Sousa-Castillo; M. Gauthier; R. Arenal; M. Pérez-Lorenzo; M. A. Correa-Duarte, *Nanoscale* **2015**, 7, 20584-20592.
[34] R. Otero-Lorenzo; A. B. Dávila-Ibáñez; M. Comesaña-Hermo; M. A. Correa-Duarte; Verónica Salgueiriño, *J. Mater. Chem. B* **2014**, 2, 2645-2653.
[35] P. Rivera-Gil; C. Vázquez-Vázquez; V. Giannini; M. P. Callao; W. J. Parak; M. A. Correa-Duarte; R. A. Álvarez-Puebla, *Angew. Chem. Int. Ed.* **2013**, 52, 13694-13698.

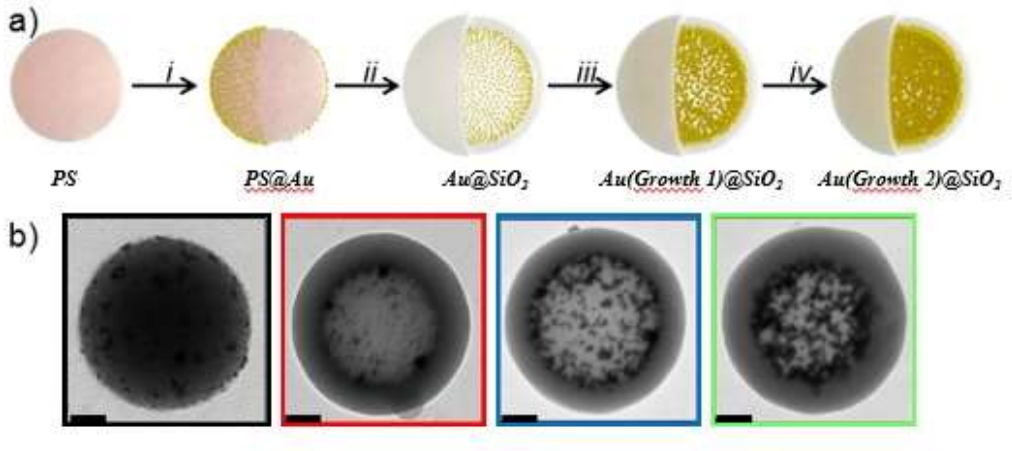

Figure 1. . a) Schematic illustration of the plasmonic capsules fabrication: i. polyelectrolyte coating through LbL method and 3 nm AuNPs adsorption on 530 nm PS beads via electrostatic interaction. ii. Silica coating and calcination at 550 °C. iii. and iv. Consecutive gold growth on the AuNPs confined inside the silica capsule via Au^{+} reduction with formaldehyde. b) Representative TEM micrographs (scale bars: 100 nm) of capsules studied here: PS@Au (black), Au@SiO_2 (red), Au(Growth 1)@SiO_2 (blue) and Au(Growth 2)@SiO_2 (green).

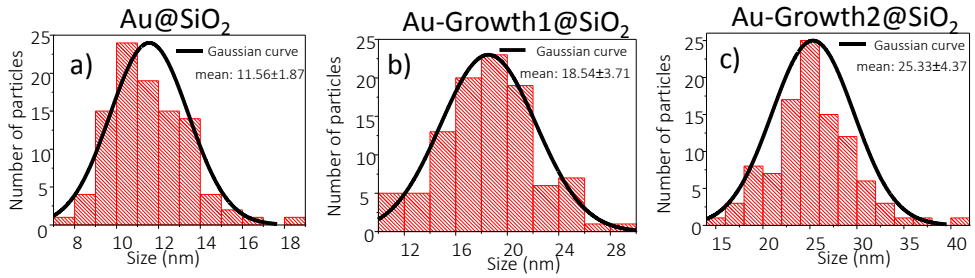

Figure 2. Histograms with statistical distribution of gold nanoparticles diameters in the different steps of the synthesis of nanocapsules with the average in nanometers.

The optical properties of the plasmonic capsules were characterized by UV-vis-NIR spectroscopy (Figure 3a). Au@SiO_2, generated a well-defined LSPR band centered at 532 nm and therefore AuNPs did not interact each other as shown by TEM (figure 1b, red). In contrast, LSPR band became broad and red-shifted by growing gold extensively increasing the density of

AuNPs and assemblies inside the hollow capsules (Figure 1b, blue and green). Consistently, the UV-vis-NIR spectra of Au(Growth 1)@SiO_2 and Au(Growth 2)@SiO_2 show a broad band with the maximum centered at 549 nm and 562 nm respectively, typical of highly interacting plasmonic aggregates, as previously reported by Sanles-Sobrido et al.[31] The increase of AuNPs aggregation inside the capsule generates thus a very high density of hot spots, which were expected to result in the generation of huge electromagnetic fields capable of enhancing the Raman signal accordingly.

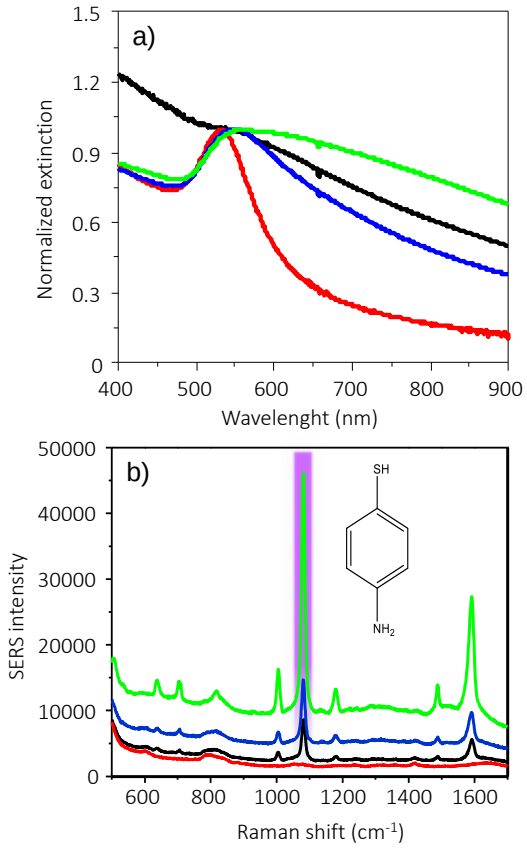

Figure 3. a) Vis-NIR spectra of plasmonic nanocapsules before and after consecutive gold growth: Au@SiO_2 (red), Au(Growth 1)@SiO_2 (blue) and Au(Growth 2)@SiO_2 (green). The black spectrum corresponds to a gold growth on PS bead which acts as a control. The arrow indicates the wavelength of the excitation laser (785 nm) for SERS measurements. b) SERS spectra of 4-ATP into plasmonic capsules and PS@Au upon excitation with a 785 nm laser line.

To prove this latter statement, the optical-enhancing activity in suspension of the plasmonic capsule set was tested using 4-aminothiophenol (4-ATP), a well-known Raman probe,[36,37] and two laser excitation lines ranging from the visible (633 nm) to the near infrared (NIR) (785 nm). The strongest SERS signals were acquired upon excitation with a 785 nm laser line using Au(Growth 2)@SiO_2 (Figure 4).

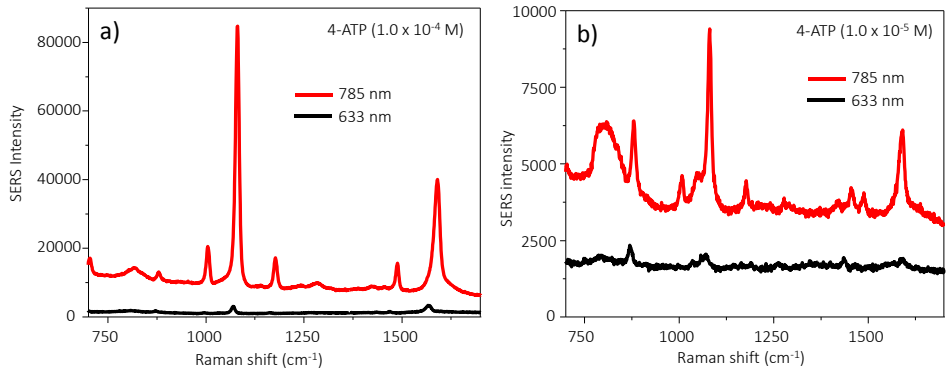

Figure 4. SERS spectra of the 4-ATP in the Au(Growth 2)@SiO_2 nanocapsules comparing the 633 nm and 785 nm lasers.

4-ATP diffuses through the mesoporous silica shell and attaches on the gold surface *via* S-Au bond. The vibrational pattern of 4-ATP was thus clearly identified for all capsule set, except for Au@SiO_2 (Figure 3b): 1003 cm^{-1} (CH bending), 1077 cm^{-1} (CC stretching and CS stretching), 1175 cm^{-1} (CH bending) and 1588 cm^{-1} (CC stretching). The absence of SERS signals in the Au@SiO_2 nanostructure is consistent with the absence of Au assemblies, as shown by TEM and UV-vis spectroscopy (Figure 1b red and 3a). Comparing the enhancement of the Raman signal obtained for the rest of the capsule, the highest enhancement was given by the Au(Growth 2)@SiO_2: 5.8-fold than that found for PS@Au and 3.8-

[36] S. Tian; Q. Zhou; C. Li; Z. Gu; J. R. Lombardi; J. Zheng, *J. Phys. Chem. C* **2013**, 117, 556-563.
[37] Q. Zhang; N. Large; P. Nordlander; H. Wang, *J. Phys. Chem. Lett.* **2014**, 5, 370-374.

fold than that observed for the Au(Growth 1)@SiO_2. Such a SERS intensity difference is mainly ascribed to the formation of hot spots into the capsule, as well as the better coupling between the LSPR and the excitation laser line.[38] Notably, the generation of a highly hot spot density was more efficient inside the capsule comparing with the PS@Au-Grown nanostructure. This can be attributed to the "confinement effect" since the capsule has a finite volume where the gold ions can accumulate, increasing the local concentration and improving the gold growth on the Au seed.

Given its higher SERS enhancement, Au (Growth 2)@SiO_2 was selected as the optimal SERS platform for direct detection of TMP in wastewater. First, the Raman spectrum of TMP powder under excitation with the 785 laser line was acquired (Figure 5). The spectrum is dominated by pyrimidine ring breathing (very strong (vs), 784 cm^{-1}), COC bending (medium (m); 378 cm^{-1}), benzene coupled to pyrimidine bending (m, 585 cm^{-1}), COC stretching coupled to pyrimidine ring stretching (m, 773 cm^{-1}), benzene ring stretching coupled to CO stretching (m, 1327 cm^{-1}), CH wagging coupled to NH rocking (m, 1357 cm^{-1}) and benzene ring stretching (m, 1603 cm^{-1}).[39] This Raman fingerprint corresponds to Form I of TMP, which is the most stable polymorphism that can present TMP molecule.[40]

[38] S. L. Kleinman; R. R. Frontiera; A.-I. Henry; J. A. Dieringer; R. P. Van Duyne, *Phys. Chem. Chem. Phys.* **2013**, 15, 21-36.

[39] A. Ungurean; N. Leopold; L. David; V. Chis, *Spectrochim. Acta A: Mol. Biomol. Spectrosc.* **2013**, 102, 52-58.

[40] D. Maddileti; B. Swapna; A. Nangia, *Cryst. Growth Des.* **2015**, 15, 1745-1756.

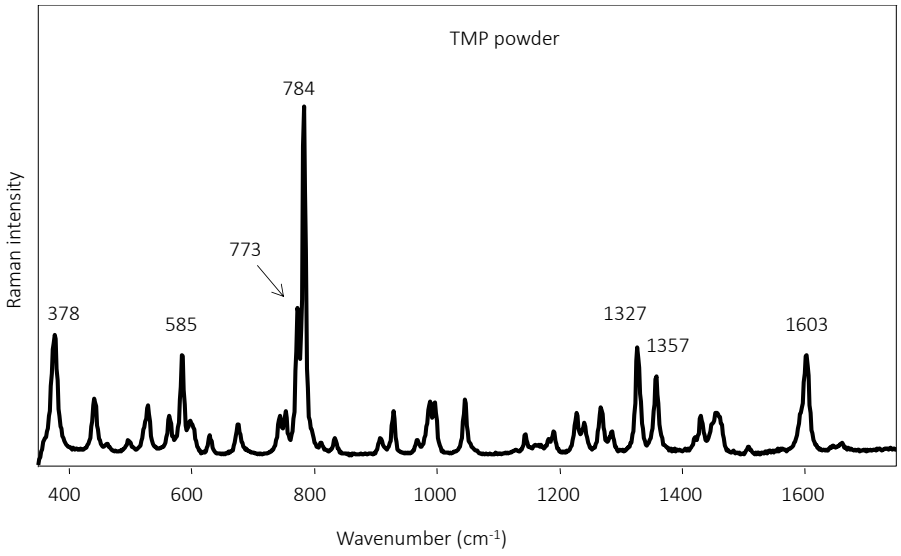

Figure 5. Raman spectrum of 4-ATP in powder under excitation with a 785 nm laser line.

Figure 6 shows the SERS spectrum of TMP on Au (Growth 2)@SiO_2. As usual, the SERS spectrum fits with the Raman spectrum but the relative band intensities are different, dominated in SERS by pyrimidine ring stretching coupled to NH bending (vs, 1653 cm^{-1}) benzene ring stretching coupled to CO stretching (s, 1321 cm^{-1}), benzene ring bending (m, 685 cm^{-1}), COC coupled to benzene ring stretching (m, 788 cm^{-1}), CO stretching (m, 1031 and 1226 cm^{-1}) and pyrimidine ring stretching (m, 1377 cm^{-1}). Interestingly, the SERS spectrum acquired here shows discrepancies with respect to those previously reported. Ungurean et al.,[39] showed the SERS spectrum of TMP on silver colloids in which the predominant band was at 777 cm^{-1}, pyridine ring breathing. This suggests a perpendicular and parallel orientation of the pyrimidine ring and benzene ring, respectively, with respect to the surfaces of the colloidal particles. However, TMP affinity for gold surfaces is likely based on π system interactions, which are weaker than amine-Ag

interaction.[41,42] Therefore, the orientation of TMP with respect to the gold surface is probably different, producing differences in both the relative band intensity and Raman shift position. As the goal here is the robust and reproducible TMP detection by SERS, the study in detail of TMP orientation on gold surfaces will be done in the future.

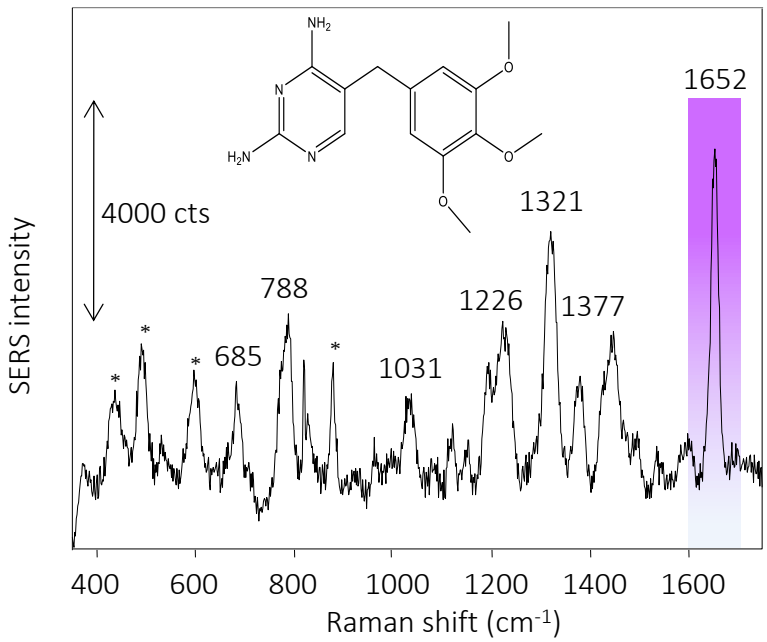

*Figure 6. SERS spectrum of TMP into Au (Growth 2)@SiO_2 capsules in wastewater upon excitation with a 785 nm laser line. The baseline was performed using software Wire 7.0. * indicates the bands corresponding to impurities from the synthetic procedure of the plasmonic capsules (details in the SI). Nevertheless, these bands do not interfere in the TMP recognition.*

[41] I. Izquierdo-Lorenzo; I. Alda; S. Sánchez-Cortés; J. V. García-Ramos, *Langmuir* **2012**, 28, 8891-8901.
[42] K. Mukherjee; S. Sánchez-Cortés; J.V. García-Ramos, *Vib. Spectrosc.* **2001**, 25, 91-99.

Looking for a reproducible, robust and selective method to establish TMP as WQS, the SERS spectra in independent samples was acquired, obtaining the same fingerprint in all cases (Figure 7).

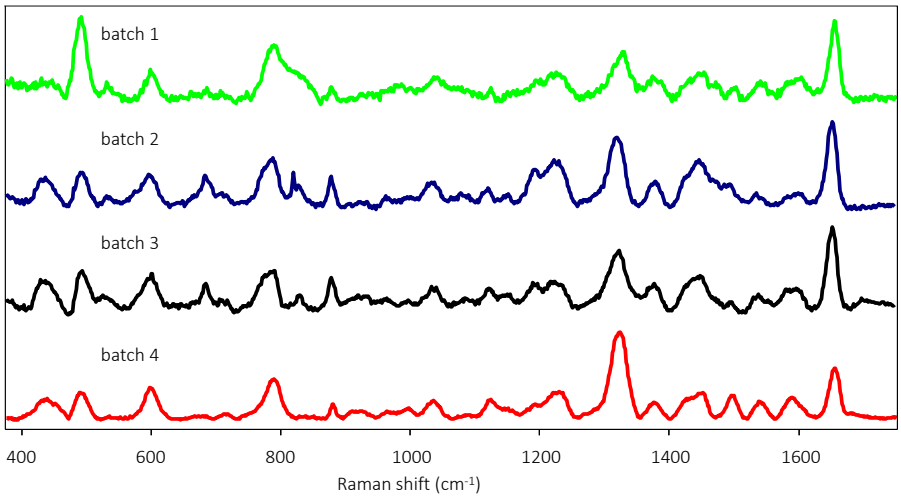

Figure 7. SERS spectrum of 4-ATP in solution under excitation with a 785 nm laser line. Each spectrum corresponds to a different batch of plasmonic capsules obtaining the same fingerprinter in all cases.

This demonstrates the efficiency of our platform due to its configuration: gold assemblies confined into the capsule. Thus, the density of hot spot does not change in the measurement, ensuring the reproducibility of the method. Next, the SERS signal of TMP was evaluated at a concentration range from 10^{-4} to 10^{-7} M. Figure 8 shows the spectral evolution centered around1652 cm^{-1}.

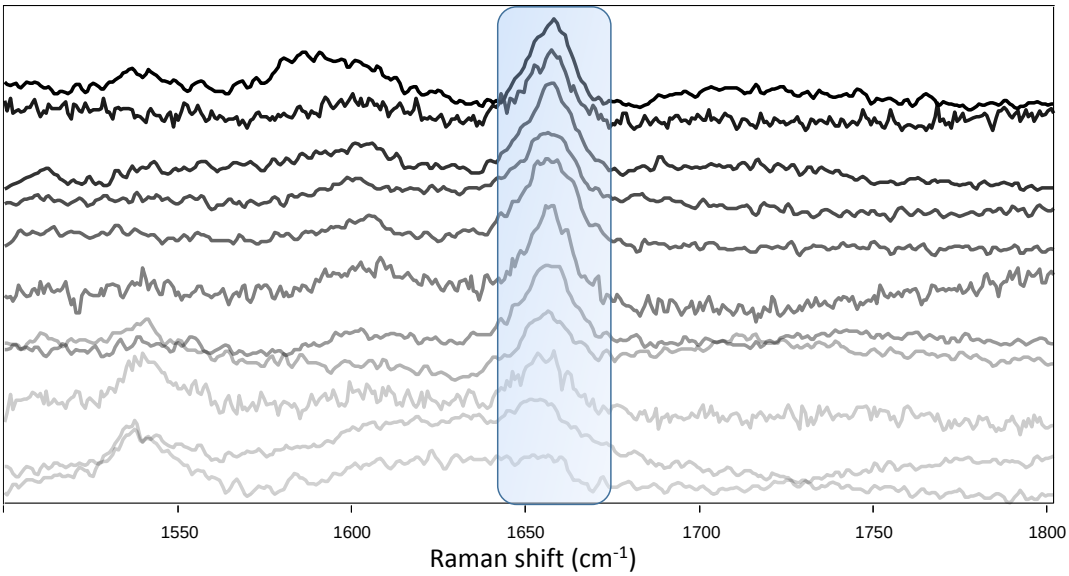

Figure 8. SERS spectra of TMP centered at 1652cm^{-1} recorded at different concentrations (from 6.0 x 10^{-5} to 2.0 x 10^{-7} M). Excitation with a 785 nm laser line.

As expected, SERS intensity was concentration-dependent and the profile of the peak became broad with the decrease of TMP concentration. This latter feature can be related to the loss of ensemble average, due to this low concentration.[43] The plot of the area under the band at 1652 cm^{-1} versus molar concentration of TMP (range 10^{-6} – 10^{-7} M) in wastewater gives rise to a linear correlation as shown Figure 9, with a remarkable r^2 =0.9882. Moreover, the sensitivity of the method was not affected by measuring the sample in wastewater because the slope of the calibration line presented a similarvalue than in pure water (3.57 × 10^{10} in wastewater vs 4,48 × 10^{10} in ultrapure water). Thus, we demonstrate the quantitative nature of this analytical method as well as the protective environment for Au assemblies against microorganism and macromolecules due to mesoporous nature of the silica capsule. The coefficient of variation (CV), a measure of

[43] L. N. Furini; S. Sánchez-Cortés; I. López-Tocón; J. C. Otero; R. F. Aroca; C. J. Leopoldo-Constantino, *J. Raman Spectrosc.* **2015**, 46, 1095-1101.

precision of the method, ranged from 3.5 – 9.3 %, showing an acceptable reproducibility for TMP analysis by SERS.

The limit of detection and quantification (LOD and LOQ) was calculated for TMP in wastewater being 3.02×10^{-8} M and 26.70×10^{-8} M (8.78 and 29.3 ppb), respectively. These values are comparable with the conventional techniques used for detection of TMP such as, extraction method[44] or HPLC with diode-array detection.[45] However, the method presented here has the advantage that does not require extensive sample preparation and is suitable for *in situ* detection, reducing time and cost of the measurement.

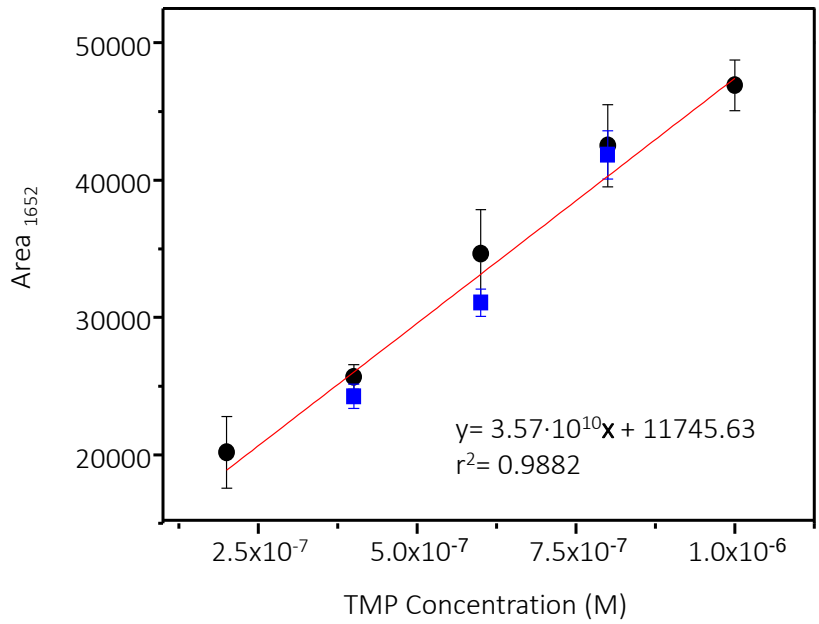

Figure 9. A linear relationship (red solid line) between the TMP concentration in wastewater and the band area at 1652 cm^{-1} (pyrimidine ring stretching and NH bending) was found at the concentration range studied here. Area values for a five-point dilution series of TMP in wastewater were measured using a Raman microscope and integrated from 1629 to 1675cm^{-1}. Each TMP concentration was measured three times. The red dots correspond to the SERS signal of TMP obtained in presence of other CECs. No matrix effect is observed.

[44] X. Zhi-Gang; D. Zhuo; H. Yu-Ling; H. Yu-Fei; P. Ying-Peng; L. Gong-Ke**,** *Chinese J. Anal. Chem.* **2012**, 40, 1002-1010.
[45] D. Mutavdžić-Pavlović; D. Ašperger; D. Tolić; S. Babić, *J. Spe. Sci.* **2013**, 36, 3042-3049.

In a real situation the wastewater will contain not only organic matter and microorganisms but also other organic pollutants (e.g. pesticide, pharmaceuticals and PAHs). These organic pollutants are generally small organic molecules, which will diffuse through the mesoporous silica shell and may produce interferences that reduce the sensitivity of the SERS method. To assess the possible suppression/enhancement of the SERS signal by the presence of these organic pollutants, we performed the TMP detection at different concentrations in the presence of other pharmaceuticals such as ibuprofen (ibu), carbamazepine (CBZ), ethinylestradiol (EE2) and diclofenac (DCF). As shown in Figure 3b, no influence of the matrix in the SERS signal of TMP is observed. This is supported by the matrix factor (%MF) which ranged from 2 to 12 %, demonstrating the specificity of the SERS platform for TMP.

2.4 Conclusions

In summary, it was devised a reproducible, robust and sensible SERS platform composed of silica capsules with highly aggregated gold nanoparticles in their inner, capable of detecting trimethoprim in the presence of other pharmaceuticals in wastewater. The sophisticated design of this SERS platform prevented the interaction of AuNPs with soil or organic matter generally present in wastewater samples, avoiding the degradation of the sensor. The specificity for trimethoprim demonstrated here will allow adopting this common antibiotic as a water quality standard. Through the *in situ* detection of trimethoprim it will be possible to monitor and improve the efficiency and costs of the water purification treatments.

Chapter 3

Design and fabrication of plasmonic capsules to detect several emerging contaminants by a multiplex detection

SERS-based direct detection can only be used to detect emerging contaminants with affinity for metal nanoparticles. In other cases, such affinity does not exist being necessary a linker between the nanoparticles and the target. This is the case of carbamezapine, diclofenac, and ethinylestradiol, among others, where detection is performed in an indirect way through the use of a linking molecule. Such molecule can be modified to obtain a functional group more reactive towards the emerging contaminant, even allowing multiplex detection.

3.1 Introduction

In the previous chapter, it was demonstrated how a contaminant can be detected by direct detection due to the affinity between a gold surface and the target molecule. Direct detection or label-free detection aims at acquiring SERS spectra of molecules without Raman dyes, while extrinsic SERS labelling methods employ Raman labels to detect molecules indirectly. Obviously, direct detection it is more convenient, for example in detection of biomolecules.[1] However, it is complicated to implement in some cases. Such cases are connected to the limited sensitivity or the poor selectivity of some molecules.

Therefore, if there is not affinity between the molecule and the metallic surface, the molecule does not provide a SERS spectrum since it is necessary that the molecule attaches to the metallic surface to enhance the Raman signal. It is worth highlighting the case of molecules with phenolic groups where the affinity between phenolic groups and the metallic surface is weak.[2,3]

In this scenario, Raman labels or Raman dyes provide an anchor point to the molecules that do not have a good affinity for the metal surface. Additionally, they afford a known SERS spectrum (Raman labels use to be a well-known Raman probe with a good Raman signal).

In this chapter, the SERS detection of different contaminants will be performed in an indirect way being necessary a ligand to link the gold nanoparticles (AuNPs) and the target given the intrinsically low affinity between both. In this regard, mixing Au-

[1] X. X. Han; B. Zhao; Y. Ozaki, *Trends in Analytical Chemistry* **2012**, 38, 2012, 67-78.
[2] S. M. Barnett; B. Vlcková; I. S. Butler; T. S. Kanigan, *Anal. Chem.* **1994**, 66, 1762-1765.
[3] L. Rodríguez-Lorenzo; R. A. Álvarez-Puebla; F. J. García-de-Abajo; L. M. Liz-Marzán, *J. Phys. Chem. C* **2010**, 114, 7336-7340.

containing nanocapsules with the contaminants does not provide and observable SERS signal.

In this case, the ligand will exhibit a functional group with a good affinity for gold (a thiol group is a very good option due to the covalent S–Au bond). Moreover, the linking molecule will present an additional functional group that will be used to trap the contaminant. This functional group will be even modified to obtain a higher affinity and specificity for the analytes under study.

The emerging contaminants studied in this work are aromatic compounds. For this reason, we selected a diazo coupling reaction as linking process. As known, diazo coupling is an organic reaction between a diazonium compound and an aromatic compound. In this case, this diazonium compound can be obtained from an aniline group.[4]

Diazo coupling consist in two steps, being the first the synthesis of an aromatic diazonium ion from an aniline derivative. The second step is the coupling of the diazonium salt with an aromatic compound yielding an azo compound. The highly electron-deficient diazonium salt of the p-nitroaniline is widely used as a coupling reagent.

These reactions are typically used to obtain azo dyes (which are a type of organic compound that contains the –N=N– functional group) as methyl orange or yellow orange.[5,6]

The diazo coupling reaction dates back to the 1850s and its mechanism was much studied in the heyday of physical organic chemistry.[7] The applications of azo dyes are numerous in today's society. Since the founding of their synthesis, aryl azo compounds

[4] N. M. Aljamali, *Biochem. Anal. Biochem.* **2015**, 4, 1000169.
[5] D. L. Astolfi; F. C. Mayville Jr., *Tetrahedron Letters* **2003**, 44, 9223–9224.
[6] R. R. Weikel; J. P. Hallett; C. L. Liotta; C. A. Eckert, *Ind. Eng. Chem. Res.* **2007**, 46, 5252-5257.
[7] S. B. Hanna; C. Jermini; H. Loewenschuss; H. Zollinger, *JACS* **1974**, 96, 7222-7228.

have served an important role in such industries as ink jet printing, textile production and coloring, and in laboratories as biological stains and also pH indicators. Being this reaction, the most widely used industrial reaction in the production of dyes, lakes and pigments.[8]

The reaction is not very selective because of the aerodizonium ion reacts with the aromatic compounds (benzene is activated in the p-position of the electron donor group). Therefore, an aerodizonium ion can react with several compounds. In this case, this will be exploited to perform a multiplex detection.

Multiplex detection enables the simultaneous detection of two or more targets and can be used in several areas as disease diagnostics, biomarket discovery, food safety and pollutant monitoring. For example, Ju-Me Li et al.[9] synthesize a nano-SERS-probes with a great potential for the detection of widespread biological molecules with exceptional selectivity, extraordinary sensitivity and tremendous multiplexing capability.

Also, the determination of vibrational frequencies by ab initio computational methods is becoming increasingly important in many areas of chemistry. The advent of density functional theory (DFT)[10] has provided an alternative means of including electron correlation in the study of the vibrational frequencies of moderately large molecules. Scott and Random have shown that DFT predicts harmonic frequencies in excellent agreement with experimental frequencies.[11] Therefore, obtaining theoretically

[8] M. Yazdanbakhsh; M. Abbasnia; M. Sheykhan; L. Ma'mani, *Journal of Molecular Structure.* **2010**, 977, 266-273.
[9] J. M. Li; C. Wei; W. F. Ma; Q. An; J. Guo; J. Hu; C.C. Wang, *J. Mater. Chem.* **2012**, 22, 12100-12106.
[10] J. Hutter; H. P. Luthi;F. Diederich, *J. Am. Chem. Soc.* **1994**, 116, 750.
[11] A. P. Scott; L. Radom, *J. Phys. Chem.* **1996**, 100, 16502.

vibrational spectra can be used to solve the interpretation of the experimental results.[12]

A hybrid B3-LYP[13] uses a combination between Becke's three-parameter exchange functional and the correlational functional of Lee, Yang and Parr.[14] A variant of density functional theory (B3-LYP) have been examined in conjunction with the 6-311G ++ (d,p) and LanL2DZ basis sets. Most frequently used for vibrational calculations.

3.2 Experimental section

3.2.1 Fabrication of plasmonic silica capsules

Polystyrene beads functionalization

Plasmonic capsules were synthesized by a templating procedure described previously in our group with slight modifications.[15] Briefly, surface functionalization of polystyrene beads (PS, 530 nm in diameter; Ikerlat Polymers) was carried out by a layer-by-layer assembly method[16,17] using positively charge poly(allylamine hydrochloride) (PAH, Mw=17500; Sigma-Aldrich) and negatively charged poly(sodium styrene sulfonate) (PSS, Mw= 70000; Sigma-Aldrich) until obtaining an external and uniform positive surface.

---

[12] M. D. Halls; H. B. Schlegel, *J. Chem. Phys.* **1999**, 11, 8819.

[13] P. J. Stephens; F. J. Devlin; C. F. Chabalowski; M. J. Frisch, *J. Phys. Chem.* **1994**, 98, 5612.

[14] C. Lee; W. Yang; R. G. Parr, *Phys. Rev. B* **1988**, 37, 785.

[15] C. Vázquez-Vázquez; B. Vaz; V. Giannini; M. Pérez-Lorenzo; R. A. Álvarez-Puebla; M. A. Correa-Duarte, *J. Am. Chem. Soc.* **2013**, 135, 13616.

[16] E. Donath; G. B. Sukhorukov; F. Caruso; S. A. Davis; H. Möhwald, *Angew. Chem. Int. Ed.* **1998**, 37, 2201.

[17] H. Ejima; J. J. Richardson; K. Liang; J. P. Best; M. P. van Koeverden; G. K. Such; J. Cui; F. Caruso, *Science* **1998**, 282, 1111.

Synthesis and adsorption of the gold seeds

AuNPs (3 nm [Au]= 10^{-4}M) were produced as described by Duff et al.[18] and subsequently adsorbed onto functionalized PS beads. In this case, 6 mL of 3 nm AuNPs were added to 50 mL of positively charged PS beads (0.25 mg/mL) under sonication. The suspension was then centrifuged to remove the excess of 3 nm AuNPs (3500 rpm, 20 min) and redispersed in ultrapure water (18.2 MΩ cm). The final concentration was 1.25mg/mL.

Mesoporous silica coating and capsule preparation

Mesoporous silica coating was carried out following the method described by Yonghui Deng et al.[19] Briefly, 3nm AuNPs-coated PS particles (PS@Au seed) were added dropwise and under sonication to a solution containing 312.5 mg of cetyl trimethylammonium bromide (CTAB; Sigma-Aldrich), 100 mL of ultrapure water, 50 mL of ethanol (Sigma-Aldrich) and 1.5 mL of an ammonia aqueous solution (28 wt %, Sigma-Aldrich). After 20 min, 1.88 mL of a 5% (v/v) tetraethoxysilane (TEOS; Sigma-Aldrich) ethanolic solution was added dropwise under sonication for 5 min. Then, the mixture was stirred for 18 h to obtain a homogenous silica growth. The silica-coated PS@Au particles were washed by three centrifugation (3500 rpm, 20 min)-redispersion (ethanol) cycles. The organic templates, PS and CTAB, were removed by calcination at 550 °C for 6 h, giving rise to final Au-containing silica capsule (Au@SiO_2).

Confined growth of gold nanoparticles

AuNPs inside the capsules were grown *via* Au^+ reduction with formaldehyde.[20] Briefly, the Au^+ solution was obtained mixing

[18] D.G.Duff; A. Baiker, *Langmuir* **1993**, 9, 2301.
[19] Y. Deng; D. Qi; C. Deng; X. Zhang; D. Zhao, *J. Am. Chem. Soc.* **2008**, 130, 28.
[20] M. Sanles-Sobrido; W. Exner; L. Rodríguez-Lorenzo; B. Rodríguez-González; M. A. Correa-Duarte; R. A. Álvarez-Puebla; L. M. Liz-Marzán, *J. Am. Chem. Soc.* **2009**, 131, 2699.

474.4 µL of 0.11 M $HAuCl_4 \cdot 3H_2O$ (Sigma-Aldrich) and 120 mL of 1.80 mM K_2CO_3 (Sigma-Aldrich) for 1 h. Then, 5 mL of this Au^+ solution and 30 µL of formaldehyde solution (37 wt%; Sigma-Aldrich) were added to 2 mL of a $Au@SiO_2$ suspension (1.25 mg/mL) under vigorous stirring. After 10 min, the color changed from pink to purple-blue ($Au(Growth\ 1)@SiO_2$). The sample was centrifuged and washed with ethanol (4500 rpm, 15 min). All these steps were repeated to obtain a second growth ($Au(Growth\ 2)@SiO_2$).

3.2.2 Addition of the ligand

Plasmonic gold nanocapsules were mixed with a solution of 4-aminothiophenol (4-ATP). The addition was performed mixing 200 µL of a solution of 4-ATP and 200 µL of capsules 1 mg/mL for 24 h. The sample was centrifugated (4000 rpm, 15 min) and washed with ethanol twice.

3.2.3 Reaction inside the capsule

Then, the capsules with the ligand were mixed with sodium nitrite and hydrochloric acid at 0 °C for 1 h with magnetic stirring to obtain the aerodizonium ion.

The capsules with aerodizonium ion were mixed with the contaminants at 0 °C to anchor the contaminants to the inner wall of the capsules.

3.2.4 Addition of thiols

Plasmonic nanocapsules were mixed with several thiols (Figure1). The thiols used were: 4-aminothiophenol (4-ATP), 4-mercaptobenzoic acid (4-MBA) and 2-naphthalenthiol (2-NAT). The addition was performed mixing 200 µL of a solution of the thiol and 200 µL of capsules 1 mg/mL for 24 h. The sample was centrifugated (4000 rpm, 15 min) and washed with ethanol twice. Also, we performed the simultaneous addition of the three thiols,

mixing 200 µL of each one and 200 µL of capsules 1 mg/mL for 24 h.

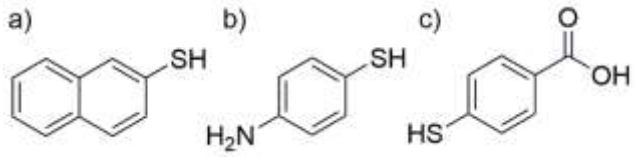

Figure 1. Thiols employed in this work: a) 2-naphthalenethiol; b) 4-aminothiophenol; and c) 4-mercaptobenzoic acid.

3.3 Results and discussion

Au-containing nanocapsules were synthesized and characterized in the same way that in the previous chapter.

Briefly, the structure obtained is based on a layer of mesoporous silica with AuNPs in the inner wall. The size of the structure is about 520 nm and the size of the AuNPs is about 20 nm. Figure 2 shows the basically characterization by transmission electron microscopy (TEM) and UV-vis spectroscopy.

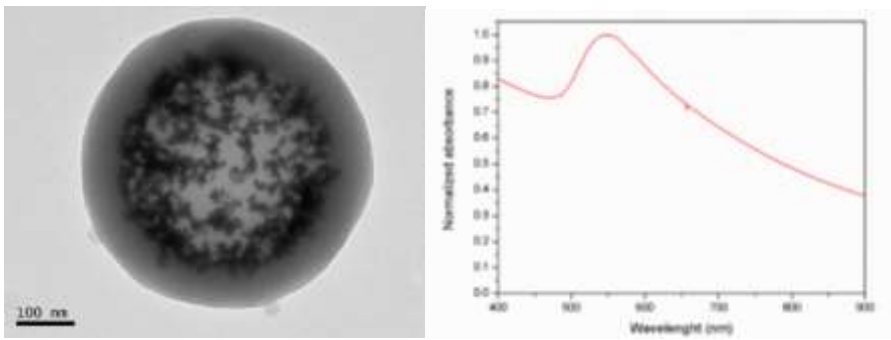

Figure 2. Characterization of the plasmonic nanocapsules by TEM and UV-Vis.

The Raman label will be 4-aminothiophenol (4-ATP). This molecule diffuses through the silica layer reaching and anchoring to the AuNPs due to the affinity between gold and the thiol group. Figure 3 shows the SERS spectrum of 4-ATP confirming the presence of the molecule inside the capsule.

A process of centrifugation and washing was performed to remove the excess of 4-ATP (the molecules that were not chemically bound to the gold).

So the molecules are trapped inside the capsule providing a good SERS spectrum because they exhibit a good cross-section (4-ATP, a well-known Raman probe[21,22] will act as a Raman linker).

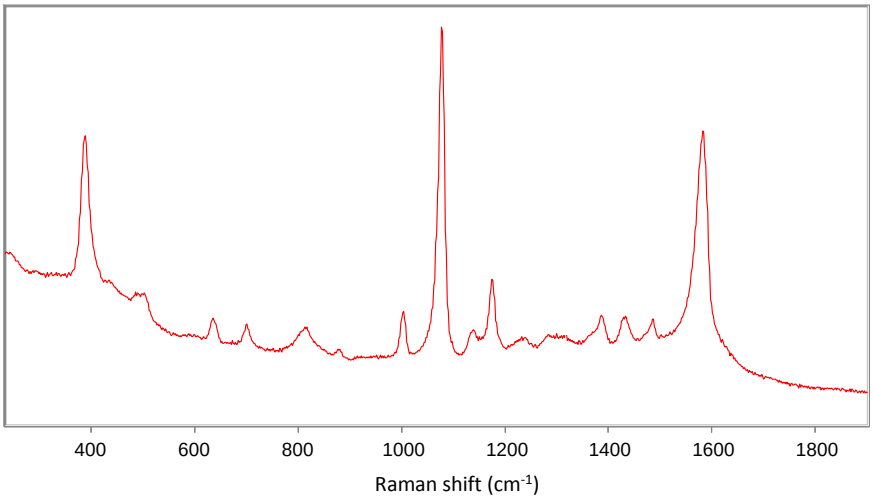

Figure 3. SERS spectrum of 4-aminothiophenol in the plasmonic nanocapsules.

Table 1. Assignment of the SERS spectrum of the 4-aminothiphenol.

Position of band (cm^{-1})	Band assignment
366	ν CS
1003	δ CH
1077	ν CC + ν CS
1135	
1175	δ CH
1382	ν CC + ν CN
1427	ν CN
1482	ν CC
1588	ν CC

[21] S. Tian; Q. Zhou; C. Li; Z. Gu; J. R. Lombardi; J. Zheng, *J. Phys. Chem. C* **2013**, 117, 556.
[22] Q. Zhang; N. Large; P. Nordlander; H. Wang, *J. Phys. Chem. Lett.* **2014**, 5, 370.

Therefore, 4-ATP stays anchored in the capsules due to the affinity between the gold and the thiol group of the 4-ATP affording a free amine group for the next reaction to take place.

The amine group will be further converted in a more reactive group, especially with the aromatic compounds (the emerging contaminants studied in this work have the aromatic compounds) performing a reaction inside the capsule to trap and detect the contaminants by an indirect way. For this reason, a diazotization reaction will be performed (Figure 4). This reaction is one of the most important transformations in organic chemistry and consist in the reaction between a primary amine and nitrous acid to obtain a diazonium salt (although gaseous, nitrous acid can be obtained as aqueous solution mixing alkaline nitrites with mineral acids, e.g., mixing sodium nitrite and hydrochloric acid).

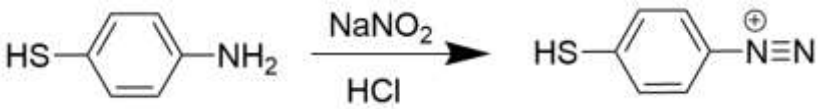

Figure 4. An aerodiazonium ion is obtained using a diazotization reaction from 4-aminothiophenol.

With this reaction, an arenediazonium ion is obtained.

When the primary amine is an aliphatic primary amine, the diazonium salt obtained is very unstable and it decomposes quickly. However, if the amine is an aromatic primary amine a diazonium salt with some stability in solution and with temperatures below 5 °C is obtained.

The SERS spectra obtained for the aerodiazonium ion is shown in the Figure 5.

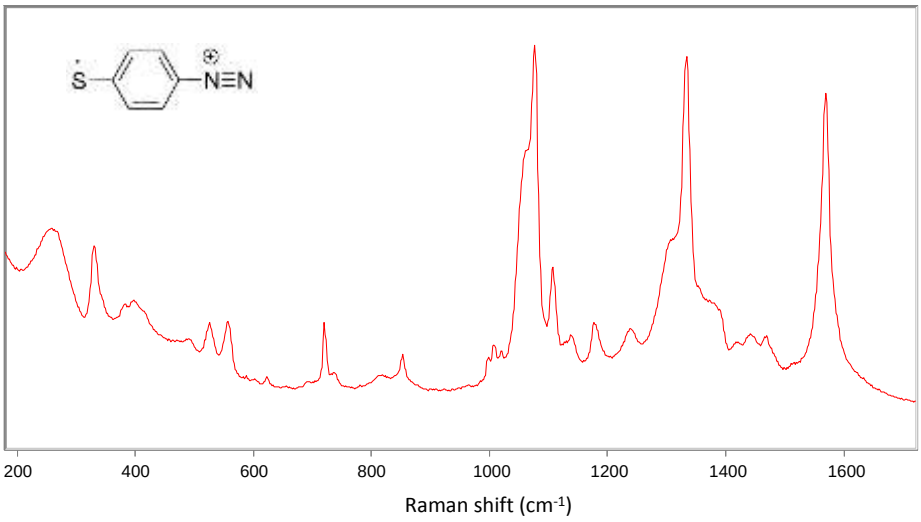

Figure 5. SERS spectrum of the arenediazonium ion.

These compounds have some stability but, even at cold temperatures, they decompose slowly. For this reason, they have to be employed with care and immediately.

The diazonium salts can react in different ways. These processes can be distributed in two groups:

- Substitution. The nitrogen atoms left the compound forming N_2 and other group enters in their place in the aromatic ring.
- Copulation reaction. The nitrogen atom stays in the final compound.

In this case, a copulation reaction is used. Diazonium salts act as an electrophile reagent in aromatic substitutions to obtain azo compounds.

Diazonium salts have a low electrophilic character, so they react only with aromatic compounds with strong electron donor groups as –OH, $–NH_2$, $–NR_2$ or –NHR. Usually, the reaction occurs in the *para* position with respect to the donor group.

The mechanism of the reaction is showed in Figure 6:

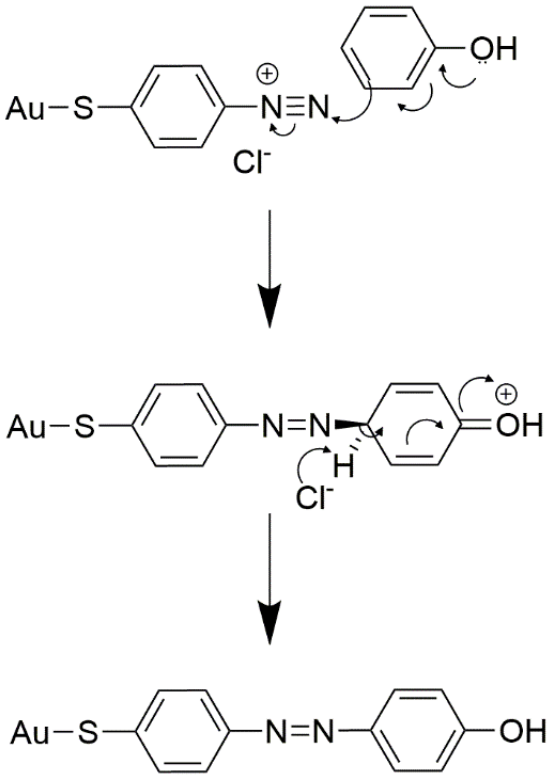

Figure 6. Reaction mechanism for a copulation reaction.

The first step of the mechanism is the attack of the π electrons of the ring to the diazonium salt due to the resonance of the pair of electrons of the electron donor group. Due the polarization, the positive charge of the nitrogen atom is neutralized forming the azo compound. A proton is delivered to restore the aromaticity of the system.

The emerging contaminants that will be studied performing the copulation reaction are: diclofenac, ibuprofen, ethynilestradiol and carbamezapine (Figure 7). These targets are aromatic compounds and some of them have several positions that can react with the arenediazonium ion since they have several electron donor groups.

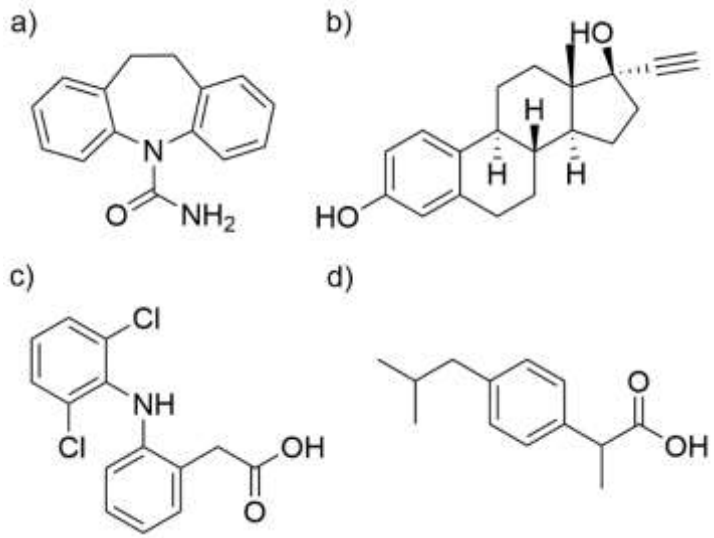

Figure 7. Emerging contaminants: a) carbamazepine; b) ethinylestradiol; c) diclofenac; and d) ibuprofen.

As aforementioned, the technique used to detect these contaminants is based on surface enhanced Raman spectroscopy (SERS). With this methodology it is possible obtain the vibrational spectrum of the molecules that are attached to the metallic surface. In this way, it is possible to check the changes produced in each step of the organic reaction. Therefore, Raman spectroscopy will allow the monitoring of the reaction with the contaminants.

The SERS spectra acquired for the compounds obtained after the reaction between arenediazonium ion and the emerging contaminants are shown in Figure 8, 9 and 10.

The copulation reaction is performed for each emerging contaminant and also is performed adding simultaneously all the emerging contaminants (SERS spectrum is shown in Figure 11). With this experiment, we aim at knowing if some of the contaminants react more intensively with the arenediazonium ion and to check if a multiplex detection can be realized.

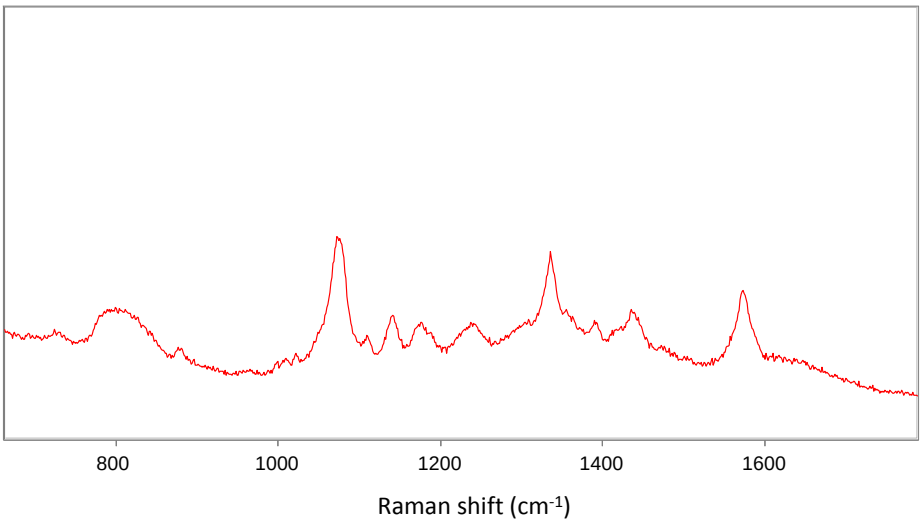

Figure 8. SERS spectrum obtained after the reaction between arenediazonium ion and carbamazepine.

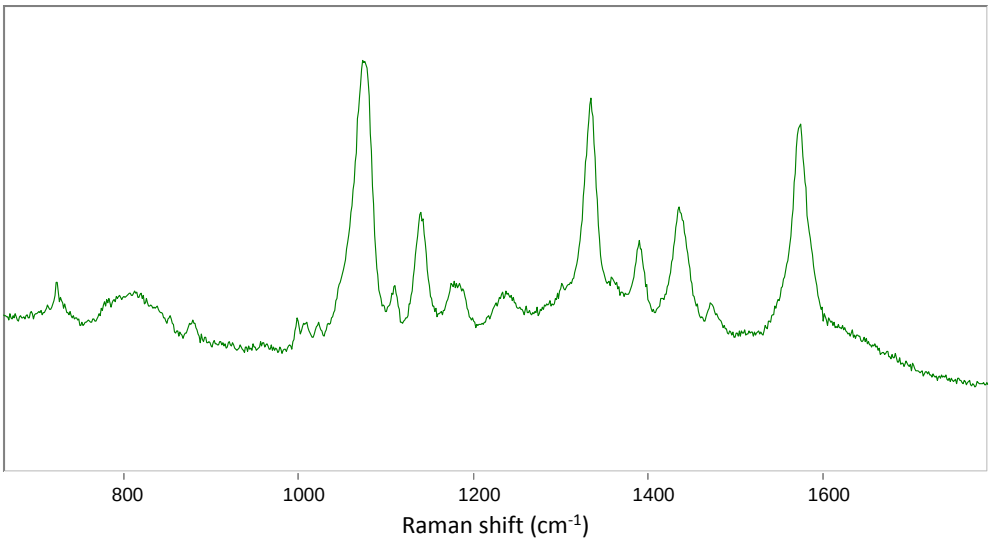

Figure 9. SERS spectrum obtained after the reaction between arenediazonium ion and ethinylestradiol.

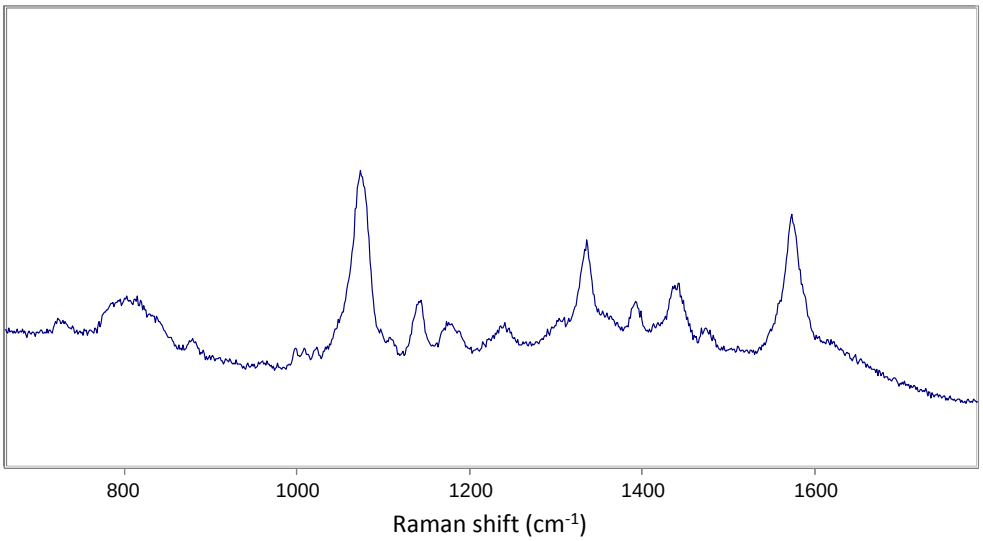

Figure 10. SERS spectrum after the reaction between arenediazonium ion and diclofenac.

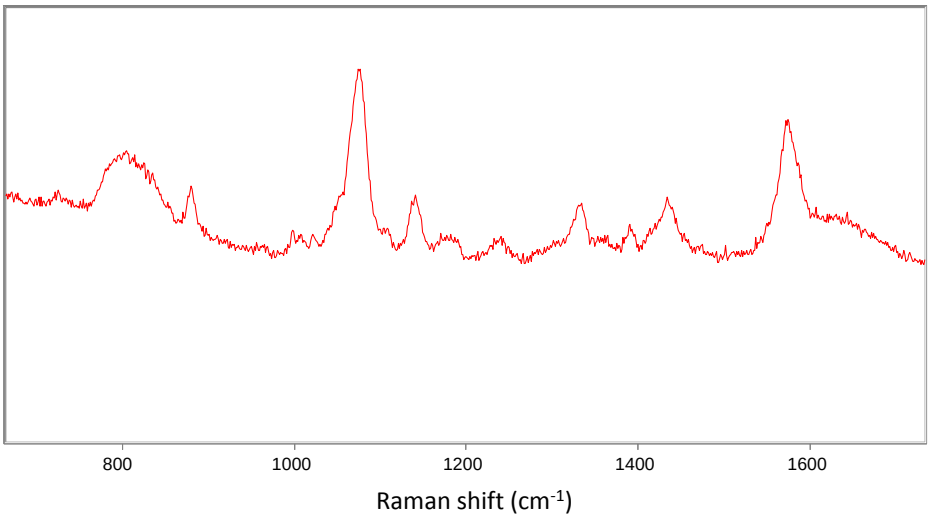

Figure 11. SERS spectrum after the reaction between arenediazonium ion and the three contaminants at the same time (ethinylestradiol, carbamazepine and diclofenac).

Spectra analysis

Once obtained the spectra are analyzed by deconvolution. This is a qualitative technique that consist in decomposing the overlapping spectral bands to identify the several peaks based on different band signatures.

Lorentzian and Gaussian fitting are the main two methods used in SERS spectra deconvolution. The Lorentzian method, the Gaussian method or a mixture of these functions can be used.

To check if the deconvolution method is a good technique to perform a multiplex detection, an experiment with several thiols was performed. Using the gold nanocapsules and three different thiols (2-NAT, 4-ATP and 4-MBA), SERS spectra were obtained.

The spectra were obtained separately (mixing just one thiol with the gold nanocapsules) and together (mixing the three thiols at the same time with the gold nanocapsules). Figure 12 shows the

SERS spectra of the three thiols used obtained separately and represented in the same figure to compare them.

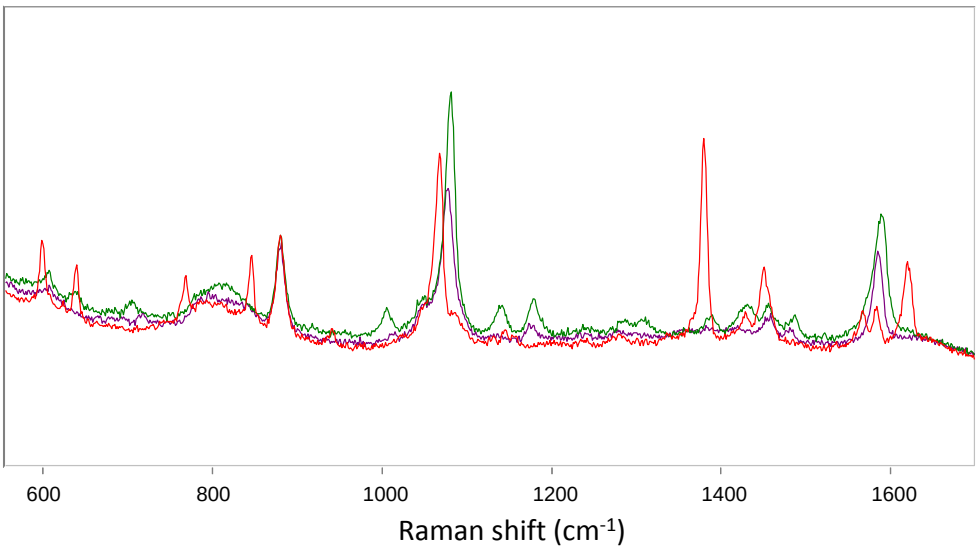

Figure 12. SERS spectra of the three thiols. Comparison of the three spectra. Red) 2-naphthalenthiol. Green) 4-aminothiophenol. Purple) 4-mercaptobenzoic acid.

Figures 13, 14 and 15 display the SERS spectrum of each thiol and it is presented a table with their assignment.

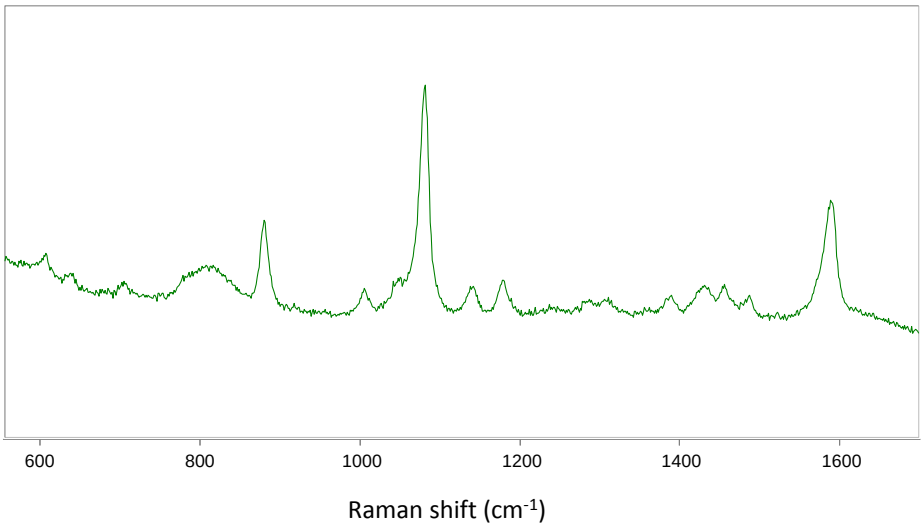

Figure 13. SERS spectrum of the 4-aminothiophenol.

Tabla 2. Assignment of the SERS spectrum of the 4-aminothiphenol. [23,24]

Band position (cm^{-1})	Band assignment
607.40	
639.91	γ C-C-C
703.67	
800.31	π wagging
1005.33	γ C-C + γ C-C-C
1049.71	
1081.38	ν C-S
1141.15	δ C-H
1178.90	δ C-H
1272.19	
1286.49	ν Ar-N
1312.52	
1389.44	δ C-H + ν C-C
1432.24	ν C-C
1456.93	
1488.23	ν C-C + δ C-H
1590.96	ν C-C

[23] Y. Liu; Y. Zhang; H. Ding; S. Xu; M. Li; F. Kong; Y. Lu; G. Li, *J. Mater. Chem. A* **2013**, 1, 3362-3371.
[24] J. Zheng; Y. Zhou; X. Li; Y. Ji; T. Lu; R. Gu, *Langmuir* **2003**, 19, 632-636.

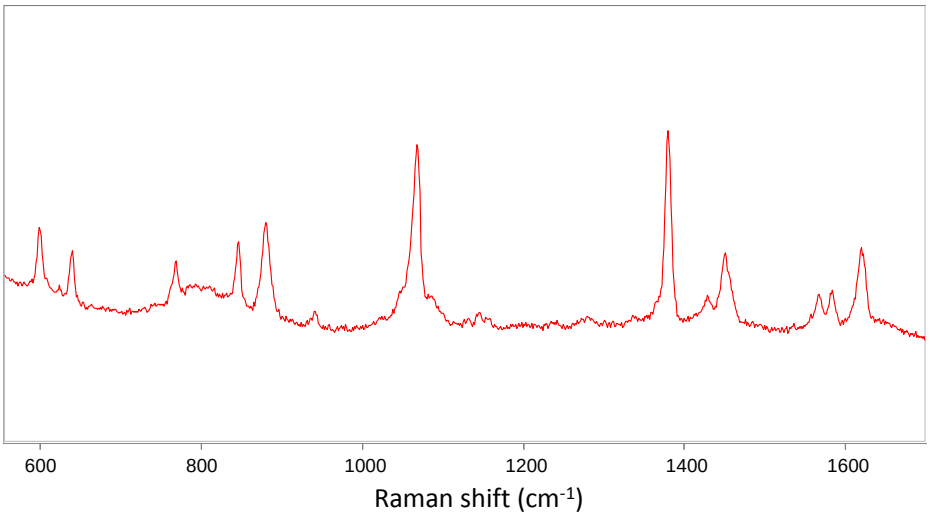

Figure 14. SERS spectrum of the 2-naphthalenthiol.

Tabla 3. Assignment of the SERS spectrum of the 2-naphthalenethiol. [25]

Position of the band (cm^{-1})	Band Assignment
599.14	δ Ring deformation
623.81	Ring twist
638.99	δ Ring deformation
768.97	δ Ring deformation
846.48	C-H twist
880.17	-
940.96	δ S-H bend
1067.77	δ C-H bend
1131.69	δ C-H bend
1145.90	δ C-H bend
1156.46	-
1380.30	ν Ring stretch
1429.29	ν Ring stretch
1450.64	ν Ring stretch
1536.33	ν Ring stretch
1568.46	ν Ring stretch
1584.42	ν Ring stretch
1620.62	ν Ring stretch

[25] R. A. Álvarez-Puebla; D. S. Dos-Santos Jr.; R. F. Aroca, *Analyst* **2004**, 129, 1251-1256.

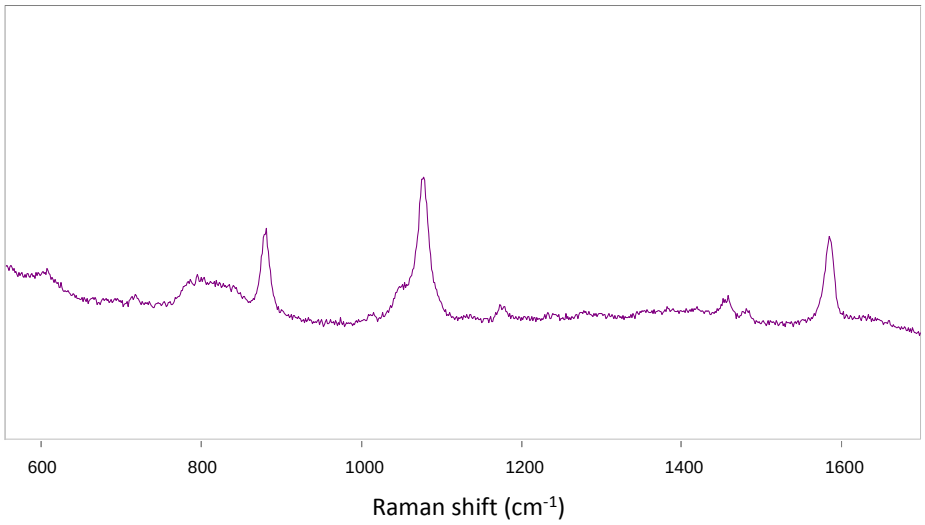

Figure 15. SERS spectrum of the 4-mercaptobenzoic acid.

Tabla 4. Assignment of the SERS spectrum of the 4-mercaptobenzoic acid. [26,27]

Position of the band (cm^{-1})	Band assignment
716.69	ϒ C-C-C out-of-plane
794.63	
881.14	
1014.50	Ring breathing
1078.17	δ C-H in plane bending
1173.67	δ C-H bending
1458.64	
1481.84	δ Ring bending
1586.11	ν C-C stretching

Also, figure 16 exhibits a comparison between the SERS spectra of the thiols and the SERS spectrum of the mixture of thiols. The table indicates the assignation of the bands obtained and the thiol that from correspond each band.

[26] W. Ma; Y. Fang; G. Hao; W. Wang, *Chin. J. Chem. Phys.* **2010**, 23, 659-663.
[27] A. Michota; J. Bukowska, *J. Raman Spectrosc.* **2003**, 34, 21-25.

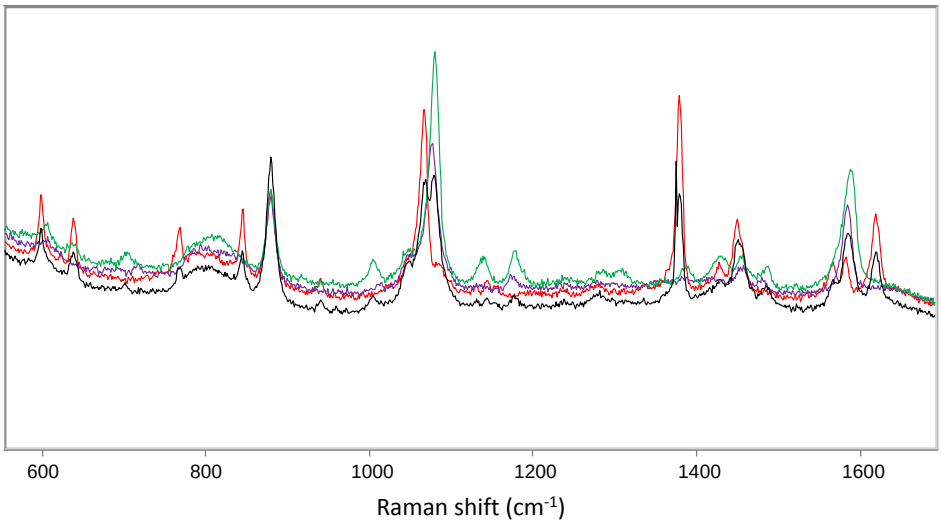

Figure 16. SERS spectrum of the three thiols separately and the mixture of all of them at the same time. Black) the mixture of the three thiols. Red) 2-naphthalene SERS spectrum. Green) 4-aminothiophenol SERS spectrum. Purple) 4-mercaptobenzoic acid SERS spectrum.

Tabla 5. Assignment of the SERS spectrum of the mixture of three thiols.

Band position (cm^{-1})	Band assignment	Belong to thiol
599.73	δ Ring deformation	2-NAT
638.44	δ Ring deformation	2-NAT
701.80		4-ATP
767.82	δ Ring deformation	2-NAT
845.64	C-H twist	2-NAT
880.58		2-NAT/4-MBA
941.01	δ S-H	2-NAT
959.72		
972.14		
1004.55	γ C-C + γ C-C-C	4-ATP
1049.93		4-ATP
1068.09	δ C-H	2-NAT
1079.32	ν C-S + C-H in plane	4-ATP/4-MBA
1131.64	δ C-H	2-NAT
1144.14	δ C-H	4-ATP/2-NAT
1177.74	δ C-H	4-ATP/4-MBA
1281.18		4-ATP
1337.24		
1380.45	δ C-H + ν C-C ring	4-ATP/2-NAT

1429.44	ν C-C ring	4-ATP/2-NAT
1451.90	ν ring	4-ATP/2-NAT/4-MBA
1485.58	ν C-C + δ C-H bend + δ ring	4-ATP/4-MBA
1576.67	ν ring	2-NAT
1587.39	ν ring + ν C-C	2-NAT/4-MBA
1620.15	ν ring	4-MBA

In the SERS spectrum obtained mixing the plasmonic capsules and the three thiols at the same time we performed a deconvolution in the range 1030–1120 cm^{-1} obtaining a separation in three peaks as it is represented in Figure 17.

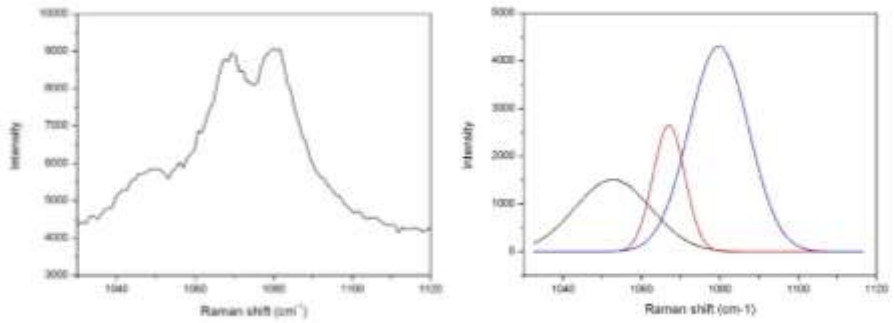

Figure 17. Left) experimental SERS spectrum for the three thiols added at the same time. Right) same experimental spectra after deconvolution.

These three peaks are 1052, 1067 and 1080 cm^{-1} and correspond to 4-aminothiophenol, 2-naphthalenethiol and 4-aminothiphenol/2-naphthalenethiol, respectively.

Therefore, with the SERS spectrum of the three thiols we can identify each thiol separately by deconvolution of the spectrum.

The same process was performed for the SERS spectrum of the arenediazonium ion and the mixture of three contaminants. In this case, it is not possible to separate the spectrum due to the similarity between the SERS spectra.

An alternative way to identify the obtained compounds is performing a simulation by computational methods to acquire the

theoretical SERS spectrum. As aforementioned in the introduction of this chapter, computational methods as DFT have demonstrated to be a good option to predict the harmonic frequencies.

Appropriate scale factors have been applied to compare the experimental spectra with the theoretical spectra obtained with computational methods. Scott and Radom's work explain how obtain these values and show the different scale factor values used depending on the DFT method employed.

In this case, the theoretical spectra were obtained by the hybrid method B3LYP/6-31G and the Hartree-Fock method (HF/6-311G), being 0.9614 the scale factor used for the hybrid method and 0.9051 the scale factor for that basis set of the Hartree-Fock method.

The comparison between experimental SERS spectra and theoretical spectra are shown in the figures 18-24:

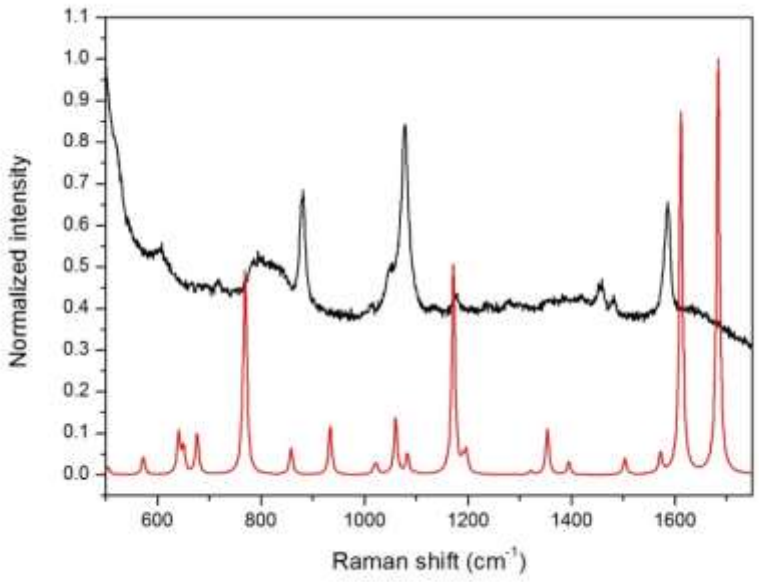

Figure 18. SERS spectra of 4-mercaptobenzoic acid. Red) theoretical spectrum. Black) experimental spectrum.

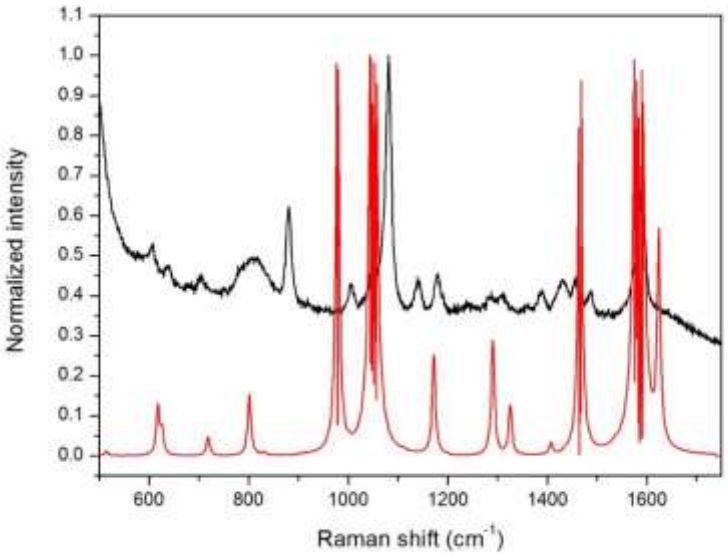

Figure 19. SERS spectra of 4-aminothiophenol. Red) theoretical spectrum. Black) experimental spectrum.

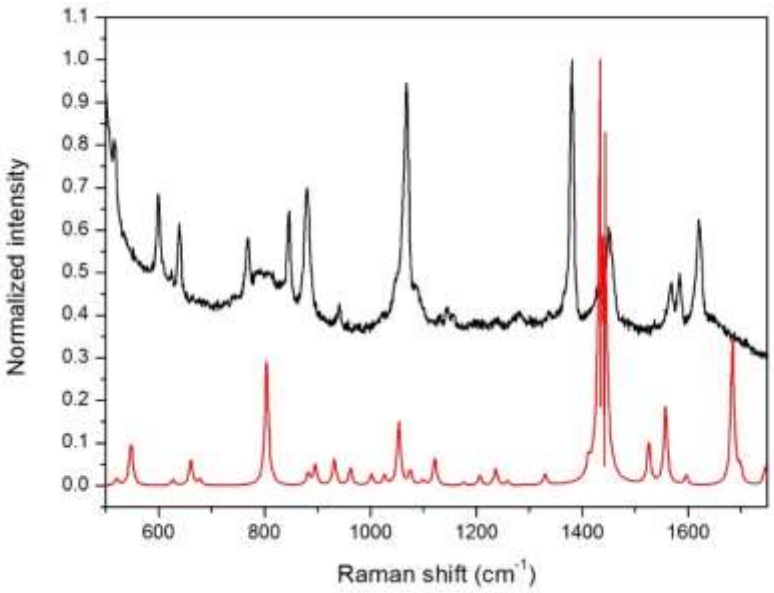

Figure 20. SERS spectra of 2-naphthalenethiol. Red) theoretical spectrum. Black) experimental spectrum.

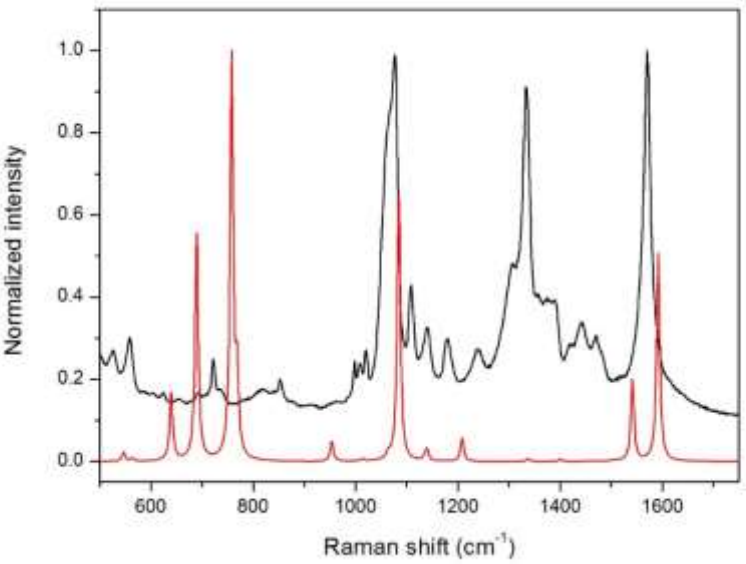

Figure 21. SERS spectra of arenediazonium ion. Red) theoretical spectrum. Black) experimental spectrum.

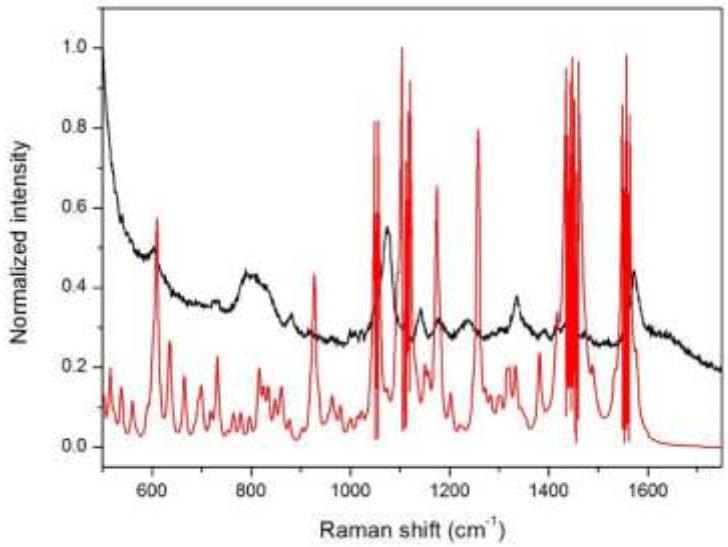

Figure 22. SERS spectra obtained after the reaction between the arenediazonium ion and ethinylestradiol. Red) theoretical spectrum. Black) experimental spectrum.

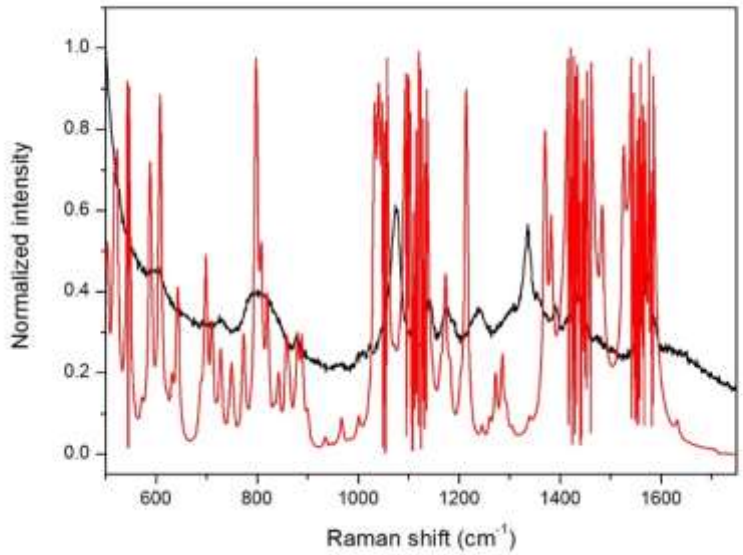

Figure 23. SERS spectra obtained after the reaction between arenediazonium ion and diclofenac. Red) theoretical spectrum. Black) experimental spectrum.

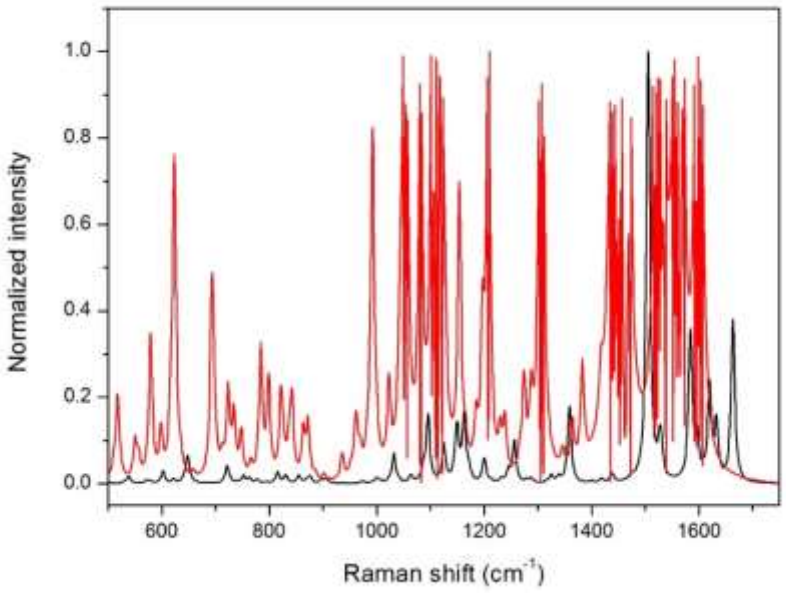

Figure 24. SERS spectra obtained after the reaction between arenediazonium ion and carbamezapine. Red) theoretical spectrum. Black) experimental spectrum.

3.4 Conclusion

As conclusion, a diazo coupling will be used to trap the contaminant using the amine group of 4-ATP. Diazo coupling is an organic reaction between a diazonium compound and an aromatic compound. Emerging contaminants are, mainly, aromatic compounds, for this reason in the capsule from the amine group of the 4-ATP can be obtained a diazonium compound to react with the emerging contaminants. In this way, emerging contaminants are trapped and detected by an indirect detection.

The multiplex detection can be performed and it is demonstrated for the thiols although for emerging contaminants is more complicated due to the similarity between the spectra of the different compounds.

About the comparison between the theoretical SERS spectra and the experimental SERS spectra obtained, it is demonstrated that it does not correspond perfectly but even in this way, it can help to perform the assignment of the bands.

Chapter 4

Plasmonic capsules as local SERS probes in Raman tweezers for detection

The optical trapping of plasmonic silica-gold capsules and their use as local SERS probes in Raman tweezers is demonstratated. These novel hybrid dielectric-metal particles, designed for optoplasmonic applications, are mesoscopic porous silica shells embedding gold nanospheres on their inner wall. It is observed a high trapping efficiency due to the plasmon-enhanced optical trapping of the gold component. Furthermore, it has been developed an accurate model of optical trapping of this hybrid system in the T-matrix framework studying how the plasmon-enhanced optical forces scale with the number of gold nanoparticles in the capsule. The relevance of the effective optical trapping in the plasmonic capsules is twofold for detection and delivery technologies: positioning and activation processes. In fact, the presented system allows to drag and locate cargo capsules embedded with specific molecules that can be activated and released *in situ* when a precise localization is required.

4.1 Introduction

Optical tweezers (OTs) are a key technique about manipulation of micro and nanosized particles. This technique was initially discovered by Ashkin, who observed the acceleration and trapping of particles by optical trap in 1970.[1]

A highly focused laser beam forms the optical tweezers. The laser beam is focused to a spot in the same plane that the specimen. This spot creates an optical trap that allows holding the sample at its center. There are two kinds of optical forces. The first one is the scattering and absorption force that tend to destabilize the trap and the second is the gradient force that is proportional to the gradient of the light intensity and enables to drive the target particle in the focal point.[2]

To obtain a stable trap it is necessary that the gradient force would be higher than forces due to scattering and absorption. This depends on several factors: power of incident light, numerical aperture of the microscope objective, and the size and nature of particles. For example, increasing the laser beam power can be used to optimize the stiffness of optical trapping.[3]

These OTs have been used in physical chemistry with several applications: trapping and analysis of aerosols,[4] optical trapping for amino acids[5] and myoglobin,[6] and for applications as single-

[1] A. Ashkin, *Phys Rev Lett* **1970**, 24, 156–159.
[2] H. L. Guo; Z. Y. Li, *Sci China-Phys Mech Astron* **2013**, 56, 2351-2360.
[3] Y. Yuan; Y. Lin; B. Gu; N. Panwar; S. C. Tjin; J. Song; J. Qua; K.-T. Yong, *Coord. Chem. Rev* **2017**, 339, 138–152
[4] R. E. Miles; J. S. Walker; D. R. Burnham; J. P. Reid, *Phys. Chem. Chem. Phys.* **2012**, 14, 3037–
3047.
[5] Y. Tsuboi; T. Shoji; N. Kitamura, *J. Phys. Chem. C* **2010**, 114, 5589–5593.
[6] T. Shoji; N. Kitamura; Y. Tsuboi, *J. Phys. Chem. C* **2013**, 117, 10691–10697.

molecule fluorescence spectroscopy,[7] imaging and absorption of gold nanoparticles,[8] microrheology of ionic liquids,[9] self-assembly of pseudoisocyanine J-aggregates,[10] optical printing,[11] and controlled aggregation of metal nanoparticles.[12]

By capturing metal nanoparticles, optical trapping can enhance the SERS signal of target molecules at hot spots.[13] The optical trapping enables to monitor the SERS fingerprint signals of analytes in an inhomogeneous sample *in vivo* such as biological fluid, living cells and tissues. Research has focused on developing optical tweezers-assisted SERS spectroscopy as a powerful and multifunctional sensing platform for improved detection sensitivity and reproducibility of SERS sensing.[3]

For this reason, trapping and manipulation of colloidal plasmonics nanoparticles have acquired great importance. The increase the mechanical effects of light on metal nanoparticles with respect to the dielectric particles of equivalent size are related to the occurrence of their optoplasmonics response typically in the visible or near-infrared (NIR) range.[14]

In fact, at the nanoscale, optical trapping forces are typically very weak as they scale with the real part of the dipolar polarizability and ultimately with particle volume.[15] This volume scaling is detrimental for optical trapping of typical dielectric nanomaterials

---

[7] M. A. van Dijk; L. C. Kapitein; J. van Mameren; C. F. Schmidt; E. J. Peterman, *J. Phys. Chem. B* **2004**, 108, 6479−6484.
[8] M. S. Devadas; Z. Li; G. V. Hartland, *J. Phys. Chem. Lett.* **2014**, 5, 2910−2915.
[9] L. J. Moore; M. D. Summers; G. A. Ritchie, *Phys. Chem. Chem. Phys.* **2013**, 15, 13489−13498.
[10] Y. Tanaka; H. Yoshikawa; H. Masuhara, *J. Phys. Chem. C* **2007**, 111, 18457−18460.
[11] M. J. Guffey; N. F. Scherer, *Nano Lett.* **2010**, 10, 4302−4308.
[12] B. Fazio; C. D'Andrea; A. Foti; E. Messina; A. Irrera; M. G. Donato; V. Villari; N. Micali; O. M. Maragò; P. G. Gucciardi, *Sci. Rep.* **2016**, 6, 26952.
[13] F. Svedberg; M. Kall, *Faraday Discuss.* **2006**, 132, 35**–**44.
[14] K. Svoboda; S. M. Block, *Opt. Lett.* **1994**, 19, 930−932.
[15] O. M. Maragò; P. H. Jones; P. G. Gucciardi; G. Volpe; A. C. Ferrari, *Nat. Nanotechnol.* **2013**, 8, 807−819.

against the destabilizing effects of thermal fluctuations.[16] However, the optoplasmonic response of metal nanoparticles has been exploited to increase optical trapping forces so that their stable confinement is achieved in the NIR at lower power with respect to dielectric ones.[14]

Far from plasmon resonance peaks, the optical response of metal nanoparticles is (mainly) the one of the free-electron plasma, yielding a large NIR polarizability, and hence a large (generally 10 times larger) optical trapping force when compared to dielectric particles of comparable size.[17]

Gold nanoparticles as small as 10 nm in size have been stably trapped with OT.[18] However, the size range for stable optical trapping is limited since if the nanoparticle increase its size, the scattering forces are much bigger than confining forces and, therefore, the particles are expelled from the trap.[17]

Moreover, the resonant plasmonic response of metal nanoparticles is responsible for their wavelength-dependent optomechanical behavior, so that for light nearly resonant with the nanoparticle plasmonic response optical forces can be used to push them for controlled patterning,[11] sorting[19] or SERS.[12]

Several hybrid structures with two or more components have been proposed as novel colloidal materials due their additional functionalities with respect to the single plasmonic nanoparticles.[20] Changing the shape and the composition of the hybrid structure, it is possible to control their plasmonic response

[16] P. H. Jones; O. M. Maragò; G. Volpe, Optical Tweezers: Principles and Applications; Cambridge University Press: Cambridge, U.K., 2015.
[17] P. M. Hansen; V. K. Bhatia; N. Harrit; L. Oddershede, *Nano Lett.* **2005**, 5, 1937−1942.
[18] F. Hajizadeh; S. N. Reihani, *Opt. Express* **2010**, 18, 551−559.
[19] M. Ploschner; T. Cizmar; M. Mazilu; A. Di Falco; K. Dholakia, *Nano Lett.* **2012**, 12, 1923−1927.
[20] A. De Luca; M. P. Grzelczak; I. Pastoriza-Santos; L. M. Liz-Marzan; M. La Deda; M. Striccoli; G. Strangi, *ACS Nano* **2011**, 5, 5823−5829.

as well as their aggregation or compatibility with a solvent, their strength or their magnetic or fluorescent properties.[21]

In the case of inorganic hybrid capsules, the position of the plasmonic nanoparticles on the inner wall of the capsule allows to create a plasmonic environment in a hollow capsule due to the confinement of plasmonic nanoparticles forming hot spots.[22] The spatial distribution of noble metal nanospheres gives rise to localized and collective plasmonic modes within the capsules that result in broadband plasmon fields that are harnessed for both enhanced optical trapping and metal enhanced spectroscopies.

Moving away from the inner walls, a fast gradient field takes place, leading to a much less intense plasmon field at the center of the cavity. This intense plasmon field gradient is at the basis of catalytic reaction control,[22] metal enhancement effects,[20] and scattering field distributions for effective optical trapping.[23]

In this chapter, the optical trapping of a novel type of hybrid dielectric-metal particle designed for optoplasmonic applications it was studied. In this case, reverse bumpy ball architectures composed of mesoporous silica shells embedding gold nanospheres.[24] Thus, we measured the optical trapping efficiency for the plasmonic capsules and we compared it with that of a solid latex particle of similar size and of with an individual gold nanoparticle of size close to the gold nanospheres embedded in the capsule inner shell. The hybrid capsule shows a trapping efficiency much higher than that of the individual gold nanoparticle due to gold clusterization inside the mesoporous

---

[21] X. Lu; M. Rycenga; S. E. Skrabalak; B. Wiley; Y Xia, *Annu. Rev. Phys. Chem.* **2009**, 60, 167−192.
[22] M. Pérez-Lorenzo; B. Vaz; V. Salgueiriño; M. A. Correa-Duarte, *Chem. Eur. J.* **2013**, 19, 12196−12211.
[23] N. Motl; A. Smith; C. DeSantis; S. Skrabalak, *Chem. Soc. Rev.* **2014**, 43, 3823−3834.
[24] M. Infusino; A. De Luca; A. Veltri; C. Vázquez-Vázquez; M. A. Correa-Duarte; R. Dhama; G. Strangi, *ACS Photonics* **2014**, 1, 371−376.

shell. Moreover, we found a trapping efficiency comparable to that of the solid microparticle despite the much (about 20 times) smaller interaction volume of the hollow plasmonic capsule. This large trapping efficiency for the capsule is due to the plasmon-enhanced optical forces acting on its hybridized shell. Experimental results are supported by accurate theoretical light scattering calculations in the T-matrix framework that show how optical forces on a gold shell-cluster increase with the square of the gold nanoparticle number on the shell. Additionally, as a proof of concept that further extends the multifunctionality of these hybrid materials, it was shown how the plasmonic characteristics of such particles enable their use as single-particle probes for surface enhanced Raman spectroscopy (SERS) of molecules dispersed in the liquid environment.

4.2 Experimental section

4.2.1 Fabrication of plasmonic silica capsules

Polystyrene beads functionalization

Plasmonic capsules are synthesized using polystyrene (PS) beads ~1400 nm as templates. These PS beads are first functionalized by an alternate deposition of a positive poly(allylamine hydrochloride) (PAH, Mw=17500) and negative poly(sodium styrenesulfonate) (PSS, Mw=70000) polyelectrolytes, following the layer-by-layer assembly technique.[25] The deposition of a final layer of PAH provides the surface of the PS beads with a homogeneous positive charge, which ensures the later adsorption of the gold seeds.

[25] F. Caruso, *Angew. Chem. Int. Ed.* **1998**, 37, 2201-2205.

Synthesis and adsorption of gold seeds

Gold seeds (1−3 nm [Au] = 10^{-4} M) are produced as described by Duff et al.[26] Thus, 6 mL of Au seeds solution are added to 50 mL of previously functionalized PS beads (0.25 mg/mL) under sonication. Then, the solution is centrifuged (4000 rpm, 20 min) and redispersed with milli-Q water three times, to remove the excess of Au seeds not adsorbed on the PS surface. The concentration of PS beads is adjusted to 1.25 mg/mL.

Mesoporous silica coating and preparation of the capsule

Mesoporous silica coating is obtained following the method described by Vázquez-Vázquez et al.[27]who performed some variations from Deng's work.[28] Briefly, the previous solution of PS@Au seeds is added dropwise and under sonication to a mixed solution of cetyltrimethylammonium bromide (CTAB) (100 mg), deionized water (40 mL), ethanol (30 mL), and ammonia aqueous solution (28 wt %, 365 µL). The resulting solution is homogenized by sonication for 20 min. Then, 1 mL of a 5% (v/v) solution tetraethoxysilane solution (TEOS) in ethanol is added drop by drop under sonication. The mixture is stirred for 2 days in order to have a homogeneous silica growth. Then, it is centrifuged and washed with ethanol three times. Finally, the PS templates are removed by calcination at 500 °C for 10 h.

Confined growth of gold nanoparticles

Gold seeds in the inner of the capsule are grown using a solution of Au^+ and formaldehyde as a reducing agent. The Au^+ solution is obtained mixing 459.3 µL of $HAuCl_4$ 0.1138 M and 120 mL of K_2CO_3 1.8 mM for 1 h. Then, 5 mL of this Au^+ solution and 30 µL of formaldehyde solution (37 wt %) are added to 2 mL Au-

[26] D. G. Duff; A. Baiker; P. P. Edwards, *Langmuir* **1993**, 9, 2301−2309.
[27] C. Vazquez-Vazquez; B. Vaz; V. Giannini; M. Perez-Lorenzo; R. A. Alvarez-Puebla; M. A. Correa-Duarte, *J. Am. Chem. Soc.* **2013**, 135, 13616−13619.
[28] Y. Deng; D. Qi; C. Deng; X. Zhang; D. Zhao, *J. Am. Chem. Soc.* **2008**, 130, 28-29.

seeds@SiO_2 mesoporous (1.25 mg/mL) under vigorous stirring. After 10 min, the color changes from pink to purple-blue. Finally, the sample is centrifuged (4500 rpm, 15 min) and washed with ethanol.

4.2.2 Experimental setups for optical trapping

The experimental setups for optical trapping in the NIR (830 and 785 nm) are based on inverted microscopes[29] (the light propagates upward, Figure 1). In a first setup (Figure 1a) the light from a NIR laser diode at 830 nm is focused in a sample chamber (80 µL) by a high numerical aperture (NA = 1.3) oil immersion objective. This objective lens tightly focuses the NIR light beam for optical trapping, imaging and Raman scattering. The available maximum power at the sample is about 26 mW. Note that at our near-infrared trapping wavelengths the absorption of ethanol or water is negligible,[16] and thus, related heating effects of the surrounding medium can be ignored. A CCD camera was used to image the trapped particles.

Particle tracking and force sensing are obtained through back focal plane interferometry, where the interference pattern from the unscattered and scattered light by the trapped particle is collected onto a quadrant photodiode (QPD). After a suitable calibration, QPD voltage signals give direct information on the trapped particle position. [30]

Additionally, Raman tweezers experiments at 785 nm are carried out in a different home-built setup (Figure 1b). The beam of a diode laser, delivering about 7 mW at the sample, serves both the purposes of optical trapping and Raman excitation. It is expanded by a telescope to overfill the microscope objective (100x oil, NA =

[29] E. Messina; E. Cavallaro; A. Cacciola; R. Saija; F. Borghese; P. Denti; B. Fazio; C. D'Andrea; P. G. Gucciardi; M. A. Iatì, *J. Phys. Chem. C* **2011**, 115, 5115−5122.
[30] G. Pesce; G. Volpe; O. M. Maragò; P. H. Jones; S. Gigan; A. Sasso; Volpe, G. *J. Opt. Soc. Am. B* **2015**, 32, B84−B98.

1.3), then it is reflected by a mirror toward a notch filter (Semrock NF03-785E-25) which, again, reflects the laser beam toward the objective lens. The sample chamber is mounted on a piezostage (Physics Instruments, P-517.3 CL) with 1 nm resolution. The backscattered light passes through the notch filter, used for Rayleigh scattering removal, and is subsequently focused by a 50 mm lens onto a Horiba Jobin-Yvon Triax 190 spectrometer (190 mm focal length) equipped with a 1200 L/mm grating blazed at 650 nm. A high sensitivity CCD (Horiba Jobin-Yvon Synapse) is used for the signal detection. A beam splitter is inserted in the optical path to reflect 50 % of the scattered light toward a CCD camera (Thorlabs USB 2.0, DCU223M), allowing for visual inspection of the trapped particle.

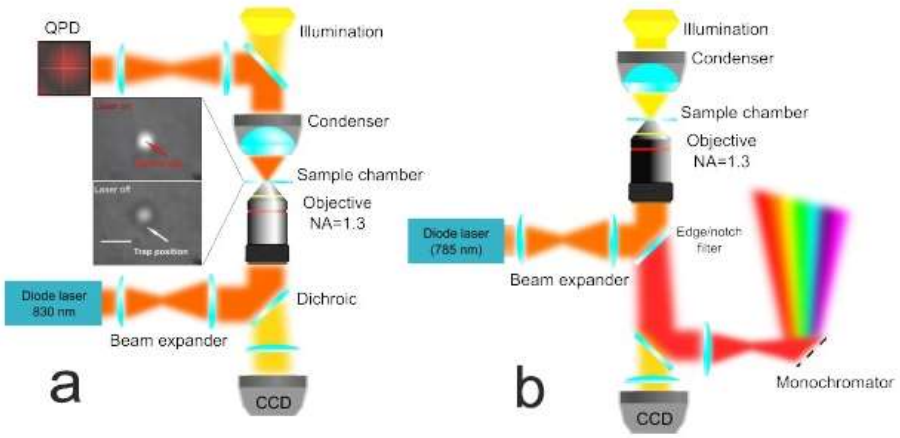

Figure 1. Experimental setups. (a) Sketch of the NIR optical tweezers. The light from a laser diode at 830 nm is expanded by a telescope and sent through an oil immersion (NA=1.3) microscope objective. Samples are loaded in a small chamber where individual capsules are optically trap in the focal spot. Accurate optical force measurements are achieved by particle tracking in the OT through back focal plane interferometry, i.e., by collecting the forward scattered and unscattered light onto a QPD. The same optics is used to image the sample with a lamp on a CCD camera. (b) Sketch of the Raman tweezers. Light at 785 nm from a laser diode is used to both trap and perform Raman spectroscopy. As for the NIR OT setup, the laser is tightly focused through an oil immersion objective (NA=1.3) into a chamber containing the capsules dispersion. Raman characterization and SERS are obtained by collecting the backscattered light from the trapped capsules through the same objective onto a grating spectrometer. A notch filter is used to both reflect the laser light and cut the Rayleigh scattering from the back-reflected radiation. Light from the spectrometer is detected with a highly sensitive CCD camera and analyzed by a PC.

Optical forces on particles stem from the conservation of linear momentum upon light scattering.[16] We calculate them by solving the light scattering problem in the T-matrix formalism for core−shell or cluster model particles illuminated by the tightly focused fields creating the optical tweezers. First, the optical fields in the focus of the high NA objective lens are calculated by means of the angular spectrum representation[31] in the absence of any particle. The resulting field is the field incident on the particles, and the radiation force exerted on any particle within the focal region is calculated by integrating the time-averaged Maxwell stress tensor in the far field:[31]

$$F_{rad} = r^2 \oint_{\Omega} \bar{T}_M \cdot \hat{r} d\Omega \qquad \text{(Equation 1)}$$

where the integration is over the full solid angle, r is the radius of a large sphere surrounding the particle, and $\bar{T}_M$ is the time-averaged Maxwell stress tensor in the Minkowski form in a homogeneous, linear and nondispersive medium.[16] Thus, the radiation force is expressed in terms of incident and scattered fields that can be expanded in vector spherical harmonics regular at the origin (Bessel multipoles) or at infinity (Hankel multipoles), respectively.[16] The linear relation between the scattered expansion amplitudes and the incident ones defines the T-matrix for the scattering process.[32] Optical force components are calculated by considering the projections of the radiation force vector on the different coordinate axes, e.g., $F_x = F_{rad} \cdot \hat{x}$, and calculating the corresponding numerical integral.[31] Optical forces on shell model particles (silica or silica-gold shells) are obtained using the Wyatt generalization of Mie theory for radially symmetric spheres,[33] while for the plasmonic shell-cluster model a T-matrix formulation of light scattering by a cluster of spheres[31] was used, where the

[31] F. Borghese; P. Denti; R. Saija; M. A. Iatì, *Opt. Express* **2007**, 15, 11984−11998.
[32] R. Saija; M. A. Iatì; F. Borghese; P. Denti; S. Aiello; C. Cecchi- Pestellini, *Astrophys. J.* **2001**, 559, 993−1004.
[33] P. J. Wyatt, *Phys. Rev.* **1962**, 127,1837−1843.

fields scattered by the spherical subunits comprising the aggregate are combined by using the addition theorem of multipole fields through a transfer matrix.[16]

4.3 Results and discussion

4.3.1 Plasmonic Capsules

The plasmonic capsules studied in these experiments have a hybrid structure that extends itself on two different length scales, that is, they are constituted by a microscopic porous hollow silica shell with a 1.4 μm diameter and a 30 nm thickness embedding plasmonic Au nanospheres. These mesoporous capsules are hollow and permeable, and Au nanoparticles are embedded on their inner walls. Figure 2a,c shows TEM images at different magnifications of the as-prepared plasmonic capsules after calcination, where individual Au nanoparticles are clearly distinguished in their inner cavity. According to the statistical distribution analysis (Figure 2d), the size of the Au nanoparticles is around 11 nm. The increase of the particle size, starting from the initial 2−3 nm Au particles, is achieved via a thermal process used also to remove the polymeric template. Hence, the large amount of small nanoparticles deposited onto the polystyrene template during the first step ensures the close vicinity of the nanoparticles necessary for the occurrence of collective plasmonic properties as a consequence of the thermal growth. Dispersions of 2−3 nm Au nanoparticles do not show localized surface plasmon resonances (LSPR), whereas plasmonic features appear only for larger particles (Figure 2b) as shown in the final structure.

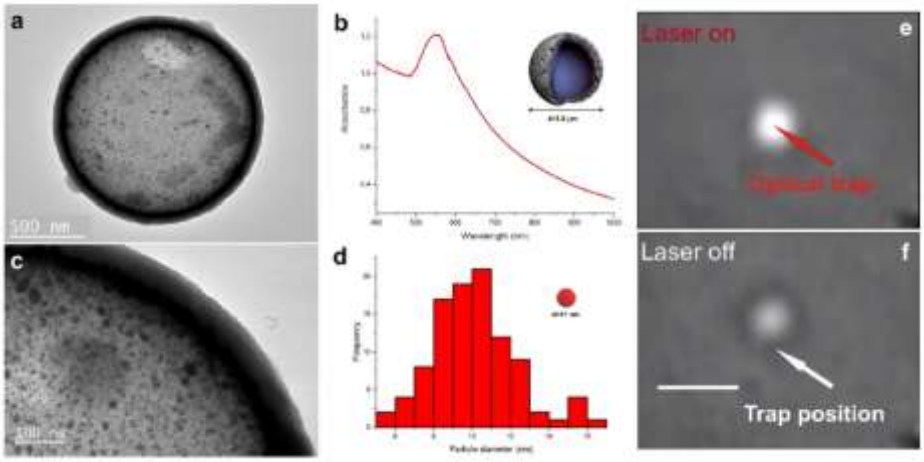

Figure 2. (a) TEM image of a 1.4 µm plasmonic mesoporous capsule. (b) Extinction spectrum of plasmonic mesoporus capsules dissolved in solution and sketch of the capsule structure (inset). (c) TEM image close-up of a mesoporous capsule evidencing the Au nanoparticle size distribution, whose histogram is shown in (d), on the inner side of the capsules. The averaged size of the Au nanoparticle is about 11 nm. (e,f) CCD images of a capsule when trapped in the optical tweezers (e) and when released from the trap (f). Scale bar is 2 µm.

4.3.2 Optical Trapping

Mesoporous capsules dispersed in ethanol have been used for optical trapping experiments in the NIR at 830 nm with 26 mW trapping power. The starting point for the measurement of optical forces is thermal noise analysis.[30] The three-dimensional motion of the optically trapped capsule is well described by the Langevin equation in the overdamped regime:[34]

$$\frac{dx_i(t)}{dt} = -\frac{k_i}{\gamma}x_i + \sqrt{2D}\,W_i(t), \quad \text{i= x, y, z} \qquad \text{(Equation 2)}$$

Where:

- $x_i(t)$ is the capsule displacement in the i-direction.
- k_i is the trap stiffness.
- $\gamma = 6\pi\eta R$ is the friction coefficient for a spherical particle of radius R with η being the medium (ethanol) dynamical viscosity.
- $D = k_B T/\gamma$ is the Stokes−Einstein diffusion coefficient.

[34] G. Volpe; G. Volpe, *Am. J. Phys.* **2013**, 81, 224–230.

- $W_i(t)$ is a white noise having $\langle W_i(t)\rangle = 0$, $\langle W_i^2(t)\rangle = 1$ for each value t, and $W_i(t)$ independent of $W_i(t + \tau)$ for $\tau \neq 0$.[16]

Equation 2 gives rise to first-order differential equations for the autocorrelation functions (ACFs) of the particle's displacements, $C_{ii}(\tau) = \langle x_i(t)x_i(t + \tau)\rangle$, that lead to simple exponential decays for the ACFs, $C_{ii}(\tau) = C_{ii}(0)\exp(-k_i\tau/\gamma)$, i.e., the autocorrelation function of the particle fluctuations decays in time with the relaxation rate $\omega_i = k_i/\gamma$. Thus, for an optically trapped spherical capsule a single-exponential fit to the displacement ACFs allows to measure the trap spring constants k_i, since η = 1.144 mPa·s (for ethanol at 20 °C) and R = 700 nm are known.

Figure 3 shows the statistical analysis of the tracking signal (Figure 3a) that points out, as usually observed with ordinary Gaussian beams,[30] how the trapped particles are more confined in the radial (x or y) than in the axial (z) direction (Figure 3b–d), i.e., the width of the particle position probability distribution $\rho(x_i)$ (solid line in Figure 3b) in the radial direction is smaller than in the axial direction (Figure 3b).

The single-exponential fit of the autocorrelation functions of the particle position (Figure 3c) gives higher relaxation rates in the radial than in the axial directions. 10 different capsules were trapped at a depth of about 20 µm for which three different QPD tracking signals were collected. The corresponding averaged force constants from all the measurements are normalized to the power at the sample. Thus, the values obtained were k_x/P = 0.9 ± 0.4 pN/(nm W), k_y/P = 1.0 ± 0.5 pN/(nm W), and k_z/P = 0.5 ± 0.2 pN/(nm W). Finally, by exploiting the particle position probability distribution (Figure 3b), the optical potential $U(x_i) = -k_bT\log[\rho(x_i)] + U_0$ can be calculated (Figure 3d). The optical trap is well approximated by a harmonic potential and it is steeper in the radial than in the axial direction.

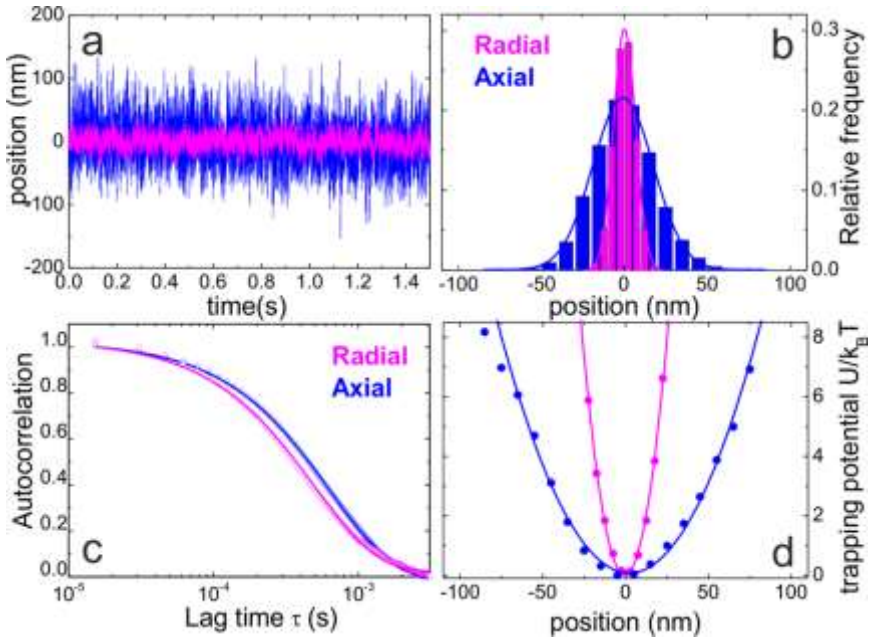

Figure 3. Optical force calibration for optoplasmonic capsules. (a) Measured tracking signals in the radial (magenta) and axial (blue) directions of the trap, representing the positional thermal fluctuations of a trapped mesoporous capsule. (b) Corresponding histograms of the capsule position related to the probability distribution in the confining potential. (c) Autocorrelation function analysis obtained from the positional fluctuations in (a). Their decay rates are related to the spring constants of the trap and serve for the full force calibration. (d) Reconstruction of the effective optical confining potential in the radial (magenta) and axial (blue) directions.

The calibration of the positional fluctuations and of the effective optical trapping potential enables the accurate reconstruction of the Brownian dynamics in the OT and their use for force sensing with femtonewton resolution.[30]

Figure 4 compares the Brownian motion of an optically trapped plasmonic capsule (Figure 4a) to that of a latex bead (Figure 4b) with radius (R = 1 μm) close to that of the capsule and to that of an individual spherical AuNP (Figure 4c) with a radius (R = 10 nm) close to that of the AuNPs embedded in the plasmonic capsule. This comparison shows visually how plasmonic capsules are optically confined with a strength close to that of solid latex beads despite their interaction volume is reduced to their hybridized shell. On the contrary, individual bare AuNPs are much less confined and difficult to trap, showing how hybridization of the

silica shell with AuNPs plays the key role in increasing optical trapping efficiency in the plasmonic capsule.

For a direct quantitative comparison of optical forces on different particles, it is often useful to divide optical forces by n_mP/c, with n_m being the refractive index of the surrounding medium (ethanol or water), c the velocity of light in vacuum, and P the laser power at the sample. This enables to normalize for the effects of different trapping power and surrounding medium refractive index. Thus, from our trapping measurements the optical trapping efficiencies in terms of reduced spring constants were calculated, $q_i = ck_i/n_mP$.

Table 1. Optical Trapping Efficiencies for Different Types of Particles: Plasmonic Capsules, Latex Beads, and Gold Nanoparticles (The efficiency values are averaged over the spring constant measurements from 10 different particles. Uncertainties represent the standard deviation from the mean values).

Efficiency (μm^{-1})	Capsules 0.7 µm	Latex beads 1 µm	AuNP 10 nm
q_x	0.20 ± 0.08	0.55 ± 0.03	(1.0 ± 0.3) x 10^{-2}
q_y	0.2 ± 0.1	0.56 ± 0.04	(1.1 ± 0.3) x 10^{-2}
q_z	0.10 ± 0.05	0.11 ± 0.01	(0.9 ± 0.5) x 10^{-2}

Table 1 compares the measured reduced spring constants, q_i, calculated for the three samples shown in Figure 4. The best trapping is obtained with latex beads, but also silica−Au capsules have quite good efficiencies, considering that they are smaller and also hollow, and they are almost 2 orders of magnitude better confined than individual AuNPs, which have very small trapping efficiencies due to the volumetric scaling of optical forces at the nanoscale.[15]

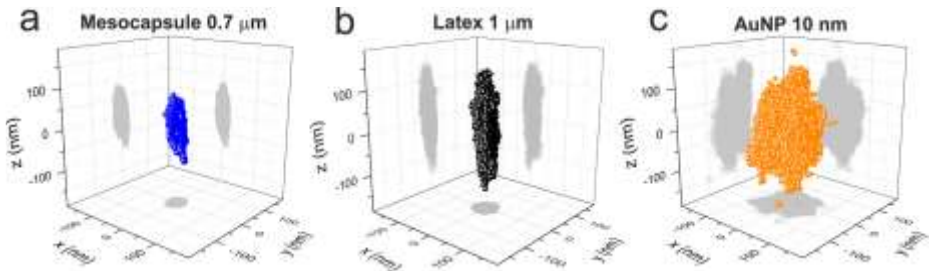

Figure 4. Reconstruction of Brownian motion for different types of spherical particles in the optical trap for similar experimental conditions: (a) optoplasmonic capsule trapped in ethanol, R = 0.7 μm, (b) solid latex particle trapped in water, R = 1 μm, and (c) individual gold nanoparticle trapped in water, R = 10 nm. Despite the hollow optoplasmonic capsule has an interaction volume much smaller than the solid latex bead, it is optically confined with a similar strength due to the hybridization of its silica shell with plasmonic nanoparticles.

In the hybrid capsule, the presence and aggregation of the metal nanoparticles in the inner (30 nm) shell yield an effective increase of the optical trapping force of the whole structure. Moreover, the trapping efficiency was comparable to that of a solid microparticle despite the much smaller (about 20 times) interaction volume of the hollow plasmonic capsule. This observed large trapping efficiency for the hollow plasmonic capsule is due to the plasmon-enhanced optical forces acting on the hybridized mesoporous shell.

Finally, it is remarkable that heating effects of the plasmonic samples in the trap are negligible as they generally occur at higher power[35] (above 50 mW) or for wavelengths resonant with the particle plasmonic response so that enough absorption is converted into heat.[36] We are far from both conditions. However, these are intriguing aspects as plasmonic capsules can act as thermally activated cargos to release molecules chemically attached to the gold component. Further studies in a double-wavelength configuration,[7] where a NIR beam traps the capsule and a visible resonant beam thermally excites the structure, can gain insights on this perspective.

[35] Y. Seol; A. E. Carpenter; T. T. Perkins, *Opt. Lett.* **2006**, 31, 2429–2431.
[36] M. Šiler; J. Ježek; P. Jákl; Z. Pilát; P. Zemánek, *Opt. Lett.* **2016**, 41, 870–873.

4.3.3 Theory

To understand the experimental results, the optical trapping forces were calculated by solving the electromagnetic scattering problem in the T-matrix[32] approach for tightly focused fields.[31]

While hollow spheres, with an inner index of refraction lower than the surrounding medium, cannot be trapped[37] in an ordinary Gaussian beam, the silica shells are permeable to ethanol and, thus, internal and external refractive indexes are the same (nm = 1.36). Moreover, the silica shells embed small Au nanoparticles on the inner silica shell wall with a random spatial distribution. To understand the role played by both the silica shell and the distribution of AuNPs in the optical trapping mechanism of the hybrid capsule, the scattering process and optical forces were calculated for several model particles and compared with those obtained for a solid latex bead and gold nanoparticles with a 6 nm radius equal to the average radius of the AuNPs of the hybrid capsule. In Figure 5, the optical force efficiencies, $Q_i = cF_i/n_mP$ (i = x,y,z), calculated for several models are presented. Optical trapping occurs when all Q_i vanish with a negative derivative.[31] As expected, both a 1 μm latex bead (Figure 5a) and an individual AuNP (Figure 5b) can be trapped with different efficiencies dictated by size and material properties. Interestingly, also a 30 nm thick permeable silica shell (Figure 5c) without AuNP inclusions can be trapped in two equilibrium positions, even if the trapping efficiency is about 2 orders of magnitude lower than that of a solid latex bead (Figure 5a). However, if it is used a model (Figure 5d) consisting of an outer silica shell and an inner homogeneous Au shell with 12 nm thickness (corresponding to the hybridizing AuNPs diameter), no trapping is obtained, as scattering forces are much stronger than trapping ones because of the gold shell large extinction at this trapping wavelength (830 nm). Thus, optical

[37] S. E. Skelton; M. Sergides; G. Memoli; O. M. Maragó; P. H. Jones, *J. Opt.* **2012**, 14, 075706.

forces were calculated for a spherical shell cluster (Figure 5e) of gold particles with 6 nm radius containing an increasing number, N, of AuNPs in a regular configuration, shell-cluster model. By increasing the number of AuNPs, a crossover in the optical trapping behavior for about 50 particles in the shell-cluster is observed (Figure 5f). When the particle number is too small (low number density), the optical trapping strength is related to the individual AuNP trapping, that is, the distance between AuNPs is so large that the interaction between the high intensity region of the OT occurs only with one particle. However, when the particle number is above 50, the increase in optical trapping follows a N^2 scaling law (dashed line in Figure 5f). In fact, in the shell-cluster calculations, the interparticle distance considered (>80 nm) is always much larger than the particle diameter (12 nm) and a weak plasmonic coupling and small red shift occur. Thus, the increase of optical trapping is consistent with the particle number density increase on the shell within the focal interaction region. Clustering at a large number density can make the plasmon band red shift when plasmonic coupling occurs for short (roughly the particle size) interparticle distance. This can also contribute to enhancing optical trapping forces in the NIR.[38]

[38] E. Messina; E. Cavallaro; A. Cacciola; M. A. Iatì; P. G. Gucciardi; F. Borghese; P. Denti; R. Saija; G. Compagnini; M. Meneghetti, *ACS Nano* **2011**, 5, 905–913.

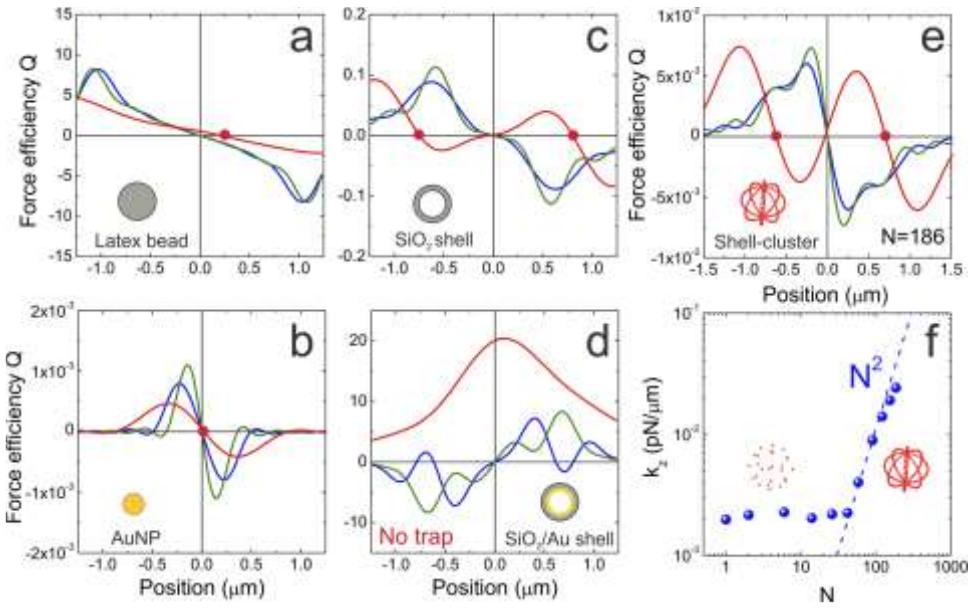

Figure 5. Optical trapping efficiencies, Qx (blue lines), Qy (green lines), Qz (red lines), calculated through the T-matrix approach for different types of model particles and cluster: (a) a latex bead (R = 1 μm), (b) an individual AuNP (R = 6 nm) similar to the particles hybridizing the capsules, (c) a 30 nm thick permeable silica shell, (d) an hybrid silica-gold double shell, and (e) a shell-cluster composed of 186 AuNPs distributed over a spherical surface equal to the capsule one. Note how the model shell particles in (c) and (e) have two stable axial trapping positions (red dots) corresponding to their maximum overlap with the high intensity spot of the OT. Instead, when a full silica-gold double shell is considered, there is no trapping point as scattering forces increase because of the large extinction of the full gold shell. (f) Optical force constant for the shell-cluster model in the axial (light propagation) direction as a function of AuNPs number, N. A quadratic power law scaling (dashed line) is superposed to the numerical data points.

4.3.4 Spectroscopic Applications

Finally, as a proof-of-concept, the use of optically trapped plasmonic capsules for SERS applications was explored. OT are tools that work intrinsically in liquid with the capability to explore soft surroundings in three-dimensions with nanoscopic precision.[39] They offer the opportunity to spectroscopically

[39] T. F. Bartsch; M. D. Kochanczyk; E. N. Lissek; J. R. Lange; E. L. Florin, *Nat. Commun.* **2016**, 7, 12729.

explore a region of interest in the surface or even inside biological samples.[40]

Thus, having the opportunity to combine OT with SERS (SERS tweezers) is key to probe the physical chemistry of soft environments and to observe the Raman response of molecules directly in their natural state,[12] with particular relevance for the case of *in situ* monitoring the evolution of analytes at very specific locations when dealing with biological systems at a cellular scale. However, devising the most efficient strategy for SERS tweezers is still a challenge. This is due, on one side, to the difficulty in manipulating nanoparticles with an efficient plasmonic response, and on the other side to exciting SERS without affecting the trapping behavior. The route to accomplish this is to design special SERS-active probes consisting of metal colloids bound to optically trappable microscopic particles.[41] In this context, the plasmonic capsules described herein represent a novel strategy for SERS tweezers.

We successfully used the plasmonic capsules for SERS by means of a single-beam Raman tweezers setup[29] operating at a single wavelength, 785 nm, used both for trapping and Raman excitation.

In Figure 6, the spectra obtained in 2×10^{-5} M (Figure 6a) and 5×10^{-5} M (Figure 6b), methylene blue (MB) water–ethanol solutions are shown, with (red lines) and without (purple lines) a capsule in the trap. In (a) with respect to (b), we increased 4 times the water content in the solution to reduce the Raman contribution of ethanol (asterisks in Figure 6b) to the spectrum that would make the identification of MB Raman peaks more difficult. Even at the low concentration of 2×10^{-5} M (Figure 6a), and with only one capsule in the trap, the presence of methylene blue in the solution

[40] C. Xie; C. Goodman; M. A. Dinno; Y. Q. Li, *Opt. Express* **2004**, 12, 6208–6214.
[41] S. Balint; M. P. Kreuzer; S. Rao; G. Badenes; P. Miskovsky; D. Petrov, *J. Phys. Chem. C* **2009**, 113, 17724–17729.

is recognized, as the most representative peaks at approximately 450, 503 (δ(C−N−C) doublet) and 1440 cm^{-1} (α(C−H)) are observed.[42] On the contrary, no MB peaks are observed in the spectrum obtained without the capsule in the trap (purple line, Figure 6a), where only a small band at 450 cm^{-1} due to ethanol background is observed. Thus, the SERS enhancement of MB peaks is clearly due to the AuNPs on the inner walls of the capsule itself, which can be reached by methylene blue due to the porosity of the silica shell.

For reference and comparison, we performed SERS on a drop cast dry (without ethanol) capsule sample with a commercial Jobin-Yvon HR800 micro-Raman setup at 785 nm excitation wavelength.[43] Figure 6c shows the spectrum of a 1×10^{-4} M aqueous solution of MB molecules drop cast and dried on a glass slide (black line) and the SERS spectrum (blue line) obtained when capsules are dispersed in MB solution at the same concentration, drop cast, and dried on the glass substrate. On dry samples, the MB Raman signal is increased about 40 times in the presence of capsules (estimated from the peak at 450 cm^{-1}). This amplification factor or SERS gain,[43] $I_{SERS}/I_{Raman} \sim 40$, measures the absolute signal enhancement that a SERS substrate (the capsule) can provide for SERS-active molecules (MB). This factor is much smaller than the so-called SERS enhancement factor, EF, defined as the scattering enhancement provided by each gold nanoparticle on a single molecule. The latter can be calculated upon normalizing the SERS and the Raman signals to the number of probed molecules in each experiment, $EF = I_{SERS}n_{Raman}/I_{Raman}n_{SERS}$, where n_{Raman} and n_{SERS} are the number of

[42] A. Camposeo; D. Spadaro; D. Magrì; M. Moffa; P. G. Gucciardi; L. Persano; O. M. Maragò;D. Pisignano,
Anal. Bioanal. Chem. **2016**, 408, 1357−1364.
[43] C. D'Andrea; B. Fazio; P. Gucciardi; M. Giordano; C. Martella; D. Chiappe; A. Toma; F. Buatier de Mongeot; F. Tantussi; P. Vasanthakumar, *J. Phys. Chem. C* **2014**, 118, 8571−8580.

probed molecules in the Raman and SERS experiments, respectively. An estimate of the number of probed molecules, n_{Raman}, can be obtained assuming that all molecules within the 785 nm laser spot area, $A_{las} = \pi d_{las}^2/4 \sim 2\ \mu m^2$, do contribute to the Raman signal (I_{Raman}), where $d_{las} \sim 1.5\ \mu m$ is the laser spot diameter used in the micro-Raman spectrometer. On the other hand, only MB molecules adsorbed on the gold nanoparticles surface within the capsule, $A_{meso} = N\pi d_{np}^2 \sim 0.7\ \mu m^2$, will contribute to the SERS signal (I_{SERS}), where $N \sim 2 \times 10^3$ and $d_{np} \sim 11$ nm are, respectively, the average number and average diameter of gold nanoparticles in the capsule (estimated from TEM images, Figure 2). Thus, assuming that in both cases are probed the same number of MB layers, it is estimated an enhancement factor of about $EF = I_{SERS}A_{las}/I_{Raman}A_{meso} \sim 10^2$, which is a reasonable number for weakly coupled nanoparticles excited out of resonance.[42] Finally, it is remarkable that while using 785 nm wavelength ensures stable optical trapping of the capsules in the Raman tweezers, this is not the most efficient wavelength for SERS detection on these structures.

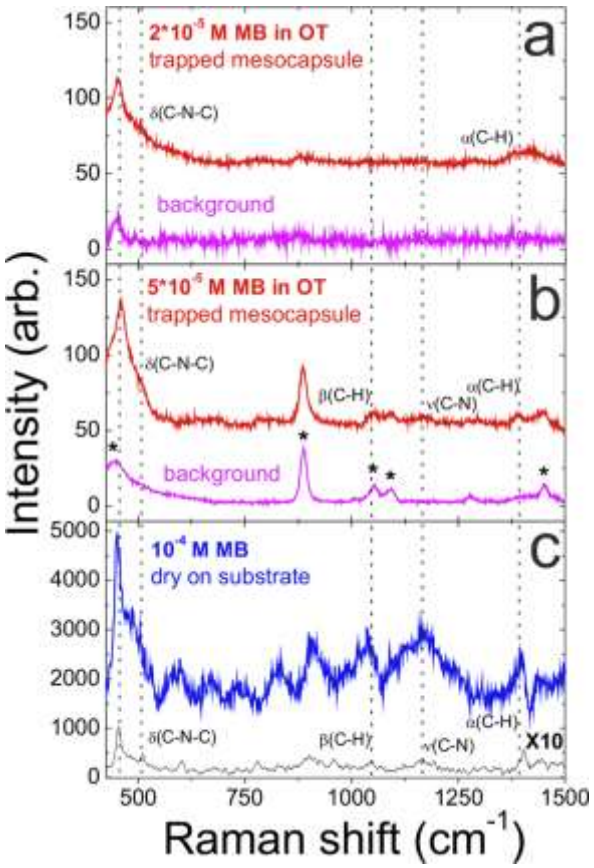

Figure 6. (a,b) SERS spectra obtained by trapping a plasmonic capsule in a Raman tweezers (785 nm trapping and excitation wavelength). Spectra in red are obtained by trapping a capsule in a 2×10^{-5} M (a) and 5×10^{-5} M (b) methylene blue–water–ethanol solution. Few of the MB peaks are evident even at the lowest concentration (the δ(C–N–C) doublet and the α(C–H)). Spectra in purple are obtained in the same solution without trapped particle showing only the ethanol background. For reference and comparison, in (c) it is shown the spectrum of a 1×10^{-4} M aqueous solution of methylene blue drop cast and dried on a glass slide (black line) and the SERS spectrum (blue line) obtained when capsules are dispersed in the MB solution, drop cast, and dried on the glass substrate. These spectra were obtained with a commercial Jobin-Yvon HR800 micro-Raman spectrometer at 785 nm excitation wavelength. The assignment of the most representative MB Raman peaks are indicated. On dry samples, the MB Raman signal is increased about 40 times in the presence of capsules. Data are displaced for clarity.

However, while a wavelength more resonant with the plasmon band is expected to yield a larger SERS signal, this would be less suitable for trapping as the increased radiation pressure would destabilize the optical trap. In order to improve SERS detection with trapped capsules, a double wavelength setup[7] with independent trapping (in the NIR) and resonant SERS excitation

could be used. Another possible strategy could be to modify the gold nanoparticle shape, e.g., using nanorods instead of spheres, or increasing their aggregation and coupling so that plasmon resonance peaks in the red would appear, enhancing SERS with 785 nm excitation.[44]

4.4 Conclusion

In conclusion, the optical trapping forces on hybrid silica-gold optoplasmonic capsules was investigated. Their increased trapping efficiency is governed by the plasmonic enhancement of optical forces due to the AuNP distribution inside the permeable silica shell. By accurately solving the light scattering problem in the tightly focused spot of the OT, it was calculated and compared optical forces for several model particles, finding a quadratic number scaling law for a shell-cluster model mimicking the optoplasmonic hybridized capsule. Finally, by means of Raman tweezers, the trapped capsules were used as local SERS molecular probes at 10^{-5} M concentration in a liquid environment. Hybridization of optical forces at the mesoscale hold perspectives to combine plasmonic response with dielectric scaffolding for smart cargos driven by light with an unprecedented ability for their individual localization. The opportunity to trap and direct hollow and porous capsules in biological fluids is of paramount importance for theranostics, high resolution imaging, and controlled drug release.

[44] C. D'Andrea; A. Irrera; B. Fazio; A Foti; E. Messina; O. Marago; S. Kessentini; P. Artoni; C. David; P. Gucciardi, *J. Opt.* **2015**, 17, 114016.

General Conclusions

Although some conclusions have been presented in each chapter, here a compilation of the most relevant are shown as global conclusions of the work.

The synthesis of plasmonic nanocapsules have been performed successful. The size of the gold nanoparticles can be controlled. In this way, the optical properties can be modified.

This nanostructures can be used to detection by Surface Enhanced Raman Spectroscopy (SERS) due to the confinement of gold nanoparticles inside of the capsule in the inner wall.

The trimethoprim, an antibacterial compound, have been detected using this kind of nanocapsules by direct detection. The molecule of trimethoprim has affinity for the gold nanoparticles, therefore the trimethoprim is anchored inside of the plasmonic nanocapsules and can be detected by optical spectroscopy.

The detection of trimethoprim was performed in wastewater (a complex matrix) and, even, in presence of other contaminants. So, trimethoprim detection is a specific detection.

Other contaminants can be detected by indirect detection. Using a Raman linker that connect the gold nanoparticles with the emerging contaminants. The Raman linker can be modify to acquire more affinity with the compound that it has to be detected.

A multiplex detection can be performed if the linker has affinity for several targets. In this case, a deconvolution of spectra can be used to separate the bands of the spectrum and perform the assignment easily.

Theoretical spectra were obtained using computational methods. Gaussian program was used to obtain them through Hartree-Fock and DFT methods. This spectra provide information that can help to the assignment of the bands.

Optical tweezers are a key technique about manipulation of micro and nanosized particles.

Optical trapping can enhance the signal SERS. For this reason, the combination between optical tweezer and SERS spectroscopy can be used a powerful and multifunctional sensing platform.

Plasmonic capsules show a trapping efficiency much higher than an individual gold nanoparticle due to the confinement of the gold nanoparticles in the plasmonic capsule.

Plasmonic capsules were used as local SERS probes. This technique can be very useful for the case of *in situ* monitoring.

Resumen

En este resumen se pretende plasmar la idea de este trabajo que se centra en la síntesis de cápsulas plasmónicas con el objetivo de utilizarlas como sensores de contaminantes emergentes. Para ello se muestra un extracto de la introducción que acerca los conceptos clave que se tratan en este trabajo y se hace un breve resumen de los capítulos 2, 3 y 4.

5. 1 Objetivo

La síntesis de nanocápsulas ha atraído un gran interés en los últimos años debido a su gran número de aplicaciones en diferentes áreas de la ciencia y la tecnología.

Esto es debido a sus propiedades únicas como la capacidad de encapsular, el control en la permeabilidad de la superficie y la posible funcionalización de ésta.

Entre las posibles aplicaciones de estas nanoestructuras huecas están: transportar y liberar fármacos de forma controlada, su utilización como nanorreactores, estabilización de catalizadores, almacenamiento de hidrógeno, construcción de bloques para cristales fotónicos, células artificiales y biosensores.

El objetivo de este trabajo es realizar la síntesis de cápsulas plasmónicas que permitan la detección óptica de contaminantes emergentes. Éstos han adquirido gran relevancia en los últimos años debido a que la exposición prolongada puede causar daños en los organismos siendo un problema medio ambiental.

5.2 Introducción

5.2.1 Nanopartículas

Se consideran nanopartículas aquellas partículas que su tamaño está entre 1 y 100 nanómetros. Mientras que partículas micrométricas presentan propiedades muy similares a las del sólido volumétrico del mismo material, las nanopartículas debido a su reducido tamaño presentan propiedades bastante distintas del sólido macroscópico.

En estas pequeñas partículas, tanto el tamaño como la forma son muy determinantes en las propiedades electrónicas. Esto se debe, básicamente, a un aumento en la relación superficie/volumen que también puede afectar a otras propiedades de las partículas: termodinámicas, químicas, espectroscópicas, electromagnéticas, etc.

Estas distintas propiedades han provocado una gran atención para conseguir crear materiales, aparatos y sistemas novedosos con propiedades únicas y posibles aplicaciones muy relevantes.

Dentro de las nanopartículas destacan las de oro, plata y cobre debido a las importantes variaciones de sus propiedades ópticas. El caso del oro es muy visual ya que a medida que se reduce su tamaño sufre importantes variaciones de color.

En el siglo XX muchos métodos de síntesis de nanopartículas metálicas han sido desarrollados. A partir del método de síntesis elegido se puede controlar el tamaño, la forma y la dispersión de las nanopartículas, pudiendo así variar la resonancia de plasmón superficial y controlando, por tanto. las propiedades ópticas, eléctricas, catalíticas, etc.

5.2.2 Nanoestructuras huecas

La síntesis de nanocápsulas es de gran interés debido a las aplicaciones potenciales que tiene en catálisis, cristales fotónicos, cromatografía, nanomedicina, baterías recargables, sensores y materiales antibacterias.

La gran ventaja que aportan estas estructuras es que sus propiedades cambian variando su composición química. Esto hace posible diseñar cápsulas que respondan a un estímulo específico

como, por ejemplo, el pH, el campo magnético o el calor. Así se podría liberar el contenido de la cápsula en el lugar y en el momento deseados.

Muchas han sido las estrategias desarrolladas para obtener nanocápsulas huecas aunque la técnica más frecuentemente utilizada es la que emplea una plantilla, debido a que permite sintetizar nanocápsulas de tamaño manejable con capas densas, homogéneas y del grosor deseado.

5.2.3 Modificación superficial

Como se ha mencionado anteriormente, la gran peculiaridad de las partículas a nivel nanométrico es su elevada relación superficie/volumen siendo las propiedades superficiales las que determinan las propiedades del sistema. Por este motivo, adquiere gran importancia el poder modificar la superficie, proporcionándole a ésta las características y propiedades que se desean. Por tanto, la modificación superficial en nanopartículas permite que las propiedades que dependen de su estructura electrónica y de su organización espacial se puedan modificar, prácticamente, a voluntad.

El método más conocido de modificación superficial es el Layer-by-Layer, siendo una técnica sencilla y asequible. Utilizando esta técnica se pueden formar multicapas alrededor de una partícula permitiendo, además, incorporar nuevos materiales.

Es importante destacar que la formación de multicapas por el método layer-by-layer no está restringida a sustratos con la superficie plana, ya que esta técnica es independiente del tamaño y forma del sustrato.

Otra de las grandes ventajas de esta técnica es que permite controlar el espesor de la capa con gran precisión (resolución nanométrica) variando los materiales específicos usados, el número de capa ensambladas y las condiciones usadas en la adsorción específica (temperatura, fuerza iónica y polaridad de disolvente).

También es muy utilizado el recubrimiento de sílice que puede modificar las propiedades de las nanopartículas. Estas esferas de sílice que recubren las nanocápsulas pueden ser preparadas por el método de Stober, el cual consiste en la hidrólisis y condensación de tetraetilortosilicato (TEOS) en una mezcla de agua, amoniaco y alcohol.

La sílice es ampliamente utilizada para el recubrimiento de coloides debido a su alta estabilidad. Pero hay otras propiedades que la hacen ideal para esta función como que es químicamente inerte, la capacidad de poder controlar su porosidad y su transparencia óptica. Por tanto la capa de sílica le proporciona a las partículas protección estérica y electroestática y además actúa como agente dispersante de mucho coloides electroestáticos dándole gran estabilidad. Además, este recubrimiento permite que se pueda seguir funcionalizando y proporciona biocompatibilidad permitiendo así, que se puedan utilizar estos nanomateriales en el campo de la nanomedicina.

5.2.4 Propiedades ópticas

Las propiedades ópticas de ciertos metales de tamaño nanométrico están fuertemente dominadas por el fenómeno conocido como resonancia de plasmón superficial. Este fenómeno tiene más relevancia en el oro, la plata y el cobre ya que para ellos

la frecuencia de resonancia está en la región visible del espectro electromagnético.

Los plasmones son ondas generadas por el movimiento colectivo de electrones libres en la superficie de un metal. Por tanto el fenómeno de resonancia plasmónica se puede definir como el acoplamiento del campo eléctrico de la radiación electromagnética incidente con la vibración de los electrones de conducción del metal.

5.2.5 Espectroscopía Raman

Una técnica que está relacionada con las propiedades ópticas es la espectroscopía Raman.

Cuando un haz de luz monocromática incide sobre la materia puede ocurrir que parte de la luz sea reflejada, que parte de la luz sea refrectada, que toda o parte de la radiación incidente sea absorbida o puede cambiar su dirección al interaccionar con la materia y ser dispersada en todas las direcciones. Éste último fenómeno es conocido como dispersión o scattering.

Cuando el fotón y la molécula chocan, la colisión puede ser elástica, es decir, ni la molécula ni el fotón ganan o pierden energía. Pero puede suceder que la colisión entre el fotón y la molécula sea inelástica. En este caso la molécula puede ganar o perder energía (rotacional o vibracional) y emitirse, por tanto, un fotón de energía menor o mayor que la radiación incidente. Este efecto se denomina efecto Raman.

Por tanto, el efecto Raman es un fenómeno de la dispersión de la luz.

Un espectro Raman comprende varias líneas Raman diferentes generadas por dispersión de diferentes vibraciones moleculares. La dispersión Raman proporciona una gran información de la estructura y composición de la materia. Esto ha hecho posible que se aplique en distintos campos como la industria alimentaria, la industria petroquímica, en biomedicina o medioambientalmente. Sin embargo, el efecto Raman es excesivamente débil.

5.2.6 Espectroscopía Raman amplificada por supercie (SERS)

Esta espectroscopía conocida como SERS, por sus siglas en inglés (Surface Enhanced Raman Scattering), es una técnica para el estudio de superficies cuyo fundamento consiste en la intensificación de la dispersión Raman de moléculas adsorbidas sobre superficies metálicas rugosas.

Los efectos espectroscópicos pueden verse fuertemente afectados cuando ellos tienen lugar justamente al lado de superficies y nanoestructuras metálicas debido al acoplamiento con los plasmones superficiales. Los campos electromagnéticos mejoran debido a estas resonancias entre los campos ópticos y los plasmones superficiales. Esto permite una redistribución de intensidades de campo en la vecindad de las nanopartículas provocando áreas de mejora para el proceso Raman.

Las mejores nanoestructuras metálicas para llevar a cabo esta gran mejora en la señal Raman son el oro, la plata y el cobre debido a que cumplen la condición de tener la resonancia plasmónica en el rango visible e infrarrojo cercano.

Esta señal registrada es, básicamente, un espectro vibracional por lo que proporciona información del sistema molecular estudiado.

Esto hace que la espectroscopía SERS sea considerada una técnica analítica con una gran sensibilidad.

La técnica SERS tiene como limitación, y por eso no está más ampliamente utilizada en ciencia de superficies, que está esencialmente restringida a substratos metálicos nobles. Ya que la actividad del SERS depende críticamente de la naturaleza del metal y la rugosidad de la superficie.

Por tanto, en resumen, el factor de intensificación de la señal Raman en la espectroscopía Raman amplificada por superficie depende de: la longitud de onda del láser, de la naturaleza del sustrato, de la morfología de la superficie (su rugosidad) y de la distancia y orientación de la molécula respecto a la superficie.

Es una técnica muy sensible que permite detectar moléculas sencillas. Utilizar esta técnica también conlleva un aumento de la selectividad. Esto permite que sea un método prometedor para bioanalítica ya que combina el alto nivel de información estructural que aporta la espectroscopía vibracional con límites de detección ultrasensibles.

Actualmente se acepta que el gran aumento de la intensidad de la señal respecto al Raman original se debe a dos mecanismos fundamentales:

- El modelo electromagnético (EM): la radiación se intensifica enormemente en las inmediaciones de una superficie metálica rugosa.
- El modelo químico o de transferencia de carga (TC): la sección eficaz de una molécula se intensifica por la formación de un complejo molécula-metal y la transferencia de carga de uno a otro.

Ambos contribuyen al modelo SERS aunque la contribución de cada uno depende del sistema a estudiar. Siendo el EM el que hace la principal contribución.

5.2.7 Contaminantes emergentes

Los contaminantes emergentes se han convertido en un riesgo ambiental para la salud pública.

Se llama contaminantes emergentes a los productos químicos, tanto naturales como sintéticos, que no se miden ni controlan habitualmente en el medio ambiente pero que pueden producir efectos perjudiciales tanto en el medio como en la salud humana.

Entre ellos destacan los principios activos farmacéuticos debido a que son compuestos relativamente poco biodegradables que se vierten continuamente (especialmente en hospitales) y que los sistemas de depuración actuales no están preparados para eliminarlos completamente.

Estos principios activos farmacéuticos que son utilizados a nivel mundial incrementándose su presencia en el medio acuático han generado gran preocupación por los riesgos ecológicos derivados de su liberación al medio ambiente.

5.3 Capítulo 2

Este capítulo abordará la posibilidad de utilizar las cápsulas plasmónicas sintetizadas como sensores para detectar contaminantes emergentes.

La trimetoprima es un agente antibacteriano, ampliamente utilizado en medicina y en veterinaria, siendo uno de los contaminantes emergentes más comúnes. Este compuesto puede

ser combinado con el sulfametoxazol para obtener un compuesto antibacteriano de amplio espectro. Prácticamente el 90% de la trimetoprima no es metabolizada siendo excretada en la orina sin modificación alguna.

Debido a su gran uso, se ha elegido a este contaminante como prueba para la comprobación de si las plantas de tratamiento de aguas residuales funcionan correctamente.

La trimetoprima tiene un pequeño tamaño que le permite difundir a través de los poros de la capa de sílice mesoporosa y así entrar en el interior de la cápsula hueca. El grupo amino de la trimetoprima hace posible que éste contaminante quede retenido en el interior de las nanocápsulas plasmónicas debido a la afinidad que hay entre el grupo amino y el oro.

La detección del contaminante se llevará a cabo mediante espectroscopía Raman. Esta técnica proporciona el espectro vibracional de las moléculas, el cuál es único para cada una de ellas por lo que puede actuar cómo una huella dactilar. El principal problema de la espectroscopía Raman es que la señal normalmente es muy débil. Por lo tanto, es necesario aumentar la intensidad Raman. La técnica SERS posibilita obtener una mayor intensidad Raman si la molécula a estudiar está muy cerca de una superficie metálica ya que el campo electromagnético aumenta.

La caracterización del sensor se realiza mediante TEM y espectroscopía de UV-Vis. Este sensor de un tamaño de 530 nm está formado por una capa de sílice mesoporosa y las nanopartículas de oro del interior. El tamaño de estas partículas de oro del interior puede ser controlado. Para este trabajo han sido utilizadas las siguientes muestras:

- PS@Au: Las partículas poliméricas de poliestireno funcionalizadas por nanopartículas de oro de 3 nm.
- PS@AuGrown: Partículas de poliestireno con nanopartículas de oro crecidas de un tamaño aproximado de 24 nm.
- Au@SiO_2: Estas partículas están formadas por una capa de sílice mesoporosa y nanopartículas de oro en el interior de un tamaño de 12 nm. Las partículas PS@Au son recubiertas por sílice mesoporosa y posteriormente calcinadas a altas temperaturas para eliminar el poliestireno obteniendo la estructura hueca. En el proceso del tratamiento térmico las nanopartículas de oro aumentan su tamaño.
- Au(Growth 1)@SiO_2: Las nanopartículas de oro del interior son más grandes (22 nm) debido a que se ha realizado un proceso de crecimiento con ácido tetracloroáurico y formaldehído que actúa como reductor.
- Au(Growth 2)@SiO_2: Se realiza un segundo crecimiento para obtener esta muestra con las nanopartículas de oro más grandes (30 nm).

En la caracterización de estas muestras mediante espectroscopía UV-Vis se observa que al aumentar el tamaño de las nanopartículas del interior, la banda del plasmón superficial se desplaza hacia el infrarrojo. Esto demuestra que al variar el tamaño de las nanopartículas del interior se varían las propiedades ópticas de la estructura.

Para evaluar la eficiencia de las cápsulas como plataforma SERS se utilizó la molécula 4-Aminotiofenol (molécula que proporciona un buen espectro Raman) y se comprobó la intensidad obtenida para las distintas estructuras. Para la estructura Au@SiO2 no se observa una buena señal SERS debido al pequeño tamaño de las nanopartículas de oro y, por tanto, la poca cantidad de hot spots

formados. Es reseñable que la estructura con la que se obtiene mayor señal SERS es Au(Growth 2)@SiO_2 siendo la intensidad obtenida tres veces mayor que las cápsulas a las que se le ha realizado un solo crecimiento.

Por lo tanto será la estructura Au(Growth 2)@SiO_2 la utilizada para detectar la trimetoprima, siendo el láser utilizado el 785 nm (que comparado con los láseres 633 nm y 532 nm, es con el que se obtiene mejor señal en este caso).

El uso de cápsulas plasmónicas para la detección de trimetoprima ofrece varias ventajas. La principal es que la sílice mesoporosa proporciona un lugar más protegido dónde realizar la detección y así evitar posibles interferencias en la medida (hay que tener en cuenta que la detección se realiza en muestras de aguas residuales, por tanto es una matriz compleja). Además, como se ha mencionado el uso de las nanopartículas de oro confinadas formando hot spots hace que la señal SERS sea mayor.

Para evaluar la sensibilidad del sensor se detectó la trimetoprima en un rango entre 10^{-4} y 10^{-7} M. Se observa cómo la intensidad de algunos picos disminuye al disminuir la concentración siendo, por tanto, la intensidad SERS dependiente de la concentración. Centrándonos en la banda de 1652 cm^{-1}, se representa la concentración de trimetoprima frente al área de esa banda y se consigue una curva de calibrado.

Para el análisis cualitativo, hay que destacar que las cápsulas plasmónicas son una buena elección ya que al evitar la agregación del oro ofrecen una buena reproducibilidad.

Para el análisis cuantitativo, se obtuvo el límite de detección a partir de la recta de calibrado llegando a detectar hasta 8,78 ppb. Esta detección es realizada en muestras reales de aguas residuales.

Además, hay que resaltar que esta detección es específica porque se han realizado medidas en presencia de otros contaminantes como ibuprofeno o diclofenaco y se ha podido detectar perfectamente la trimetoprima.

5.4 Capítulo 3

En este capítulo se muestra que para algunos contaminantes, la detección con las cápsulas plasmónicas no se puede realizar de forma directa ya que no existe afinidad entre el contaminante y las nanopartículas de oro. Por tanto, es necesario la utilización de un linker que los conecte. Así, el linker proporciona un punto de anclaje para los analitos que tengan baja afinidad con las nanopartículas metálicas.

En este trabajo se ha utilizado el 4-Aminotiofenol como linker debido a que cumple todas las características necesarias. Se trata de una molécula pequeña que puede penetrar a través de los poros de la sílice mesoporosa, es una molécula que proporciona una buena señal Raman y además contiene dos grupos funcionales que le permitirán unirse a las nanopartículas metálicas como al analito. El grupo tiol tiene gran afinidad por las nanopartículas metálicas dejando libre el grupo amino.

Se demuestra que el 4-aminotiofenol entra en el interior de la cápsula y queda atrapada en el interior mediante espectroscopía SERS ya que se obtiene se espectro. Así que el linker queda anclado por el lado del tiol (debido a la afinidad del enlace covalente Au-S) quedando disponible el grupo amino que sería el encargado de reaccionar con el analito.

En este caso, y con el objetivo de obtener un grupo más reactivo se realiza una reacción de diazoación para obtener una sal de

diazonio. Esta reacción es una de las más importantes en química orgánica y consiste en la reacción de una amina primaria y ácido nitroso. Cuando la amina primaria es alifática, la sal de diazonio obtenida es muy inestable y se descompone rápidamente. Sin embargo, si la amina primaria es aromática se genera una sal de diazonio que tiene cierta estabilidad en disolución y a bajas temperaturas.

Esta sal de diazonio formada es muy reactiva con los compuestos aromáticos, especialmente con los que tienen grupos dadores de electrones en la posición *para* (esto es debido a que la sal de diazonio tiene un carácter poco electrófilo). Como los contaminantes emergentes tratados en este trabajo son compuestos aromáticos se ha decidido que esta es la reacción idónea para detectarlos, pudiendo realizar incluso una detección múltiple.

El seguimiento de esta reacción se ha llevado a cabo mediante SERS, comparando los espectros obtenidos del linker antes y después de la reacción.

Además, al poder reaccionar con distintos contaminantes emergentes, el espectro SERS obtenido será una mezcla así que será necesario separar las señales mediante una deconvolución. Para comprobar si esto es posible, se realizó un experimento mezclando tres tioles al mismo tiempo con las cápsulas plasmónicas. En primer lugar, se obtuvieron los espectros individuales de cada tiol, asignando las bandas de cada espectro. Posteriormente, se realizó la asignación al espectro SERS de la mezcla observando que algún pico ha variado. En uno de estos picos se ha realizado una deconvolución obteniendo tres señales perfectamente diferencidas y que gracias a este proceso se pueden asignar correctamente.

Se trata de realizar este proceso de deconvolución para los espectros obtenidos después de la reacción entre la sal de diazonio y los contaminantes emergentes pero resulta complicado obtener una clara separación ya que los espectros individuales son muy similares entre sí.

Otro método posible para poder identificar los compuestos obtenidos, identificando así a los contaminantes es mediante la comparación de los espectros experimentales con espectros teóricos. Estos espectros son calculados mediante cálculos teóricos. Los métodos computacionales utilizados como DTF o Hartree-Fock han sido empleados en distintas ocasiones para obtener las frecuencias vibracionales. En este trabajo concreto, aunque los espectros teóricos y experimentales no concuerdan exactamente se han podido emplear los espectros teóricos para la asignación de algunas bandas.

5.5 Capítulo 4

En este capítulo se introduce el término de pinzas ópticas, una técnica que consiste en la manipulación de micro y nanopartículas. Un haz de láser altamente enfocado es la base de esta técnica ya que cuando es enfocado en el mismo plano de la muestra se crea una trampa óptica que permite sujetar a la muestra en el centro.

Esta técnica se ha utilizado en diferentes aplicaciones pero en los últimos años ha adquirido gran importancia el atrapamiento y manipulación de nanopartículas plasmónicas ya que capturando partículas metálicas, la trampa óptica puede mejorar la señal SERS. Siendo la trampa óptica con SERS una poderosa y multifuncional plataforma de detección.

En este trabajo se ha medido la eficiencia del atrapamiento óptico de las cápsulas plásmonicas y se ha comparado con una párticula de látex del mismo tamaño y con una sola nanopartícula de oro de un tamaño similar a las nanopartículas de oro que se encuentran en el interior de la nanocápsula. Las cápsulas plasmónicas muestran una mayor eficiencia de atrapamiento óptico que la nanopartícula individual debido al confinamiento de las nanopartículas de oro en el interior de las cápsulas. Además, comparando la cápsula plasmónica con la partícula de látex se obtiene una eficiencia similar, siendo muy reseñable ya que la cápsula es hueca y tiene un volumen de 20 veces menos que la partícula de látex.

Estos resultados experimentales fueron comparados con cálculos teóricos siendo los resultados similares y confirmando las conclusiones extraídas.

Finalmente, se realiza alguna prueba para demostrar cómo funciona el acoplamiento de dos técnicas como las pinzas ópticas y el SERS. En este caso, se utilizan las cápsulas plasmónicas para la detección de una molécula en disolución. Se comprueba que da buen resultado y que permite usar esta técnica para monitorizar *in situ*. Aunque este sistema tiene un amplio margen de mejora, se podría utilizar el acoplamiento de estas dos técnicas para la detección de contaminantes emergentes.